Departamento de Ciências da Vida

The Role Of Autophagy Activation-Mediated By Let-7 In A Transgenic Mouse Model Of Machado- Joseph Disease

Beatriz Filipa Varela Estremores

Dissertação no âmbito do Mestrado em Biologia Celular e Molecular com especialização em Neurobiologia, orientada pela Doutora Sónia Duarte (Centro de Neurociências e Biologia Celular) e co-orientada pelo Professor Doutor Carlos Duarte (Departamento de Ciência da Vida) e apresentada ao Departamento de Ciências da Vida da Faculdade de Ciências e Tecnologia da Universidade de Coimbra

Setembro de 2018

UNIVERSIDADE D
COIMBRA

This work was performed in Professor Luís Almeida's Group "Vectors and Gene Therapy" at Center for Neuroscience and Cell Biology (CNC), University of Coimbra, Portugal, under scientific guidance of Doctor Sónia Patricia Dias Duarte.

This work was financed by the European Regional Development Fund (ERDF), through the CENTRO 2020 Regional Operational Programme under project CENTRO-01-0145-FEDER-000008:BrainHealth 2020, through the COMPETE 2020 - Operational Programme for Competitiveness and Internationalization and Portuguese national funds via FCT – Fundação para a Ciência e a Tecnologia, I.P., under projects: POCI-01-0145-FEDER-032309, POCI-01-0145-FEDER-016719 (PTDC/NEU-NMC/0084/2014), POCI-01-0145-FEDER-007440 (UID/NEU/04539/2013) and POCI-01-0145-FEDER-016390:CANCEL STEM, and through CENTRO 2020 and FCT under project CENTRO-01-0145-FEDER-022095:ViraVector; also by projects ESMI (JPCOFUND/0001/2015) and ModelPolyQ (JPCOFUND/0005/2015) under the EU Joint Program - Neurodegenerative Disease Research (JPND), the last two co-funded by the European Union H2020 program, GA No.643417 and national funds (FCT), by and the National Ataxia Foundation, the American-Portuguese Biomedical Research Foundation, and by the Richard Chin and Lily Lock Machado Joseph Disease Research Fund. Sónia Duarte, was supported by an FCT fellowship (SFRH/BPD/87552/2012).

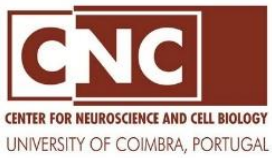

“I believe that God put us in this jolly world to be happy and enjoy life”

Sir Robert Baden-Powell

Agradecimentos

Em primeiro lugar, gostaria de agradecer ao Professor Luís Almeida por me ter aceitado no seu grupo de investigação para que pudesse realizar a minha dissertação. Obrigada por toda a preocupação, apoio e interesse ao longo deste ano de trabalho e por toda a transmissão de conhecimento.

À Doutora Sónia Duarte, um obrigado muito especial. Obrigada por todo o apoio, paciência, por todo o conhecimento partilhado, por todos os risos. Sem ti seria impossível chegar até aqui. Mais do que uma orientadora senti que ao longo desde ano tive ao meu lado uma pessoa em quem podia de facto confiar (e isso é importantíssimo para quem está a centenas de km de casa, como eu).

Ao Professor Carlos Duarte, obrigada por me ter acompanhado não só ao longo deste ano, mas também ao longo destes dois anos do mestrado. O seu apoio é muito importante para este mestrado.

A todo o grupo de Vetores e Terapia genética. Fizeram sentir-me em casa. Foi bom saber que sempre que ia para o laboratório havia sempre alguém para dar apoio quando precisei. Muito obrigada a todos!!

Aos meus "amigos locais" de sempre muito obrigada! É sempre tão bom voltar a casa e estar convosco, mesmo estando afastada tanto tempo.

Às minhas "defesas" Inês e Dori. Mesmo não estando todos os dias juntas continuamos iguais. Obrigada, miúdas!

À minha grupeta, Catarina, Rafael e Diana, obrigada por todos os encontros e momentos mais parvos que vivemos. Sem vocês isto não teria sido a mesma coisa. Obrigada!

Ao grupinho da sala de mestrado, obrigada a todos. Zé Pedro, Beltrão, Cristiana, Marta, Rita, Miguel, Patrick, Tânia, Mariana, Carina, Jéssica, Daniel, Inês e Ricardo. Foi tão importante ter-vos ao meu lado durante esta caminhada. Levo-vos a todos no coração. À Mariana um obrigado muito especial (sabes porquê e não preciso de escrever aqui). Ganhaste um lugar especial na minha vida. Obrigada! À Carina obrigada por teres sido o furacão daquela sala (no bom sentido, claro). Quase que se pode dizer que deste vida àquela sala. Foste a maior surpresa este ano, e que bom que foi. E claro que também ganhaste um lugar na minha vida (não fiques ciumenta). Obrigada!

À Carina Maranga. Acho que as palavras nunca serão suficientes para te agradecer. Obrigada por estares sempre ao meu lado, por não me deixares cair, por "ralhares" quando é preciso. Obrigada por olhares por mim como quem olha para a irmã mais nova. É isso, não é? És das maiores bênçãos da minha vida!

À Corporação de Bombeiros Voluntário de Monchique: Muito Obrigada! Obrigada por me mostrarem todos os dias que somos uma família. Obrigada por me terem feito crescer tanto ao longo destes anos. Os BVM são essenciais à minha vida. Sei que sou melhor hoje por vossa causa. São incríveis. Tenho tanto orgulho por fazer parte desta família. Somos Incríveis juntos. E será sempre "Vida por Vida".

Aos meus avós, irmão, tios, primos, obrigada a todos individualmente. Sem o vosso apoio incondicional não seria possível. Muito obrigada!

Aos meus pais. Por acreditarem sempre em mim, até de olhos fechados. Obrigada por me permitirem tudo isto, por não me cortarem as asas. Espero continuar a orgulhar-vos como até agora.

Por fim, quero agradecer a Deus, que nunca me deixou sozinha até nos momentos mais difíceis. Continuarei a acreditar e a confiar, sempre.

Table of contents

Table of Figures

List of tables

Abbreviations list

Ago2 - Argonaut 2

ASO – Oligonucleotides

ATGs - Autophagy related gene proteins

Atx3 - ataxin 3

CAG – Citosine-Adenine - Guanine

CMA - Chaperone-mediated autophagy

CMV – Cytomegalovirus

CREB - cAMP-response-element binding protein

DAPI - nuclear marker 4',6'-diamidino-2-phenylindole

DRPLA - Dentatorubropallidoluysian Atrophy

DGCR8 - DiGeorge critical region 8

EPO - External progressive ophthalmoplegia

ESCRT - Endosomal sorting complexes for transport

FIP200 - focal adhesion-interacting protein of 200 kDa

GFAP - Polyclonal anti-glial fibrillary acidic protein

GLK - Germinal center kinase-like kinase

HA - *Hemagglutinin*

HEK293 - *Human Embryonic Kidney 293*

hiPSCs - *Human induced pluripotent stem cells*

Iba-1 - Anti-ionized calcium binding adaptor molecule 1

IHC - Immunohistochemistry

JNK1 - c-Jun N-terminal Kinase 1

LAMP2A - Lysosomal-associated membrane protein 2A

LV - Lentiviral vectors

MAP1-LC3 - Microtubule-associated protein 1 light chain 3

MAP2 - Microtubule-associated protein 2

Map4k3 - Mitogen-activated protein kinase kinase kinase kinase 3

miRISC - RNA induced silencing complex

miRNAs - MicroRNAs

mir-scr - mir-scramble

MJD - Machado-Joseph disease

MMP-2 - Matrix metalloproteinase 2

monoU – Mono-uridylate

mTORC1 - Mammalian Target of Rapamycin Complex 1

NES - Nuclear export signals

NII - Neuronal intranuclear inclusions

NGS - normal goat serum

NLS - Nuclear localization signal

NMJ - Neuromuscular junction

PAS - Phagophore assembly site

PFA - Paraformaldehyde

PBS – Phosphate Buffer Saline

PI-3-P - Phosphatidylinositol-3-phosphate

PolyQ - Poly-glutamine

polyU - Poly-uridylate

pre-miRNA - premature-miRNA

pre-let-7 - Precursor of let-7

pri-miRNA - primary-miRNA

PVDF - polyvinylidene fluoride

Rag GTP-ases - Ras-related GTP-binding protein

RNAi - RNA interference

SBMA - Spinal and bulbar muscular atrophy

SCAs - Spinocerebellar ataxia

SNAREs - N-ethylmaleimide-sensitive factor attachment protein receptors

SQSTM1/p62 - Sequestosome 1/p62

TFEB - Transcription Factor EB

Tg - Transgenic

TRBP - Transactivation-response RNA-binding protein

TBS - Tris-buffered saline

TUT4/7 – terminal uridylyl transferase 4/7

UIM - Ubiquitin interacting motifs

UVRAG - Ultra-violet resistance-associated gene

UPP - Ubiquitin Proteasome Pathway

Vps34 - Vacuole protein sorting 34

WT – Wild-type

YAC - *Yeast artificial chromosom*

Abstract

Machado-Joseph Disease (MJD), also known as Spinocerebellar ataxia type 3 (SCA3), is a neurogenerative disorder caused by an expansion of the trinucleotide cytosine-adenine-guanine (CAG) in the *MJD1* gene, which translates into a polyglutamine tract within ataxin-3 protein that carries more than 55 CAG repeats in pathogenic conditions. MJD is the most common autosomal dominant ataxia worldwide and is characterized by several motors and non-motor clinical features with ataxia being the most common. Pathological mechanisms underlying MJD are still unclear, however it is accepted that mutant ataxin-3 gains toxic functions related to protein cleavage, oligomerization and aggregation, dysfunction of cellular quality control mechanisms and transcriptional and translational dysregulation, among others.

Our group provided evidence of an autophagy impairment in MJD. We have shown that MJD pathogenesis is associated with accumulation of autophagosomes, decrease of autophagy-related proteins and accumulation of mutant ataxin-3 and neurodegeneration. However, the cause of autophagy deregulation in MJD remains unknown.

Autophagy is a highly complex mechanism regulated by several molecules, namely by microRNAs (miRNAs). MiRNAs, being small non-coding RNAs, play an important regulatory role in animal cells by targeting mRNA transcripts for cleavage or translational repression. These small RNAs are involved in a broad range of biological functions, are expressed in a tissue specific manner and have been increasingly implicated in several disorders including neurodegenerative diseases and particularly in PolyQ diseases. Let-7 is a highly conserved miRNA, which showed to be able to activate autophagy and ameliorate neuropathology in a lentiviral- mouse model of MJD. Moreover, let-7 was shown to regulate several genes that block mTORC1 complex leading to autophagy activation.

Thus, we hypothesized whether let-7 would be able to activate autophagy and consequently alleviate motor incoordination and inbalance in a Transgenic (Tg) MJD mouse model. For that, lentivirus coding for let-7 or mir-scramble (mir-scr), as a control, were injected into the cerebellum of Tg MJD mice. In this study, we observed that let-7 was able to ameliorate motor coordination and balance, being this effect more prominent after 9 weeks of treatment. We also observed at a neuropathological level, evaluated at 12 weeks post-injection, that let-7 treatment led to an increase of layers thickness in lobules VIII and IX and seemed to partially decrease the levels of aggregates in whole cerebellum. Moreover, we have also observed that the MJD Tg mouse model used in this work exhibited an impairment in autophagy that was partially rescued upon let-7 treatment. In the last part of this work, we also observed that RagC, being a let-7 target, was upregulated at a basal level in MJD Tg mice, and

showed a tendency to be downregulated upon let-7 treatment. These results confirmed once more that autophagy is a good target for MJD treatment. In addition, this work provides new insights about the role of let-7 in the context of MJD and at the same time also opens new perspectives to a new possible approach based on miRNAs for MJD therapy.

Keywords: Machado-Joseph Disease (MJD), MicroRNAs (miRNAs), let-7, Autophagy, let-7 targets

Resumo

A doença de Machado-Joseph (DMJ), também conhecida como Ataxia Espinocerebelosa do tipo 3, é uma doença neurodegenerativa causada por uma expansão do trinucleótido citosina-adenina-guanina (CAG) no gene *MJD1*, que é depois traduzida numa cadeia de poliglutaminas na proteína ataxina-3, transportando mais de 55 repetições CAG em condições patogénicas. A DMJ é a ataxia autossómica dominante mais comum a nível mundial e caracteriza-se por vários sintomas motores e não-motores, sendo a ataxia o mais comum. Os mecanismos patogénicos subjacentes à DMJ ainda estão por esclarecer, no entanto, aceita-se que a ataxina-3 mutante ganha funções tóxicas relacionadas com a clivagem proteica, oligomerização e agregação, disfunção dos mecanismos celulares de controlo de qualidade e da desregulação a nível da transcrição e tradução, entre outras.

O nosso grupo já providenciou evidências do comprometimento do mecanismo de autofagia na DMJ. Com estes estudos mostrámos que a patogénese da DMJ está associada à acumulação de autofagossomas, à diminuição de proteínas relacionadas com a autofagia, bem como à acumulação da ataxina-3 e neurodegenerescência. No entanto, a causa da desregulação da autofagia na DMJ permanece desconhecida.

A autofagia é um mecanismo altamente complexo regulado por diversas moléculas, nomeadamente por microARNs (miARNs). Os miARNs, sendo pequenos ARNs não-codificantes, desempenham um importante papel regulador em células animais, tendo como alvos os transcritos de mRNA, mediando à sua clivagem ou inibição do mecanismo de tradução. Estes pequenos ARNs estão envolvidos num largo conjunto de funções biológicas, são expressos de uma forma especifica no tecido e têm sido implicados em diversas doenças incluindo doenças neurodegenerativas, particularmente em doenças de poliglutaminas. O let-7 é um miARN altamente conservado, que mostrou ter a capacidade de ativar a autofagia e melhorar a neuropatologia num modelo lentiviral da DMJ em murganho. Mais ainda, o let-7 mostrou regular diversos genes que bloqueiam o complexo mTORC1 levando à ativação da autofagia.

Assim, colocámos a hipótese se o let-7 seria capaz de ativar a autofagia e consequentemente aliviar a descoordenação motora e desequilíbrio num modelo transgénico (Tg) da DMJ em murganho. Para isso, injetámos lentivírus que codificam para o let-7 ou mir-scramble (mir-scr), como controlo, no cerebelo de murganhos transgénicos da DMJ. Neste estudo, observámos que o let-7 era capaz de melhorar a coordenação motora e equilíbrio nestes animais, sendo este efeito mais evidente às 9 semanas de tratamento. Também observámos a nível neuropatológico, avaliado às 12 semanas pós-injeção, que o tratamento com let-7 levou ao aumento da espessura das camadas nos lóbulos VIII e IX e parece diminuir parcialmente o nível de agregados em todo o cerebelo. Além disto, também observámos que

o modelo Tg da DMJ em murganho usado neste trabalho mostrava um comprometimento da autofagia, que foi parcialmente recuperado depois do tratamento com let-7. Na última parte deste trabalho, também observámos que a RagC, sendo um alvo do let-7, estava sobreexpressa a nível basal no modelo Tg da DMJ,, e mostrou uma tendência para estar diminuída após tratamento com let-7. Estes resultados confirmam uma vez mais que a autofagia é um bom alvo para o tratamento da DMJ. Mais ainda, este trabalho fornece novos conhecimentos acerca do papel do let-7 no contexto da DMJ e ao mesmo tempo abre novas perspetivas para uma nova abordagem possível baseada em miARNs para terapia em DMJ.

Palavras-chave: Doença de Machado-Joseph (DMJ); MicroARNs (miARNs); Let-7; Autofagia; Alvos do let-7

Chapter I - Introduction

1. Poly-glutamines (PolyQ) Disorders

Poly-glutamine (PolyQ) disorders are a group of 9 diseases that are characterized by a mutation on a disease-related gene, which translates into a large tract of glutamine repeats. The first disease associated with this glutamine expansion was spinal and bulbar muscular atrophy (SBMA). At that time, La Spada and its collaborators discovered an amplification of repeats number in androgen receptor gene that was associated with the pathogenesis of the disorder (La Spada et al., 1991). In addition to SBMA, Huntington's disease, Dentatorubropallidoluysian Atrophy (DRPLA), and Spinocerebellar ataxias (SCA) type -1, -2, -3 (or Machado-Joseph disease, MJD), -6, -7 and -17 (Table 1) are also part of this group of polyQ disorders. Although these disorders share a CAG expansion, this occurs in different genes, which are unrelated (Gatchel and Zoghbi, 2005; Orr and Zoghbi, 2007). Nevertheless, all polyQ disorders are characterized by neuronal loss and are associated to physical and neurological problems (Gatchel and Zoghbi, 2005). A negative correlation between CAG length and age of onset has been described in MJD, as well as in the other PolyQ diseases. Thus, when an individual carries a long segment of CAG occurs a phenomena called anticipation (Maciel et al., 1995).

Table 1: Summary of polyQ disorders (adapted from Rego & de Almeida 2005; Orr & Zoghbi 2007; Matos et al. 2011)

Disease name	Mutated gene	Protein product	CAG repeat size		Brain regions affected
			Normal	Pathogenic	
Spinocerebellar ataxia 1	SCA1	Ataxin 1	6-39	40-82	Cerebellar Purkinje cells, dentate nucleus, brainstem
Spinocerebellar ataxia 2	SCA2	Ataxin 2	15-24	32-200	Cerebellar Purkinje cells, brainstem, frontotemporal lobes
Spinocerebellar ataxia 3	ATXN3/MJD 1/SCA3	Ataxin 3	10-51	55-87	Cerebellar dentate neurons, basal ganglia, brainstem, spinal cord
Spinocerebellar ataxia 6	CACNA1A	$CACNA1_A$	4-20	20-29	Cerebellar Purkinje cells, dentate nucleus, inferior olive
Spinocerebellar ataxia 7	SCA7	Ataxin 7	4-35	37-306	Cerebellum, brainstem, macula, visual cortex
Spinocerebellar ataxia 17	SCA17	TATA-binding protein	25-42	47-63	Cerebellar Purkinje cells, inferior olive
Huntington's disease	HD	Huntingtin	3-34	36-121	Striatum, cerebral cortex
Dentatorubropallidoluysian Atrophy	DRPLA	Atrophin 1	7-34	49-88	Cerebellum, cerebral cortex, basal ganglia, Luys body
Spinal and Bulbar muscular atrophy (SBMA; kennedy disease)	AR	Androgen receptor	9-36	38-62	Anterior horn and bulbar neurons, dorsal root ganglia

1.1 Machado-Joseph Disease (MJD)

Machado-Joseph Disease (MJD), also known as Spinocerebellar ataxia type 3 (SCA3), was firstly described by Nakano et al. in 1972 in a Portuguese descendent population from Azores. This population showed motor and neurological symptoms such as ataxic gait, dysarthria, absence of tendon reflexes and nystagmus, among others. Since all the members of this family were affected and the disorder was not lethal, the investigators suggested that would be inherited and autosomal dominant naming it as "Machado disease" (family´s name) (Nakano et al., 1972). In the same year, Woods et al. described the disorder in other family designating it as "Nigro-spino-dentatal degeneration with Nuclear Ophthalmoplegia"(Woods and Schaumburg, 1972). Some years later, the disease was described in two other families with different names, as "Joseph Disease" and "Azorean Disease" and finally proposed as a unique disorder named by "Machado-Joseph Disease" (reviewed by Rosenberg 1992).

MJD is the most common autosomal dominant ataxia worldwide (1.5/100000). In Portugal, MJD shows a high prevalence in Azores (1/2554), especially in Flores island (1/158) (Araújo et al., 2016), while in Portugal mainland it is more rare (1/100000) (Bettencourt et al., 2008). Besides Portugal, there are other countries where the disorder shows to have a high relative frequency such as Brazil, Germany, Australia and Japan (Bettencourt and Lima, 2011), however in others, like Italy and Wales the disease frequency is low (Ruano et al., 2014) (Figure 1).

Figure 1 Representative image of the global prevalence of Machado-Joseph Disease (MJD). (Adapted from: http://www.physio-pedia.com/Machado-Joseph_Disease (Spinocerebellar_Ataxia_Type_3)**.**

1.1.1 Clinical features and MJD subtypes

The first common symptom occurring in MJD is the gait ataxia that is present in 98.6% of patients (Coutinho, 1992). However, since this neurodegenerative disorder affects various systems such as extrapyramidal, pyramidal cerebellar and oculomotor neurons it is associated with many other symptoms. Thus, there are motor symptoms beyond gait ataxia such as limb ataxia, nystagmus, diplopia, dystonia, dysphagia and rigidity. All of this symptoms are clinical hallmarks important for the correct diagnosis (Bettencourt and Lima, 2011; Paulson, 2012). Non-motor symptoms have also been reported, such as sleep disturbances, cognitive impairment and psychiatric symptoms (Pedroso et al., 2013).

The disorder is very heterogenous since MJD patients are not all affected by the same symptoms. Thus, it was proposed a division into 5 MJD types depending on severity (Table 2). The type 1, also termed "Type Joseph", consist of individuals with early onset that present quickly progression of ataxia, external progressive ophthalmoplegia (EPO), pyramidal (rigidity and spasticity) and extrapyramidal signs (bradykinesia and dystonia) (Bettencourt and Lima, 2011).

Table 2: MJD types depending on severity

Type	Onset	Symptoms
Type 1 or Joseph	Early (20-24 years)	• Pyramidal signs • Extrapyramidal signs • Ataxia • EPO
Type 2 or Thomas	Intermediate (30-40 years)	• Ataxia • EPO
Type 3 or Machado	Late (40-75 years)	• Ataxia • EPO • Peripheral disturbances
Type 4	_____	• Parkinsonism • Mild cerebellar deficits • Neuropathy or Amyotrophy
Type 5	_____	• Spastic paraplegia

In type 2 or Thomas, which is the most common, the affected individuals present an intermediate onset exhibiting EPO and ataxia. This type may also develop extrapyramidal signs that once present are tenuous and pyramidal signs. The patients with a late onset belongs to type 3 or "type Machado" and present ataxia, EPO and peripheral disturbances (Bettencourt and Lima, 2011; Coutinho and Andrade, 1978). The type 4 of MJD is a rare form of the disorder that present parkinsonism, mild cerebellar deficits and distal motor neuropathy or amyotrophy (Suite et al., 1986). The last type of

MJD, type 5, is also a rare form and the individuals only present spastic paraplegia (Bettencourt and Lima, 2011).

1.1.2 Neuropathology

MJD is characterized by neurodegeneration in selective brain regions. A reduction of cerebellum, caudate and putamen volumes was firstly reported in MJD patients by Klockgether and co-workers (Klockgether et al., 1998). Years later, MJD studies showed atrophy of cerebellum, pons, medulla oblongata and cranial nerves III-IX, thus resulting in a weight loss of the entire brain (Rüb et al., 2002; Schulz et al., 2010). In 2006, the same investigators also reported neurodegeneration of thalamus and hypothesized that neuronal intranuclear inclusions (NII) and its toxic effects were in the origin of neurodegeneration found in *post-mortem* brains of MJD patients (Rüb et al., 2006).

In several other studies, neuronal loss specially in striatum, brainstem, basal ganglia and spinal cord, being really marked in Clark's column and anterior horn was also described in MJD (reviewed by Rüb et al. 2008). Our group also provided evidences of neuronal dysfunction in striatum of *post-mortem* brains of MJD patients that was confirmed both in lentiviral rat model and in transgenic mouse model of MJD (Alves et al., 2008). Surprisingly, Purkinje cells in cerebellar cortex and inferior olive seemed to be relative preserved in MJD (Durr et al., 1996), however this aspect is still controversial as in some patients there was loss of granule layer and Purkinje cells, especially in vermis (Muñoz et al., 2002). Rüb and his colleagues also reported the enlargement of the 4th ventricle in some cases (Rüb et al., 2008) (Figure 2).

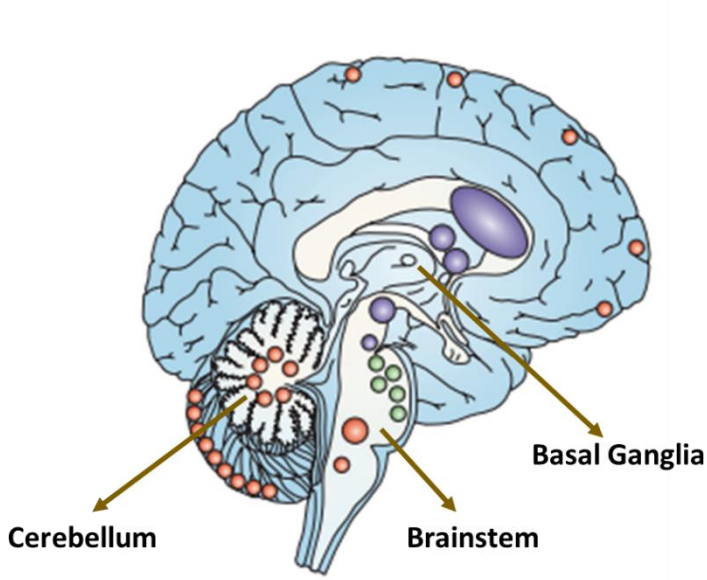

Figure 2 Neuropathology in MJD. Representative scheme of principal affected areas in MJD. Large dots indicate severe neuronal loss. Green dots indicate cranial nerves involvement. Blue dots indicate extrapyramidal nuclei involvement. Adapted from (Taroni and Didonato, 2004)

1.1.3 *MJD1* gene

MJD is associated to *MJD1* (or *ATXN3*) gene which is located on the long arm of chromosome 14 (14q32.1) and encodes for ataxin 3 (atx3) protein (Takiyama et al., 1993). In 1994, Kawaguchi and colleagues identified an unstable CAG expansion in atx3 of MJD patients (Kawaguchi et al., 1994). MJD1 gene is composed by 11 exons with CAG tract being located in exon 10. Four different transcripts were described due to different splicings in exon 10 or exon 11 (Ichikawa et al., 2001). MJD1 gene carries 10 to 51 CAG repetitions in normal population and from 55 to 87 in MJD individuals. Individuals with CAG repeats between 52 and 54 show incomplete penetrance, which means that some may develop the disease while others do not (Maciel et al., 2001; Matos et al., 2011; Orr and Zoghbi, 2007). The mean age of onset in MJD is 38 years old and the individuals normally died after 20 years of the onset, however this can be different if an individual has a higher CAG length being considered a juvenile case (Kawaguchi et al., 1994; Maciel et al., 1995).

1.1.4 Ataxin-3 (atx3) protein

1.1.4.1 Wild type (wt) Ataxin-3

Wild-type (WT) atx3 is the protein product of *MJD1* gene with a molecular weight around 42 kDa and composed by 339 amino acids, depending on the CAG stretch length. Atx3 can be found in several different types of cells and tissues in whole body and is ubiquitous expressed in the brain (Albrecht et al., 2004; Schmitt et al., 1997; Trottier et al., 1998). This protein has a catalytic domain localized in N-terminal, which is a globular structure termed Josephin domain conferring the ubiquitin protease activity and that is highly conserved between mammalian species (Masino et al., 2003). Josephin domain is followed by a flexible C-terminal tail containing the CAG tract and two or three ubiquitin interacting motifs (UIM), depending on the isoform, which allows the binding to polyubiquitylated proteins (Albrecht et al., 2004; Burnett et al., 2003) (Figure 3).

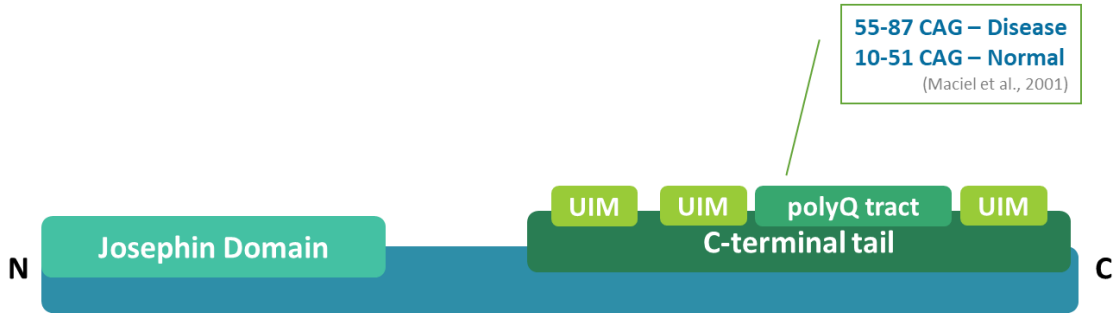

Figure 3 Scheme of ataxin 3 (atx3) protein. Atx3protein is composed by two principal domains: josephin domain, that is highly conserved, and C-terminal tail that contain two or three ubiquitin interacting motifs (UMI) and the polyglutamine (polyQ) tract.

Furthermore, the non-pathogenic atx3 has a natural tendency to aggregate. In addition, atx3 with two UIM is more prone to aggregate due to the presence of a hydrophobic domain than the atx3 that carries three UIM. This last isoform is the most common form found in the human and murine brain (Harris et al., 2010).

In cells, the atx3 protein can be found most of the time in cytoplasm, however it can also be found in nucleus may be due to a nuclear localization signal (NLS) localized upstream of polyQ tract that gives properties to the protein to enter the nucleus. Moreover, there are also three nuclear export signals (NES), one localized close to Josephin domain (NES 174) and the other two inside of Josephin domain (NES 77 and NES 141) that allows the exportation of atx3 to the cytoplasm (Albrecht et al., 2004; Antony et al., 2009; Macedo-Ribeiro et al., 2009).

Although the main function of atx3 is not clearly understood there are many evidences suggesting that its principal role is as deubiquitinating enzyme (Donaldson et al., 2003; Doss-pepe et al., 2003). Regarding this, it has been proposed that atx3 acts in Ubiquitin Proteasome Pathway (UPP), one of the major pathways to degrade proteins (Todi et al., 2010). Atx3 has also been implicated in formation and transport of aggresomes. These aggresomes are aggregates of misfolded proteins that are located near the microtubule-organizing centre and are not possible to be degraded by proteasome (Burnett and Pittman, 2005; Todi et al., 2010). Atx3 seems to interact with tubulin and microtubule-associated protein 2 (MAP2) that will contribute to aggresomes transport (Mazzucchelli et al., 2009; Todi et al., 2010). On the other hand, atx3 may also be involved in transcription of genes acting as a transcription regulator. Actually, atx3 is able to repress transcription by inactivating co-activators that mediate transcription. In 2002, Li and his colleagues found that atx3 interacts and represses cAMP-response-element binding protein (CREB) and p300 avoiding transcription. Furthermore, it was found that atx3, through Josephin domain, can inhibit histone acetylation that will also repress transcription (Li et al., 2002).

1.1.4.2 Mutant ataxin-3

The formation of mutant atx3 occurs when *MJD1* gene carries over than 55 CAG repeats (Maciel et al., 2001). This pathogenic form of atx3 is more prone to aggregate than the non-pathogenic form, forming NII. (Chai et al., 2001; Paulson et al., 1997; Perez et al., 1998). Atx3 aggregates are formed in two different stages. The first stage is shared by normal and mutant atx3, in which protein aggregate through Josephin domain, forming dimers and consequently aggregates that are SDS-soluble fibrils. However, in mutant atx3 the aggregation rate is faster than in normal atx3. The second stage only occurs in mutant atx3, where the protein aggregates through the polyQ tract developing SDS-insoluble aggregates (Ellisdon et al., 2006).

1.1.5 MJD models

In order to study molecular mechanisms and pathogenesis of MJD, different models have been generated and are essentially divided in *in vitro* models and in *in vivo* models.

1.1.5.1 *In vitro* models

1.1.5.1.1 Neuronal and non-neuronal cells

Human Embryonic Kidney 293 (HEK293) cell line has been used as an MJD model. For instance, HEK293 transfected with mutant or normal atx3 were used to assess mitochondria impairment on MJD cytotoxicity (Laço et al., 2011).

Fibroblasts are other non-neuronal cell type used to investigate mechanisms impairment in MJD. These cells are obtained through dermal biopsies from MJD patients. In our group we have used fibroblasts to investigate autophagy impairment in MJD (Onofre et al., 2016).

PC6-3 cell line is derived from rat adrenal gland pheochromocytoma used in MJD *in vitro* studies but contrarily to the cell lines mentioned above, these cells need to be differentiated into neuronal cells. In MJD studies PC6-3 were also transfected with mutant and normal atx3 and used to investigate mitochondria impairment in MJD (Laço et al., 2011).

Neuronal cell lines are also used as an MJD model *in vitro*. Neuro-2a cell line is derived from neuroblastoma, has a fast growth and are easily to manipulate. Neuro-2a cells have been used for instance to study the effect of beclin1 overexpression in MJD pathology (Nascimento-Ferreira et al., 2013). More recently, neuro-2a expressing mutant atx3 was used to investigate the effect of sirtuin 1 in autophagy mechanism (Cunha-Santos et al., 2016).

1.1.5.1.2 Human induced Pluripotent Stem Cells (hiPSCs)

Human induced pluripotent stem cells (hiPSCs) are a recent approach developed by Takahashi and collaborators in 2006 (Takahashi and Yamanaka, 2006; Takahashi et al., 2007). Since then, many studies have used this *in vitro* human cell model. hiPSCs can be obtained by reprogramming human fibroblasts of MJD patients. Then hiPSCs derived neurons can be used as an MJD model. As an example, this model was used to study the effect of autophagy induction in MJD (Ou et al., 2016).

1.1.5.2 *In vivo* models

1.1.5.2.1. Invertebrate models

Drosophila melanogaster is a fly specie used mostly in molecular genetic investigation. In order to understand the mechanism involved in MJD pathogenesis, human normal atx3 carrying 27 glutamines (Q) repeats (MJDtr-Q27) or truncated form of mutant atx3 carrying 78 Q repeats (MJDtr-Q78) were overexpressed in Drosophila. Flies carrying mutant atx3 showed NII in brain as well as in the eyes, however this model showed early death (Warrick et al., 1998). After this study, the same group generated another fly model. Using the *D. melanogaster,* the authors expressed the full-length human mutant atx3 carrying 78Q or 84Q from cDNA. This model presented NII in brain and eyes and neurodegeneration (Warrick et al., 2005).

Other invertebrate model used in MJD studies is *Caenorhabditis elegans (C. Elegans)*. The first model created in this specie occurs in 2006 by Khan et al. This model was produced by expressing the full-length mutant atx3 carrying 91Q or 130Q or also expressing truncated forms of mutant atx3 with 63Q or 127Q. These models presented motor incoordination in late stages as well as neuronal dysfunction and presence of aggregates (Khan et al., 2006).

1.1.5.2.2 Vertebrate models

1.1.5.2.2.1 Rodent models

1.1.5.2.2.1.1 Transgenic Models

The first mouse model was created in 1996 by Ikeda and his collaborators. In this model, mice expressed the full-length mutant atx3 carrying 79 repeats selectively in Purkinje cells using L7 promoter, however no alterations in behaviour or in neuropathology were reported in this model. After that, they created a mouse model expressing truncated mutant atx3 that exhibit severe atrophy of cerebellum, loss of Purkinje cells and brutal behaviours deficits. However, these clinical and neuropathologic features as well as the loss of Purkinje cells did not reproduce what occurs in MJD patients (Ikeda et al., 1996).

Some years later, Cemal and collaborators produced a mouse model mimicking MJD in humans. For that, they used yeast artificial chromosome (YAC) expressing full-length mutant atx3 with 15, 64, 67, 72, 76 and 84 repeats that have a ubiquitous expression. This mouse model presents an early onset and develops wide ataxia, tremor and sensory deficits, among others. NII and neuronal loss were observed in cerebellar nuclei and pontine (Cemal et al., 2002).

Other MJD mouse model was generated using the mouse prion protein promoter to express full-length human mutant atx3 with 71 or 20 repeats. This approach allowed to enhance the expression of mutant atx3 in brain and spinal cord, however at a neuropathological level, NII were barely found in Purkinje cells. This MJD mouse model showed ataxia, low body weight, postural instability and premature death (Goti et al., 2004).

In 2008, Torashima and colleagues created a mouse model expressing an N-terminal truncated human isoform of mutant atx3 from cDNA carrying 69 glutamines with hemagglutinin (HA) epitope. In this model, Atx3 is selectively expressed under the control of L7 promoter in Purkinje cells. Cerebellar atrophy and severe ataxia were found in this model as well as an almost complete absence of Purkinje cells (Torashima et al., 2008). In the same year, Chou and collaborators tried to use prion promoter to express full-length of an isoform of human atx3 with 79 glutamines and HA epitope. Low body weight, motor incoordination and severe ataxia were present in this mouse model. Moreover, the authors reported a transcriptional dysregulation and detected NII, as well as neuronal loss in pons, dentate nuclei and *substantia nigra* in these mice (Chou et al., 2008).

1.1.5.2.2.1.2 Lentiviral models

In 2008, our group generated for the first time a lentiviral-based genetic model of MJD in rat. This model was generated by stereotaxic injection into the rat striatum of lentivirus encoding for full-length human atx3 carrying 27Q or 72Q. This model showed presence of aggregates and neuronal loss (Alves et al., 2008).

After this study, the same approach was used to generate an MJD mouse model. For this purpose, lentivirus encoding for full-length human atx3 carrying 27Q or 72Q were injected into the mouse striatum. Evidences of neuronal loss, neurodegeneration and accumulation of mutant atx3 were found in this model (Simões et al., 2012).

In the same year, other model was produced by the injection of the same lentiviral constructs into the cerebellum vermis of mice. This approach resulted in mouse ataxia and cerebellar neuropathology (Nóbrega et al., 2012).

All in all, Lentiviral mouse models appear to be time- and cost-effective.

1.1.5.2.2.2Non-rodent models

Very recently, Watchon et al. established a non-rodent model to study MJD, using zebrafish. In this model, they expressed human atx3 with 23Q or 84Q with HuC as a neuronal promoter. Phenotypically, the 84Q zebrafish exhibit impairment in motor coordination, namely in accelerated swimming, being

progressive along ageing. At a neuropathological level, this model shows neuritic-beading staining pattern, however it failed showing the presence of neuronal intranuclear inclusions, which constitute one of the most important hallmarks of the disease (Watchon et al., 2017).

In conclusion, there are several models to study MJD and all of them were developed with the ultimate goal of mimicking what happens in human MJD patients. Each model presents advantages and disadvantages and therefore each group of investigation uses the more convenient model for their work.

1.1.6 Pathogenesis

The molecular mechanisms underlying MJD pathogenesis are still poorly understood. Nonetheless, several hypotheses have been suggested (figure 4). It has been discussed for several years whether mutant atx3 formation would lead to a loss or a gain-of-function. Regarding this, it was suggested that the mutant form of atx3 is capable of changing its conformation to a β-strand conformation, acquiring a toxic function. (Nagai et al., 2007).

Some authors have reported that due to inefficient clearance of mutant atx3, toxic C-terminal fragments are generated and will aggregate and recruit full-length mutant atx3, as well as other important proteins causing neurotoxicity (Chai et al., 2001; Ellisdon et al., 2007; Perez et al., 1998). Actually, these fragments seem to breakout the cellular quality control mechanisms and cause the neurodegeneration in MJD by a mechanism of toxic cleavage mediated by calcium-dependent calpains proteases. In 2007, Haacke and her group demonstrated that in the presence of calpastatin, a calpain inhibitor, atx3 is less prone to aggregate in neuroblastoma cells (Haacke et al., 2007). After this, our group observed that inhibition of calpains, through overexpression of calpastatin in a lentiviral MJD mouse model, was able to reduce the number of aggregates, as well as their size. Moreover, we also found that inhibition of calpains by calpastatin avoid the aggregation of mutant atx3 and its translocation to the nucleus (Simões et al., 2012). Altogether, these results suggest that proteolysis of atx3 is an MJD pathogenesis-linked mechanism (figure 4).

NII and neuronal cytoplasmic inclusions formed by mutant atx3 have also been implicated in deregulation of quality-control mechanisms. These aggregates are able to sequester other proteins such as transcription factors, chaperones, ubiquitin and proteins from the proteasome that will disturb UPP and autophagy. Disruption of these mechanisms leads to an accumulation of misfolded proteins (Chai et al., 1999; Paulson et al., 1997), thus contributing to MJD pathogenesis (figure 4).

Moreover, upregulation of neuroinflammatory molecules were also found in MJD models and further confirmed in MJD patient brains. Matrix metalloproteinase 2 (MMP-2) and interleukin- 1β, among others were found to be upregulated in MJD, thus suggesting a role of glia in MJD pathogenesis (Evert et al., 2001, 2003). In other study, neuroinflammation was not detected in early stages of MJD, but is prominent at late stages of the disease (Silva-Fernandes et al., 2010). However, the implication of neuroinflammation in MJD pathogenesis is still poorly studied (Figure 4).

Many other mechanisms have been proposed as contributing to MJD pathogenesis, as it is illustrated in Figure 4.

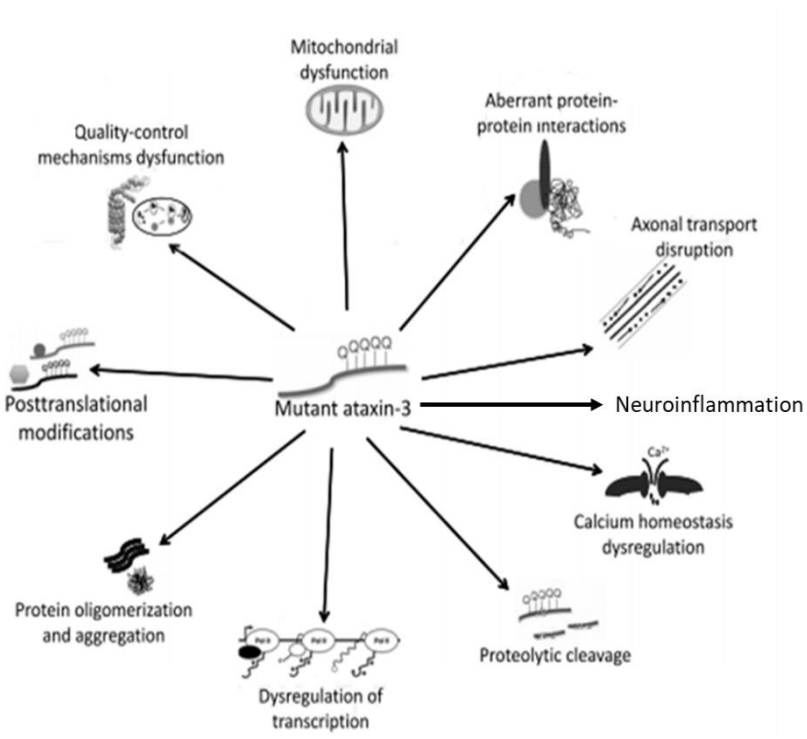

Figure 4 Mechanisms involved in MJD pathogenesis. Several mechanisms have been suggested to be linked to MJD pathogenesis. Mutant atx3 is responsible for deregulating important cell pathways such as protein oligomerization and aggregation, dysregulation of transcription, neuroinflammation, quality-control mechanisms deregulation, among others. All these mechanisms when disrupted lead to neurodegeneration in MJD. Adapted from (Nóbrega and de Almeida, 2012).

1.1.7 Therapeutic strategies for MJD

Despite the huge efforts, there is still no treatment capable of delaying or blocking the progression of the disease. One of the first approaches consisted in the silencing of mutant atx3. Our group generated an RNA interference (RNAi) that was able to target atx3 inducing non-allele specific silencing. Atx3 silencing showed to alleviate neuropathology in a MJD rat model (Alves et al., 2010). Other group tried to silence mutant atx3 using peptide nucleic acid and locked nucleic acid antisense oligomers against

its polyQ tract and the results showed that atx3 was efficiently silenced in in vitro MJD cell models (Hu et al., 2009).

One of the most promising non-viral gene therapies is named antisense oligonucleotides (ASO). These chemical molecules are single short strands of oligonucleotides, which are able to target mRNA, modelling its function. ASOs technology has been studied in several disorders, especially in brain-related diseases. In 2017, Moore and collaborators used ASOs to silence mutant atx3 in two different Transgenic (Tg) mouse models: one that carries a single atx3 isoform by expressing a cDNA (CMV-MJD-Q135) and the other that carries the full-length of mutant atx3 (YAC-MJD-Q84.2). In this study they observed that three of the five tested ASOs were very efficient in reducing mutant atx3 in YAC-MJD-Q84.2 but not in CMV-MJD-Q135 model. This means that full-length of atx3 is a more powerful target for ASOs than the cDNA (Moore et al., 2017). In the same year, Toonen and his collaborators described another approach using ASOs for MJD therapy. In this work they used ASOs that were able to remove the polyQ stretch in atx3 protein and consequently eliminate the main cause of the disease. A decrease of insoluble atx3 and nuclear accumulation was observed upon repeated intracerebroventricular injections of these ASOs in a SCA3 mouse model (Toonen et al., 2017). More recently, McLoughlin and his group made use of one of the most promising ASOs that effectively target full-length human *ATXN3* gene, described in the study of Moore et al. (Moore et al., 2017), and injected it intracerebroventricularly into an early symptomatic transgenic SCA3 mice. Following a single i.c.v. bolus injection of this ASO, apart from the prevention of oligomeric and nuclear accumulation of ATXN3, it was also reported a rescue of motor injuries and Purkinje cells dysfunction (McLoughlin et al., 2018). Since the overactivation of calpains has been showing to contribute to mutant atx3 proteolytic cleavage, translocation to the nucleus, inclusions formation and neurodegeneration, our group tried to inhibit these proteases using BDA-410, a synthetic calpain inhibitor in a lentiviral MJD mouse model. We observed that treated mice had a decrease in the number of atx3 fragment and inclusions. At a phenotypic level BDA-410 induce amelioration of motor coordination and balance observed in beam walking test (Simões et al., 2014).

Autophagy has also been studied as a possible target for MJD therapy and this point will be discussed in the next section.

2. Autophagy

Autophagy is one of the most highly conserved mechanisms from yeast to humans. This cell process, firstly discovered by De Duve and Wattiaux (de Duve and Wattiaux, 1966), aims at degrading misfolded proteins and damaged organelles, contributing for cell clearance through lysosomes under starvation and stress conditions (Mizushima et al., 2004). The general term of "autophagy" includes three different subtypes for cell clearance: macroautophagy, microautophagy and chaperone-mediated autophagy (CMA) (Figure 5). In all the three subtypes, there is delivery of cytoplasmic elements into lysosome for further degradation (Harding et al., 1996; Li et al., 2012; Neff et al., 1981; Wang and Klionsky, 2003). Lysosomes are large vacuoles that contain a lot of digestive enzymes such as proteases and lipases that will degrade proteins and organelles (de Duve and Wattiaux, 1966; Yao et al., 2017).
Macroautophagy is the better known subtype and involves formation of autophagosome that will fuse with lysosome occurring catabolism (de Duve and Wattiaux, 1966; Wang and Klionsky, 2003). Microautophagy was discovered years ago, however the mechanism underlying this process is still poorly understood. Even so, it is known that there is a direct invagination of lysosome membrane containing small portions of cytoplasm and proteins (Li et al., 2012; Mortimore et al., 1988). CMA is the most different form of autophagy and does not implicate a vacuole formation or sequestering of proteins. Thus, the cargo contains KFERQ- like pentapeptide motif that will be recognized by HSC70, a cytosolic chaperone. Instead of fusion with lysosome, this autophagy promotes translocation of cargo into the lysosome with the help of lysosomal-associated membrane protein 2A (LAMP2A) (Agarraberes and Dice, 2001; Cuervo and Dice, 1996).

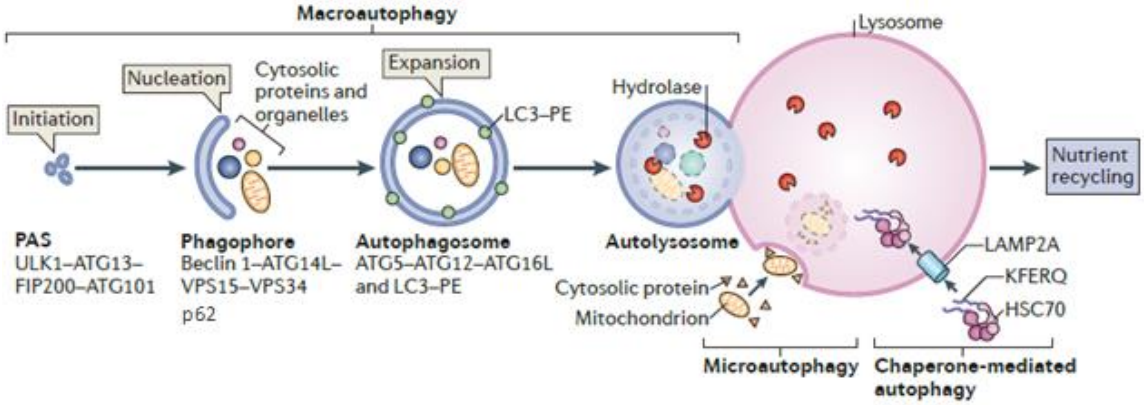

Figure 5 Autophagy mechanism. Autophagy is a molecular mechanism for cell clearance. It is divided in three different subtypes: Macroautophagy represents the most complex type, being constituted by four steps- initiation, nucleation, expansion and fusion with lysosome; Microautophagy is still unclear, but it is known that exhibits direct engulfment of lysosome membrane with small portion of cytoplasm; Chaperone-mediated autophagy (CMA) does not require vesicles formation. Instead, a motif in the cargo protein will be recognized and then the protein will be translocated into the lysosome. Adapted from (Kaur and Debnath, 2015)

2.1 Macroautophagy

Macroautophagy is the main type of autophagy in cells and also the most studied. It is currently termed "autophagy" and is an highly complex mechanism regulated by several proteins (Mizushima et al., 1998, 2004). This process is composed by three important steps, namely 1) initiation and nucleation, 2) elongation and 3) maturation and fusion (Figure 6).

- **Initiation and nucleation**

The key for autophagy induction is mostly starvation sensed by mammalian Target of Rapamycin Complex 1 (mTORC1). This complex acts as a sensor of amino acids concentrations in cells and is involved in protein biogenesis and lipogenesis, thus contributing for cell growth. MTORC1 when activated, represses autophagy by phosphorylating important proteins involved in autophagy signalling, such as autophagy related gene proteins (ATGs) (Kamada et al., 2000). Therefore, when mTORC1 is repressed under amino acid limitation, ULK1 (named Atg1 in yeast) and ULK2 will be dephosphorylated. This step leads to the formation of ULK complex that also includes focal adhesion-interacting protein of 200 kDa (FIP200), Atg13 and Atg17. The ULK complex will be important for the formation of phagophore assembly site (PAS), activating autophagy (Suzuki et al., 2007).

In this process, how phagophore membrane, the precursor of autophagosome, is formed is still a theme of discussion. Some authors defend that endoplasmic reticulum is the major organelle contributing with membrane for autophagosome formation (Dunn, 1990), whereas others defend that autophagosome is formed by the outer membrane of mitochondria (Hailey et al., 2010). Thus, it has been proposed that endoplasmic reticulum, mitochondria, recycling endosomes and plasma membrane can contribute all for autophagosome membrane formation (reviewed by Lamb et al., 2013).

Furthermore, the activity of Vacuole protein sorting 34 (Vps34) was demonstrated to be required in regulation of phagophore formation at early stages of autophagy, namely at the nucleation step. This molecule forms a complex with Beclin 1 (named Atg6 in yeast), p150/Vps15, Ultra-violet resistance-associated gene (UVRAG) and Barkor/Atg14-L. Moreover, phosphatidylinositol-3-phosphate (PI-3-P), being a Vps34 product, displays an essential role in this process through the recruitment of ATG proteins. (Fan et al., 2011; Jaber et al., 2011).

Under non-starvation conditions, Beclin 1 binds Bcl-2, an anti-apoptotic protein, inhibiting autophagy (Pattingre et al., 2005). Conversely, under nutrient starvation conditions Bcl-2 is phosphorylated by c-Jun N-terminal Kinase 1 (JNK1) and beclin 1 is activated inducing autophagy (Wei et al., 2008).

One of the principal molecules that recognize cargo for degradation is Sequestosome 1/p62 (SQSTM1/p62). p62 is able to bind ubiquitinated proteins that are aggregated and deliver them into autophagosomes to be degraded through interaction with LC3 (Bjørkøy et al., 2005). Moreover, some authors have suggested that p62 can also act as a selective autophagy receptor for ubiquitinated substrates (Ichimura et al., 2008).

- **Elongation**

The following step is the expansion of phagophore that will form the mature phagophore, called autophagosome. Elongation step involves two ubiquitin-like reactions. In the first reaction, Atg12 is activated by Atg7 (E1-like activating enzyme). Atg7 and Atg10 (E2-like activating enzyme) will allow the link between Atg12 and Atg5 (Mizushima et al., 1998). Then, the complex Atg12-Atg5 will bind to Atg16L forming Atg16L complex. This complex is essential for phagophore elongation being localized in isolated membrane but is not present in mature autophagosome (Mizushima et al., 2003). In the second reaction, one of the proteins involved is microtubule-associated protein 1 light chain 3 (MAP1-LC3, or LC3) that is firstly synthesized as pro-LC3, a precursor of LC3. Pro-LC3 will be cleaved by Atg4B generating LC3-I (Hemelaar et al., 2003). Following that, through Atg7 activity, LC3-I will bind to phosphatidylethanolamine (PE) leading to LC3-II formation, that consequently binds to autophagosome membrane. LC3-II is now able to induce the elongation of phagophore (Mizushima et al., 2002). Contrarily to Atg16L complex, LC3 remains in the membrane even after the fusion with lysosome and its presence is correlated with the number of autophagosomes present in cells (Kabeya et al., 2000).

- **Maturation and fusion**

In the last step of autophagy, usually the autophagosome fuses with lysosome, however some autophagosomes may also fuse with late endosomes forming amphisome, that will ultimately fuse with lysosome (Berg et al., 1998). In both cases, at the end there is the autolysosome formation. For the autophagosome to lysosome fusion to happen, autophagosome needs to be transported across microtubules depending on dynein proteins (Kimura et al., 2008; Ravikumar et al., 2005). The fusion process is mediated by several molecules, including soluble N-ethylmaleimide-sensitive factor attachment protein receptors (SNAREs) (Atlashkin et al., 2003; Furuta et al., 2010), endosomal sorting complexes for transport (ESCRT) (Lee et al., 2007; Rusten et al., 2007) and Rab7 (Gutierrez et al., 2004; Jäger et al., 2004).

Lysosome assumes an important role in degradation of proteins due to the presence of essentials enzymes, but also in fusion step. Yamamoto and his colleagues showed an accumulation of autophagosomes and a decrease in autolysosomes in a rat cell line after inhibition with bafilomycin A1, which blocks proton pump. Thus, these results demonstrated the essential role of lysosome in autophagy, particularly in the fusion with the autophagosome (Yamamoto et al., 1998).

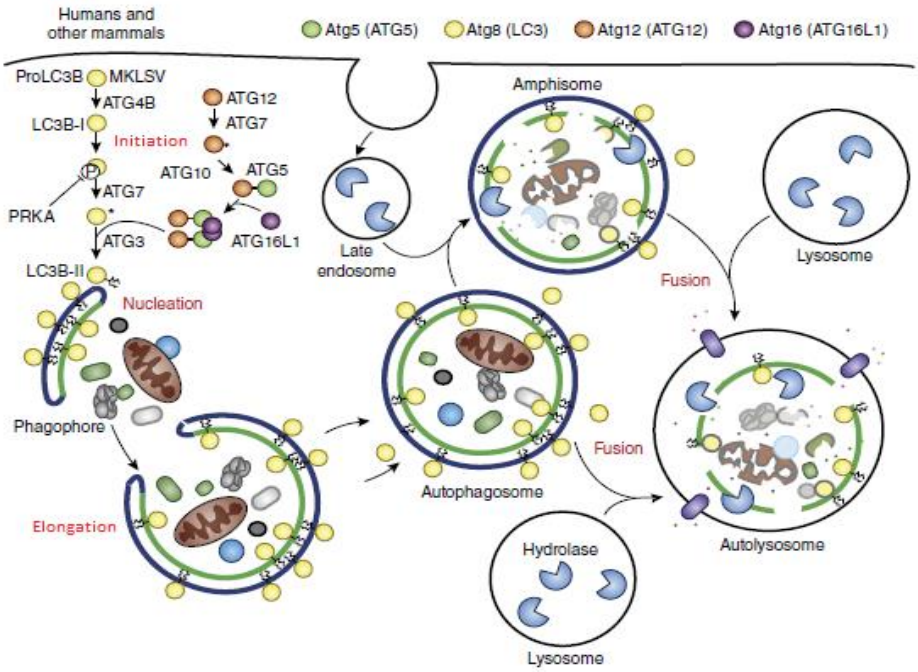

Figure 6 **Macroautophagy machinery.** Macroautophagy is a highly complex mechanism. In the first step, several molecules are important to initiate autophagy such as ULK1 and 2, FIP200, Atg13 among others. Once phagophore is created, it needs to elongate through two ubiquitin-like reactions. One of the reactions involves the complex Atg16L formation, necessary for elongation and the second generates LC3-II that will form the autophagosome. In the final step, autophagosome will fuse with late endosome forming amphisome that will fuse with lysosome or autophagosome will directly fuse to lysosome. Abbreviations: FIP200 - focal adhesion-interacting protein with 200 kDa; Atg – autophagy-related gene protein; LC3 - microtubule-associated protein 1 light chain 3. Adapted from (Lamb et al., 2013)

2.2 Autophagy and PolyQ diseases

Autophagy has been implicated in neurodegeneration. The role of autophagy in neurodegeneration was suggested when both knockout mouse models for Atg5 (Hara et al., 2006) and Atg7 (Komatsu et al., 2006) showed neurodegeneration. Thus, these studies suggested that autophagy may have a neuroprotective effect in the brain.

In polyQ diseases, one of the first evidences of the role of autophagy was reported by Ravikumar in 2002. In this study, the authors used several autophagy inhibitors in Huntington's disease models and

found an accumulation of huntingtin and autophagosomes. Furthermore, it was also found that in the presence of rapamycin, an autophagy activator, there was an increase of protein clearance. Taking this into account, the authors suggest that autophagy displays essential role in aggregates clearance (Ravikumar et al., 2002). Years later, the same group used *in vitro* models of several polyQ proteins and found that in presence of rapamycin autophagy is activated. Moreover, the authors also demonstrated the beneficial role of rapamycin for *in vivo* autophagy activation (Berger et al., 2006).

In HD, since normal huntingtin plays a role in axonal transport its mutation leads to the accumulation of autophagosomes avoiding the normal processing by autophagy. Deletion of polyQ tracts in mutant huntingtin improved autophagy (Zheng et al., 2010). There are some evidences showing that beclin 1, which displays an essential role in autophagy, is recruited into the aggregates of mutant huntingtin, thus inhibiting autophagy (Shibata et al., 2006).

In DPRLA there are also some evidences of an autophagy impairment. In a *Drosophila melanogaster* DRPLA model, it was shown that mutant atrophin caused a deregulation at the level of the lysosome, leading to a dysfunctional autolysosome and consequently to an autophagy impairment (Charroux and Fanto, 2010). Furthermore, it was also found that autophagic vesicles accumulate in glial cells of fly's models of DRPLA, may be due to the severe dysfunctional lysosome. However, in contrast with other polyQ disorders, in which induction of autophagy seems to rescue neuropathology, in fly's models of DRPLA there were no evidences of that (Nisoli et al., 2010). In mammalian models of DRPLA, there is still no report of an autophagy impairment, and so further studies are necessary in these models.

2.2.1 Autophagy and Spinocerebellar ataxias

Particularly, some evidences of autophagy impairment have been reported in spinocerebellar ataxias. In SCA1, ATXN1 is present in nucleus and cytoplasm of neurons. In Purkinje cell nuclei, an accumulation of ATXN1 was reported by Iwata in 2005. In this work, they also described the presence of vacuoles accumulation in Purkinje cells suggesting an impairment of autophagy. Nevertheless, the mutant form of ATXN1 showed to be degraded by the autophagic pathway (Iwata et al., 2005).

In SCA7, the presence of inclusions containing mutant ATXN7 localizing in nucleus has been reported in cultured cells, which was also confirmed in brain from SCA7-patients, thus suggesting deregulations of protein turnover processes, mainly autophagy (Zander et al., 2001). Later, it was described that posttranslational modifications, mainly acetylation of some amino acids of mutant atx7 could be preventing its degradation through the autophagy process. Mutant atx7 was shown to accumulate in

cells while the normal protein that was not acetylated was correctly degraded by autophagy (Mookerjee et al., 2009).

2.2.1.1 Autophagy and MJD

In MJD, the Atx3 protein has been shown to accumulate in nucleus and cytoplasm. The first evidences of the crucial role of autophagy in MJD arose in 2002 and 2006. Expanded ataxin-3, as similar as, other polyglutamine diseases proteins has shown to be degraded by the autophagic pathway (Berger et al., 2006; Ravikumar et al., 2002). In other study, the authors identified new modifiers of atx3 toxicity through genome-wide screen in an MJD *D. melanogaster* model expressing mutant atx3, and they found that most of these modifiers were involved in quality-control mechanisms, such as autophagy (Bilen and Bonini, 2007). Furthermore, they found that reducing *ATG5* autophagy gene in a MJD model of *D. melanogaster* aggravated the MJS phenotype, thus suggesting a neuroprotective role for autophagy in MJD (Bilen and Bonini, 2007). Our group have also provided evidences of autophagy impairment in MJD. An accumulation of both mutant atx3 and autophagic proteins, such as p62, LC3 and Atg16L was reported in brains from MJD patients, thus suggesting an impairment of autophagy (Nascimento-Ferreira et al., 2011). Ubiquitinated mutant atx3 aggregates were also found to co-localize with p62 in the nucleus at early stages of disease and autophagosomes accumulated in the cytoplasm at late stages of disease progression in an MJD lentiviral rat model (Nascimento-Ferreira et al., 2011). Furthermore, beclin 1 was drastically reduced in MJD patient's fibroblasts as well as in an MJD transgenic mouse model (Nascimento-Ferreira et al., 2011). In 2016, our group used fibroblasts from healthy and MJD individuals and investigated whether autophagy is impaired in MJD-fibroblasts. A tendency towards the accumulation of p62 and a reduction of LC3II were observed in MJD fibroblasts, thus corroborating all the results suggesting a defect of the autophagy pathway in MJD (Onofre et al., 2016).

2.2.1.1.1 Autophagy as a therapeutic target in MJD

Given the evidences of an impairment of autophagy in MJD, our group and others have been developing different therapeutic strategies for MJD involving autophagy induction. For example, Menzies and collaborators tried to induce autophagy using an rapamycin ester, an inhibitor of mTORC, named Temsirolimus (Menzies et al., 2010). The group injected this compound in the brain of an MJD transgenic mouse model and found that both mTORC and other proteins from mTOR pathway were repressed. Moreover, Temsirolimus was also able to decrease aggregates number and soluble mutant

atx3 in cytoplasm, while endogenous WT atx3 was not affected. This compound also demonstrated to be able to rescue motor incoordination (Menzies et al., 2010).In other study of our group, beclin 1 was overexpressed in an MJD lentiviral rat model (Nascimento-Ferreira et al., 2011). The results showed a reduction in the number of aggregates and oligomers, as well as a reduction of neuronal dysfunction upon beclin 1 overexpression (Nascimento-Ferreira et al., 2011).Later, we have also assessed whether beclin 1 overexpression would rescue motor and neuropathological impairments when administered to pre and post-symptomatic models of Machado-Joseph disease (Nascimento-Ferreira et al., 2013). The overexpression of beclin 1 resulted in significant improvements of motor coordination, gait and balance, as well as a preservation of neuronal dysfunction and neurodegeneration in both lentiviral-based and transgenic mouse models of MJD (Nascimento-Ferreira et al., 2013). In other study, it was reported that treatment with 17-DMAG, which is an Hsp90 inhibitor being an autophagy activator, was able to rescue motor incoordination of a transgenic mouse model along with a decrease in the number of inclusions (Silva-Fernandes et al., 2014). In the same year, our group have also reported that autophagy activation-mediated by let-7 ameliorated neuropathology in an MJD lentiviral-mouse model (Dubinsky et al., 2014). More recently, we also showed that caloric restriction was able to induce autophagy and rescue motor and neuropathological impairments in a transgenic mouse model (Cunha-Santos et al., 2016).

Based on our study about calpains and other important studies about proteolytic cleavage in MJD, Watchon and his collaborators investigated the effect of calpeptin, other inhibitor of calpains, in an MJD transgenic zebrafish model (Watchon et al., 2017). Here, they found that calpeptin was able to reduce atx3 fragments and improve motor impairment. Interestingly, they also found that this effect of calpeptin was directly related with autophagy, demonstrated by a decrease of beclin-1 and p62 levels and an increase of LC3II levels in calpeptin treated zebrafish. This results suggest that inhibition of calpains resulted in autophagy activation in MJD (Watchon et al., 2017).

Altogether, these studies showed that autophagy plays an important role in neuroprotection of polyQ diseases, particularly in MJD. Autophagy impairments were shown to contribute towards MJD pathogenesis and induction of this mechanism resulted in an amelioration of neuropathology and motor incoordination. Thus, this mechanism is a crucial target for polyQ therapy, especially for MJD.

3. MicroRNAs (miRNAs)

MicroRNAs (miRNAs) are endogenous molecules, highly conserved among species, which have been implicated in several mechanisms, through gene regulation. The existence of these molecules was first reported in 1993. At that time, two different groups found a gene involved in the development of *C. elegans* that did not encode for a protein, but instead encodes for a small RNA molecule, which they named lin-4. This small molecule bound complementary lin-14 mRNA regulating its expression (Lee et al., 1993; Wightman et al., 1993). These evolutionary sequences with single-strand are antisense sequences with approximately 22 nucleotides (Lagos-Quintana et al., 2001; Lee et al., 1993; Wightman et al., 1993).

3.1 miRNA biogenesis

In order to produce functional miRNA to bind mRNA target, the sequence needs to be synthesized by the cell. MiRNA gene may be localized in introns of protein-coding genes or in independent genomic transcription units (Rodriguez et al., 2004). In canonical pathway, the first part of the process occurs in nucleus where miRNA gene is transcribed into a long primary-miRNA (pri-miRNA) by RNA polymerase II (Figure7). Most of these pri-miRNAs are polyadenylated (Lee et al., 2004a). Pri-miRNA is then cleaved by Drosha complex generating a hairpin molecule with 70 to 110 nucleotides, named by premature-miRNA (pre-miRNA) (Landthaler et al., 2004; Lee et al., 2003). This complex is a microprocessor complex that remains in two forms: a smaller complex containing Drosha with cofactor DiGeorge critical region 8 (DGCR8, also known as Pasha) or in a larger complex with RNA helicases, ribonucleoproteins and Ewing's sarcoma proteins' family, in which its function remains poorly understood (Gregory et al., 2004). After that, pre-miRNA is exported to cytoplasm through exportin 5 in a complex with Ran-GTP (Yi et al., 2003) where it will be recognized and cleaved by Dicer (an RNase III enzyme) and Transactivation-response RNA-binding protein (TRBP) generating an imperfect double-strand mature miRNA with 20-24 nucleotides (Lee et al., 2004b). Finally, in the last step, one of miRNA strands will be degraded and the other mature strand will be incorporated into the RNA induced silencing complex (miRISC) through a dynamic process involving Dicer, TRBP, argonaut 2 (Ago2) and Ago-bound GW182 family proteins (Eulalio et al., 2008; Schwarz et al., 2003). Then , this complex binds complementary target mRNA inducing its cleavage or blocking its translation (Gregory et al., 2005) (Figure7).

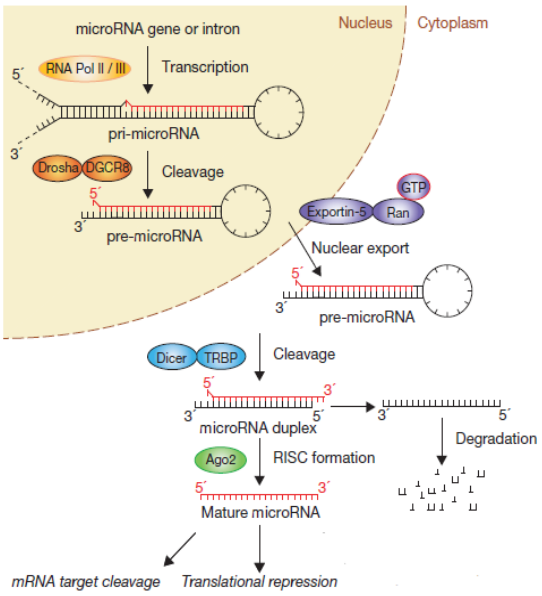

Figure 7 miRNA biogenesis - Canonical pathway. The biogenesis of miRNA begins in nucleus with miRNA gene transcription. There, the transcript of primary miRNA (pri-miRNA) is cleaved by microprocessor Drosha-DGRG8 into premature miRNA (pre-miRNA). Then, pre-miRNA, a microRNA duplex, is exported by exportin 5 complexed with RanGTP. In cytosol, it will be cleaved by complex Dicer-TRBP where one of strand will be degraded and the other will be incorporated into the miRISC complex in a dynamic process involving Dicer, TRBP, argonaut 2 (Ago2) and Ago-bound GW182 family proteins. This complex is now able to induce mRNA target cleavage or to repress its translation. Abbreviations: TRBP – transactivation response binding protein; RISC – RNA induce silencing complex; AGO – argonaute. Adapted from (Winter et al., 2009).

Alternatively, miRNA can be originated from mirtrons, short intronic hairpins generated by intron splicing. Through this non-canonical pathway, mirtron is not cleaved by Drosha being directly export to cytosol via the same mechanism in canonical pathway (exportin 5). In the cytoplasm, the two pathways converge and mirtron will be cleaved by Dicer and consequently will bind the mRNA target (Berezikov et al., 2007; Okamura et al., 2007; Ruby et al., 2007) (Figure 8).

Very recently, our group have demonstrated that impairments in miRNA biogenesis may contribute to MJD pathogenesis. A significant downregulation of genes implicated in miRNA biogenesis (DGCR8, Dicer, and FMR1), as well as of genes involved in miRNA silencing machinery (Ago2, TARBP2, and DDX6) was reported in a transgenic MJD mice model. Additionally, no significant alteration in Drosha levels was detected (Carmona et al., 2017). Therefore, these results suggest that both an impairment in the miRNA biogenesis and miRNA function may account for miRNA dysregulation and consequently contribute for a disarrangement in the control of gene expression at post-transcriptional level, that ultimately contribute for MJD pathogenesis (Carmona et al., 2017).

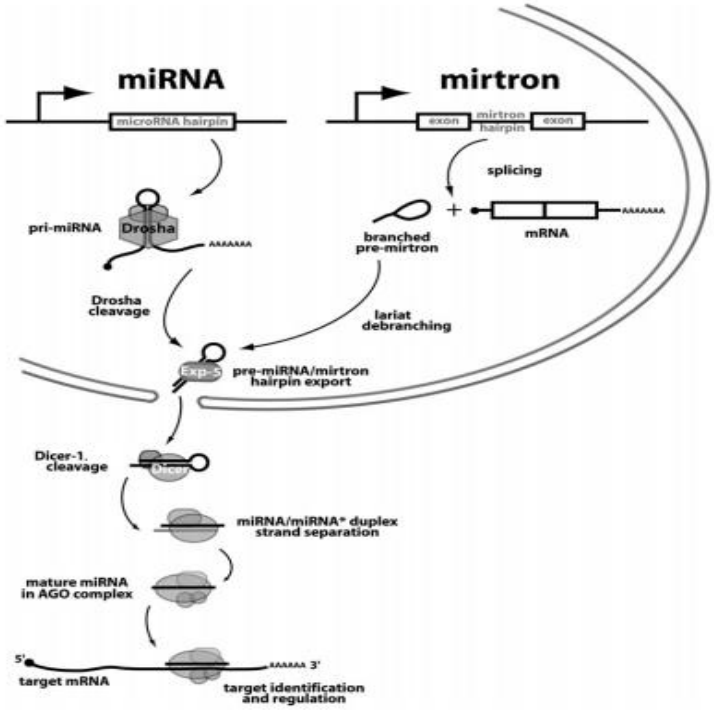

Figure 8 Canonical and mirtron pathways. By contrast with the canonical pathway, mirtron derive from intron splicing and it is not cleaved by drosha. Then, mirtron pathway merge with canonical pathway, in which mirtron is translocated to cytosol by exportin 5-RanGTP. In cytoplasm, it is cleaved by Dicer as pre-miRNA and the mature miRNA strand bind to AGO forming complex to target mRNA. Abbreviations: AGO – argonaute. Adapted from (Okamura et al., 2007)

3.2 MiRNAs and MJD

In the case of MJD, studies have reported a miRNA dysregulation in both human peripheral serum samples (miR-25, miR-125b, miR-29a and miR-34b) and in transgenic mice brain tissue (miR-15b, miR-181a, miR-361 and mir-674) (Rodríguez-Lebrón et al., 2013; Shi et al., 2014).

Our group also provided evidences of the important miRNA role in MJD pathogenesis. Three different miRNAs, such as mir-9, mir-181a and mir-494 targeting 3'UTR region of MJD1 gene, were identified as capable of regulating its gene expression (Carmona et al., 2017). MiRNAs levels of those 3 miRNA candidates were assessed by qPCR in post-mortem tissue from patients and a tendency to be decreased was found in MJD patients (Carmona et al., 2017). In MJD neurons derived from hiPSCs, which have been reprogrammed from MJD patient's fibroblasts, a downregulation of mir-181a and mir-494 was observed, while no difference in mir-9 levels was reported, when compared to control neurons (Carmona et al., 2017). Moreover, all the three miRNAs were significantly downregulated in transgenic mouse model comparing with WT mice (Carmona et al., 2017). This work also showed that overexpression of these miRNAs effectively reduced mutATXN3 levels and ameliorated the associated MJD neuropathology in a Lentiviral MJD mouse model (Carmona et al., 2017).

In conclusion, miRNAs appear to display an essential role in MJD and may be promising targets for the development of novel therapeutic approaches.

3.3 MiRNAs and autophagy

The first evidence of autophagy regulation by miRNAs was demonstrated in 2009 by Zhu and colleagues. They demonstrated that miR-30A bound to beclin 1, the protein involved in nucleation step of macroautophagy, repressing its expression. In the presence of miR-30A, they observed an inhibition of the autophagic pathway. They also observe that miR-30A was downregulated upon autophagy activation under starvation conditions (Zhu et al., 2009).

Since then, more studies have reported the role of miRNAs in autophagy regulation. Huang and collaborators demonstrated that in early steps of autophagy, ULK2 is downregulated by miR885-3p, a miRNA involved in cell viability in response of chemotherapeutics (Huang et al., 2011). As previously shown, beclin 1 can be repressed by Bcl-2 (Pattingre et al., 2005). In addition, it has been reported that Bcl-2 can be downregulated by miR-195, miR-24-2 and miR-365-2 leading to beclin 1 activation and autophagy induction (Singh and Saini, 2012). Considering this, miRNAs against Bcl-2 were proposed to act as pro-autophagic factors (Singh and Saini, 2012). Other miRNAs than miR30A appear to target beclin 1 modulating its activity. It is the case of miR-17-5p (Chatterjee et al., 2014), miR-216a (Menghini et al., 2014), isoform A and B of miR-376 (Korkmaz et al., 2012, 2013) and miR-16 (Chatterjee et al., 2015). MiR-216a was also shown to target ATG5 (Menghini et al., 2014) and miR376a to repress ATG4 (Korkmaz et al., 2013). In other studies, it was shown that miR-30d (Yang et al., 2013), miR-143 and miR-130a regulated ATG2 (Kovaleva et al., 2012), while miR-101 repressed Rab5A, which is involved in regulation of beclin1-PIK3 (Frankel et al., 2011), thus demonstrating that all of them modulate autophagosome biogenesis. MiR30d was also shown to supress beclin 1 and ATG15 (Yang et al., 2013).

In a subsequent step of autophagy mechanism, it was demonstrated that miR-375 targets Atg7, an enzyme that mediates LC3 and PE conjugation involved in the expansion of autophagosome, thus inhibiting autophagy in hepatocellular carcinoma (Chang et al., 2012). LC3-II was also shown to be directly regulated by miR-204 which leads to downregulation of clearance mechanism found in cardiomyocytes (Xiao et al., 2011). Regarding the last stage of autophagy, which corresponds to the fusion between autophagosome and lysosome, despite being the less understood some putative regulatory miRNAs have been pointed out. In 2011, a computational analysis revealed that miR-130/301/454 cluster putatively regulates several key genes of the mTOR pathway involved in autophagy-lysosomal functions, including signalling genes such as IGF1, MAPK1, ULK1, ULK2, among others, as well as autophagy mediators, such as WDFY3, ATG2B and ATG16L1 (Jegga et al., 2011).

Taking all this data into account, miRNAs seem to be good therapeutic strategies for disorders linked to autophagy deregulation.

3.4 Let-7

Let-7 was one of the first discovered miRNAs. It was originally described in *C. elegans* as being involved in the process of transition from larvae to adult stage (Reinhart et al., 2000). Lack of let-7 expression led to an abnormal switch to adult stage, while its overexpression contributed to precocious development into adult stage. In this study, it was also found that lin-28 was negatively regulated by let-7 (Reinhart et al., 2000). In *D. melanogaster,* it was found that let-7 is involved in regulation of neuromuscular junction (NMJ), since absence of let-7 led to immature NMJ (Sokol et al., 2008). More recently, let-7 was implicated in suppression of NF-kB canonical and non-canonical pathways in atherosclerosis (Wang et al., 2017). The authors showed that let-7 was able to target molecules involved in both NF-kB pathways in macrophages, thus resulting in a reduction of lipids accumulation, as wells as in a decrease of inflammatory molecules secretion. Therefore, let-7 mediated repression of NF-kB biogenesis was suggested as a potential therapy for atherosclerosis (Wang et al., 2017).

Let-7 is generated by the canonical pathway of miRNA biogenesis. However, it can also be regulated by lin28, which modulates its expression in tissues at a posttranscriptional level. After transcription, lin28 binds to conserved loop of let-7 recruiting terminal uridylyl transferase 4 or 7 (TUT4/ZCCHC11 - zinc finger, CCHC domain containing 11 or TUT7/ ZCCHC6 – zinc finger, CCHC domain containing 6) (Hagan et al., 2009) (Figure 9). TUT4/7 will poly-uridylate (polyU) the precursor of let-7 (pre-let-7), avoiding its cleavage by dicer and labelling it for degradation. Contrarily, repression of TUT4/7 and downregulation of lin28 led to an accumulation of let-7 and suppression of let-7 targets (Hagan et al., 2009). Years later, Chang et al. found that Dis3L2, a exonuclease involved in Perlman syndrome, was the responsible for let-7 degradation (Chang et al., 2013) (Figure 9). In other study, Heo and coworkers discovered that in absence of lin28, TUT4/7 was able to mono-uridylate (monoU) let-7 inducing cleavage by dicer (Heo et al., 2012). More recently, two domains in TUT4/7 were identified as being responsible for the switch between monoU and polyU. In this study, the authors found that catalytic module is responsible for mono-uridylation and poly-uridylation, while lin28-interacting module is recruited for oligo-uridylation (Faehnle et al., 2017).

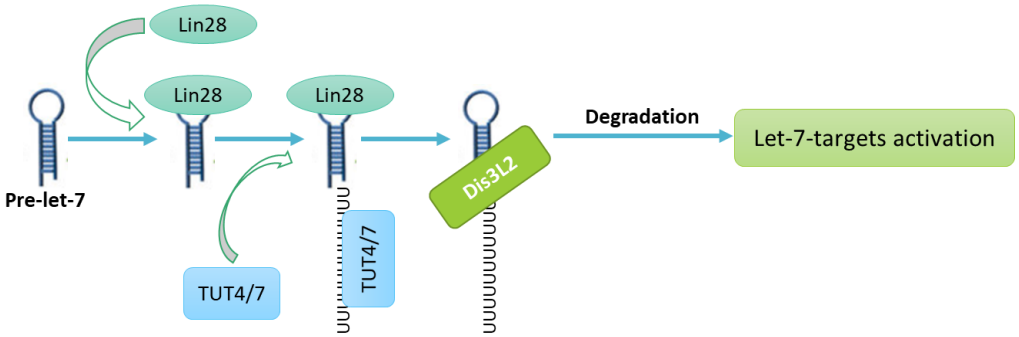

Figure 9 Lin28/let-7 pathway. Contrarily to normal biogenesis, here, let-7 once targeted by lin28 is not cleaved by Dicer. Lin28 binds conserved loop of let-7 percursor recruiting TUT4/7 that will poly-uridylate this miRNA. In this way, let-7 will be degraded by Dis3L2, thus activating let-7-targets. Abbreviations: TUT4/7 – terminal uridylyl transferase 4/7. Based on (Balzeau et al., 2017)

3.4.1 Let-7 and autophagy

Let-7 has also been indicated as a potential regulator of the autophagy mechanism. In 2011, Jegga and his colleagues described some miRNAs that might be involved in autophagy (Jegga et al., 2011). Using bioinformatics tools, they found that miR-98, a let-7 variant, may recognize several genes involved in autophagosome-lysosome fusion, such as, LAMP2 and Atg16L, however this evidence was not proved *in vitro* or *in vivo* studies (Jegga et al., 2011).

In 2014, our group in a collaboration with La Spada evaluated the role of let-7 in the autophagy mechanism (Dubinsky et al., 2014). In this study, primary cortical neurons from a GFP-LC3 transgenic mice were cultured in a nutrient-limited media for autophagy induction and deregulated miRNAs were identified. From the miRNA array analysis, it was possible to identify 19 miRNAs that were overexpressed. From these miRNAs, five of them belonged to let-7 family and so the next studies were focused on let-7 (Dubinsky et al., 2014). The results showed that in fact let-7 induces autophagy in primary cortical neurons and then they went to clarify the mechanism underlying autophagy activation mediated by let-7. mTOR protein levels were found to be significantly reduced in primary cortical neurons upon treatment with a let-7 mimic, thus indicating that let-7 regulates autophagy in an mTOR-dependent manner (Dubinsky et al., 2014). Different bioinformatics tools, such as Ago HITS-CLIP analysis, TargetScan 6.0 and scanning directly for let-7 seeds sites were used to predict possible let-7 targets involved in the repression of mTOR. Several genes were identified as putative targets of let-7, including LAMTORs (1-5), RagA/B/C/D, Map4k3, Slc1a5, Slc7a5 and Slc3a2. These genes are involved in amino acids sensing pathway, in which mTOR displays a central role (Figure 10). These results were further confirmed by qRT-PCR, in which all these genes appeared to be downregulated in the presence of let-7 (Dubinsky et al., 2014).

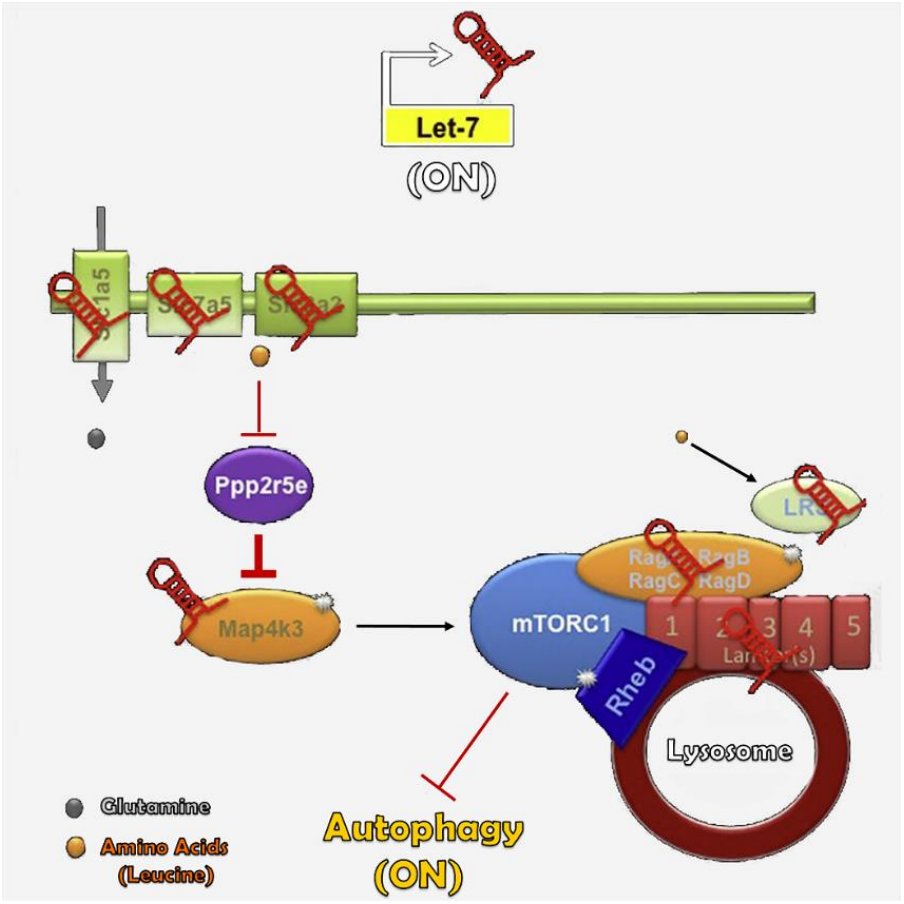

Figure 10 Illustration of the proposed mechanism for autophagy activation mediated by Let-7. Let-7 seems to target several genes from the amino acid sensing pathway. The hypothesis is that let-7 is able to silence many targets in this pathway, such as Slc1a5, Slc7a5, Slc3a2, Lamtors (1-5), Rag A/B/C/D and Map4k3, thus leading to mTORC1 repression and ultimately to autophagy activation.

As previously reported, also by our group, autophagy is impaired in MJD (Berger et al., 2006; Bilen and Bonini, 2007; Nascimento-Ferreira et al., 2011; Ravikumar et al., 2002). In addition, we have shown that let-7 is able to activate autophagy in neurons (Dubinsky et al., 2014). Taking all this into account we went to assess whether let-7 could activate autophagy in vivo and simultaneously ameliorate MJD phenotype (Dubinsky et al., 2014). Our results showed that Let-7 was able to reduce aggregates number in the context of increased levels of LC3-II in a lentiviral mouse model of MJD. Therefore, we were able to show that let-7 is capable of inducing autophagy *in vivo* and has a promising potential as a therapeutic strategy for MJD (Dubinsky et al., 2014).

3.4.2 Let-7 target genes

Mitogen-activated protein kinase kinase kinase kinase 3 (Map4k3) also known as Germinal center kinase-like kinase (GLK) belongs to a large family of kinases, Ste20 kinase family, which is involved in several cellular mechanisms and is broadly expressed in mammalians (Diener et al., 1997). In 2007,

Findlay and his group link for the first time the activity of MAP4K3 with the activation of mTORC1 via amino acid sensing pathway (Findlay et al., 2007). In this study, they found that knocking down *CG7097* in *D. melanogaster*, which corresponds to MAP4K3 in mammalians, resulted in a decrease of S6K1 phosphorylation, an important effector of mTORC1. In addition, they got into the same conclusions after testingMAP4K3 knockdown in human cells. By the opposite, an overexpression of MAP4K3 resulted in an activation of mTORC1 and in the presence of amino acids, the S6K1 was not phosphorylated due to the knockdown of MAP4K3, thus suggesting MAP4K3 is activated under non-nutrient starvation conditions (Findlay et al., 2007). Very recently, Hsu and his group tried to understand how MAP4K3 could regulate mTORC1 and consequently autophagy (Hsu et al., 2018). In this study, MAP4K3 was repressed in human cells and the results showed that autophagy was more activated compared to the control. Furthermore, MAP4K3 was also shown to regulate the cellular localization of Transcription Factor EB (TFEB), which is a positive regulator of autophagy. Once in the nucleus TFEB activates autophagy, however when located into the cytosol inhibits autophagy. Therefore, they found that in the absence of MAP4K3, TFEB remains in nucleus, whereas it is translocated to the cytosol upon overexpression of MAP4K3 (Hsu et al., 2018). In this study, TFEB was also shown to interact with mTORC1 following phosphorylation at TFEB serine 3 mediated by MAP4K3. Together these facts indicate that MAP4K3 phosphorylates TFEB, facilitating the interaction between TFEB and mTORC1 and subsequent phosphorylation of TFEB. TFEB remains sequestered in the cytoplasm, thus resulting in autophagy inhibition (Hsu et al., 2018).

Ras-related GTP-binding protein (Rag GTP-ases) is a large protein complex, which includes RagA, RagB, RagC and RagD. In the context of autophagy, Kim et al. demonstrated the direct relationship between Rag GTP-ases and mTORC1 (Kim et al., 2008). In this study, they found that Rags were able to phosphorylate S6K1, whereas their downregulation led to a reduction in S6K1 phosphorylation, thus demonstrating a direct regulation of mTORC1. Furthermore, constitutively active Rags were shown to activate mTORC1 even in the lack of amino acids conditions, thus demonstrating that sensibility of mTORC1 to amino acids conditions is mediated by other proteins than itself (Kim et al., 2008). At the same time, Sancak and his colleagues reported that Rags coimmunoprecipitated with raptor, one of the principal components of mTORC1, suggesting a role of Rag GTP-ases in mTORC1 regulation (Sancak et al., 2008). In addition, they also found that in presence of amino acids, mTORC1 changes its localization from cytoplasm to perinuclear region and to large vesicular structures where it would be activated and it will mediate cell growth (Sancak et al., 2008).

Lamtors are a gene family, which have been associated to the complex named “Ragulator”. This family is composed by five genes: Lamtor1, Lamtor2, Lamtor3, Lamtor4 and Lamtor5 which encodes for p18, p14, MP1, LAMTOR4 (C7orf59) and LAMTOR5 (HBXIP), respectively. In 2010, Sancak and his group

found that p18, p14 and MP1 interact with Rag GTP-ase proteins confirmed by coimmunoprecipitation of these proteins (Sancak et al., 2010). Besides that, the absence of p18 and p14 led to a decrease in mTORC1 activation through amino acids sensing pathway, thus resulting in autophagy activation. Ragulator has also shown to be essential for mTORC1 translocation to the lysosomal membrane where Rags GTP-ases remain (Sancak et al., 2010). In 2012, the same group have also demonstrated that LAMTOR4 and LAMTOR5 were present in precipitates containing p14, p18 or RagB (Bar-Peled et al., 2012). Moreover, they found a stronger interaction with Rags GTP-ases when in the presence of LAMTOR4 and LAMTOR5 than in their absence, thus confirming that Ragulator complex is constituted by five proteins instead of three, which were firstly described. Moreover, the authors found that Ragulator is sensitive to presence of amino acids because act as guanine nucleotide exchange factor. This property makes Ragulator a mediator of Rags binding to nucleotides and consequently confers to this complex the ability to be sensitive to the presence of amino acids regulating mTORC1 (Bar-Peled et al., 2012).

SLC7A5, also known as LAT1 is a bidirectional transporter that forms a heterodimer with SLC3A2 and both are responsible to the exchange of L-glutamine to the L-leucine. In the context of mTORC1 regulation, Nicklin and his collaborators found that cellular medium containing L-glutamine was mandatory for the activation of mTORC1 (Nicklin et al., 2009). Taking this into consideration, they wondered whether SLC7A5/SLC3A2 could regulate the activation of mTORC1 through the L-glutamine/L-leucine efflux. The knockdown of SLC7A5/SLC3A2 led to a decrease of mTORC1 activity and activation of autophagy, by decreasing L-glutamine uptake (Nicklin et al., 2009). After this, Milkereit and his group showed that LAPTM4b, which is a lysosomal protein, is essential for the recruitment of SLC7A5 transporter in SLC7A5-mediating L-leucine efflux (Milkereit et al., 2015).

All these genes, being let-7 targets, demonstrate to be important for mTORC1 and autophagy regulation.

Main goals

Autophagy is one of the compromised mechanisms in MJD contributing to neurodegeneration. Taking this into account, some therapeutic approaches had consisted of inducing autophagy to enhance degradation of the disease protein. In fact, previous works of our group demonstrated that activation of autophagy ameliorate the motor deficits observed in MJD (Cunha-Santos et al., 2016; Nascimento-Ferreira et al., 2013). Additionally, in our lentiviral mouse model it was observed that let-7 was able to activate autophagy and decrease the number of ubiquitin-positive inclusions after 4 weeks of treatment (Dubinsky et al., 2014).

Concerning this, the main goal of this work is to study the effect of autophagy activation mediated by Let-7 microRNA in a transgenic (Tg) mouse model of MJD, firstly described by Torashima et al. (Torashima et al., 2008). For that, we aimed at:

- Evaluating the effect of let-7 on motor coordination and balance, which were shown to be compromised in this Tg MJD mouse model;
- Investigating whether let-7 is capable of ameliorating neuropathological effects observed in these Tg MJD mice;
- Characterizing the autophagy impairment in this Tg MJD mouse model;
- Evaluating whether let-7 could activate autophagy in this Tg mouse model;
- Assessing the expression levels of let-7 targets in Tg MJD mice, before and after let-7 treatment, in an attempt to identify the important players in an MJD context.

Chapter II – Materials and Methods

1.1 Material

Table 3: Immunohistochemistry and western blotting primary and secondary antibodies

Immunohistochemistry			
Primary antibody	**Host**	**Dilution**	**Reference/supplier**
Monoclonal anti-haemagglutinin (HA)	Mouse	1:1000	#901501 (BioLegend, CA, USA)
Polyclonal anti-glial fibrillary acidic protein (GFAP)	Mouse	1:1000	#3670 (Cell Signaling Techonology)
Anti-ionized calcium binding adaptor molecule 1 (Iba-1)	Rabbit	1:1000	019-19741 (Wako)
Polyclonal anti-calbindin D-28k antibody	Rabbit	1:500	AB1778 (Merck Millipore, Darmstadt, Germany)
Secondary antibody	**Host**	**Dilution**	**Reference/supplier**
Anti-mouse Alexa Fluor 488	Goat	1:200	A-11029 (Invitrogen)
Anti-rabbit Alexa Fluor 488	Goat	1:200	A-11034 (Invitrogen)
Anti-rabbit Alexa Fluor 647	Goat	1:200	A-21245 (Invitrogen)
Western Blotting			
Primary antibody	**Host**	**Dilution**	**Reference/supplier**
Polyclonal anti-p62	Rabbit	1:1000	#5114 (Cell Signaling Technology)
polyclonal anti-LC3B	Rabbit	1:1000	#2775 (Cell Signaling Technology)
Monoclonal anti-haemagglutinin (HA)	Mouse	1:1000	#901501 (BioLegend, CA, USA)
Polyclonal anti-RagC	Rabbit	1:1000	#3360 (Cell Signaling Technology)
Monoclonal anti- β-actin	Mouse	1:2000 or 1:5000	AC74 A2228 (Sigma Aldrich, St. Louis, MO, USA)
Secondary antibody	**Host**	**Dilution**	**Reference/supplier**
Anti-rabbit alkaline phosphatase conjugated	Goat	1:10 000	#31340 (Thermo Scientific, Rockford, IL, USA)
Anti-mouse alkaline phosphatase conjugated	Goat	1:10 000	WP20006 (Invitrogen)

1.2 Methods

1.2.1 Lentiviral vectors production

Lentiviral vectors (LV) encoding for let-7 microRNA precursor (let-7f-2) and miR-scramble (miR-scr) were produced in human embryonic kidney 293 T cells using a four-plasmid system described previously (de Almeida et al., 2002; De Almeida et al., 2001). The lentiviral particles were produced and resuspended in 0.1 M phosphate-buffered saline (PBS) with 0.5 % bovine serum albumin, and samples were matched for particle concentration by measuring HIV-1 p24 antigen content (RETROtek, Gentaur, Belgium). Concentrated viral stocks were stored at -80 ºC until use.

1.2.2 Stereotaxic surgery procedure

The in vivo experiments were carried out in accordance with the European Community Council Directive (86/609/EEC) for the care and use of laboratory animals. The researchers received adequate training (Felasa-certified course) and certification to perform the experiments from the Portuguese authorities (Direcção Geral de Veterinária). The animals were housed in a temperature-controlled room and maintained on a 12-h light/dark cycle. Food and water were available ad libitum. Six-week-old transgenic Machado-Joseph disease mice (Torashima et al., 2008) were anaesthetized by intraperitoneal administration of ketamine (100 mg/Kg) /xylasine (10 mg/Kg) in a final proportion 2:1. These animals were stereotaxically injected with LV encoding for let-7 or mir-scr directly into the cerebellum and were kept for 12 weeks post-injection before being sacrificed for subsequent analyses, with behavior tests being performed every 3 weeks. Briefly, concentrated viral stocks were thawed on ice, resuspended by vortexing and the LV injection was performed by means of an automatic injector (Stoelting Co., Wood Dale, IL, USA) at the following coordinates: antero-posterior: - 2.3 mm; lateral: 0 mm; ventral: - 3 mm, relative to lambda. All mice received a single 5µl injection of LV (250,000 ng of p24/ml) at a rate of 0.25 µl/min into the cerebellum. After injection, the syringe needle was left in place for an additional 3 min to allow for the diffusion of vectors and minimize backflow.

1.2.3 Behavioural tests

Six-week-old mice were submitted to a battery of motor tests starting 2 days before the stereotaxic injection (t=0) and every 3 weeks until 12 weeks post-injection. All tests were performed in a dark room with, at least, 60 min of acclimatization to the experimental room and at the same period of the day (during the morning until early afternoon). Details of each test can be found as follows:

- **Beam walking test**

In beam walking test, motor coordination and balance were assessed by measuring the time mice took to cross a graded series of narrow beams towards an enclosed escape platform. This test was performed in two different square beams (1 m) with 18 mm and 9mm square wide, always sequentially from the widest to the narrowest beam. The beams were placed horizontally 25cm above the surface, with an end attached on a narrow support and the opposite end fixed to a bounded box (20 cm square) for mouse escaping. The latency time of each animal to cross each beam was recorded in two trials and the results correspond to the average.

- **Accelerated rotarod**

Motor coordination and balance were assessed using rotarod apparatus (Letica Scientific Instruments, Panlab, Spain) at an accelerated speed from 4rpm to 40 rpm, over a period of 5 min, as we previously described (Nóbrega et al., 2013). The latency time to fall off the rotarod apparatus was recorded for each animal in four different trials per time point with a minimum of 15 minutes intertrial interval and the results correspond to the average of the three first trials.

- **Swimming test**

For this test a rectangular aquarium was used (length: 150 cm; height: 20 cm; width: 11.5 cm), incorporating a platform at 10cm to the floor at the opposite site of the starting test point. The aquarium was filled up with water at 24-26ºC to the platform level. Mice were placed at one end of the aquarium and the time spent to swim until the platform plus the time needed to climb the platform was recorded. Each animal performed three trials with a minimum of 15 minutes intertrial interval and the results correspond to the average of two trials.

1.2.4 Tissue preparation for histological processing

18 weeks old treated transgenic mice were sacrificed by ketamine/xylazine (2:1) overdose intraperitoneal injection. Mice were transcardially perfused in 0.1M PBS followed by 4% paraformaldehyde solution (4% PFA). Mice brains were removed and post-fixated in 4% PFA for 24h. After cryoprotection by incubation in 30% sucrose-PBS solution for 48 h, mice brains were stored at -80°C. Sagittal slices with 30µm were cut in cryostat (Thermo Scientific CryoStar NX50) and stored at 4°C in 48-multi-well plate containing PBS supplemented with 0.12 mmol/l sodium azide.

1.2.5 Cresyl-violet staining

Free-floating sagittal sections were mounted in gelatin-coated slides. The sections were dehydrated by passing through water, 75% ethanol, 96% ethanol, 100% ethanol and xylene solutions followed by the process of hydration where sections stained 5 min in cresyl violet solution. Then the sections were dehydrated one more time and mounted in Richard-Allan Scientific™ Mounting Medium (Thermo Scientific).

Images of staining were acquired in Carl Zeiss Axio Imager Z2 equipped with AxiocamHRc and Plan-apochromat 20x/0.8.

1.2.6 Free- floating immunohistochemistry

Free-floating sagittal slices were permeabilized and blocked in PBS/ 0.1% Triton X-100 (Sigma) enriched with 10% of normal goat serum (NGS) solution (Alphagene Invitrogene) for 1h to 1.5h. Sections were then incubated at 4°C overnight in blocking solution with the primary antibodies. Depending on the antibody, free-floating sections in primary antibody stayed for an extra 1h to 2h at room temperature before the incubation for 2h in corresponding secondary antibody diluted in blocking solution (Table 3). Sections were washed three times and incubated 5 min in nuclear marker 4',6'-diamidino-2-phenylindole (DAPI; 1:500). The sections were washed three times and mounted in DAKO fluorescence mounting medium on gelatin-coated microscope slides.

Images of staining were acquired in Carl Zeiss Axio Imager Z2 equipped with AxiocamHRm and Plan-apochromat 20x/0.8, or in Cell Observer Spinning Disk equipped with Plan-apochromat 20x/0.8 M27 using Zen 2 (blue edition) software.

1.2.7 Quantification of granular and molecular layers thickness and cerebellar volumes

Quantification of granular and molecular layers thickness and lobular and cerebellar volumes were measured in 8 slices of each animal in a blind fashion (selected sagittal slices corresponding to 0.12mm, 0.36mm, 0.60mm, 0.84mm, -0.12mm, -0.36mm, -0.60mm, -0.84mm lateral plans to the midline. These plans coincide with following diagrams: Figure 102, 104, 106, 108, respectively for both hemispheres in (Paxinos and Franklin, 2001)). Thickness of granular and molecular layers were manually assessed by drawing a line vertical to the bottom of each interlobule, excluding Purkinje cell bodies. The joint measure of granular and molecular layers thickness took into account the beginning of molecular layer until the end of the granular layer vertical to the bottom interlobule including Purkinje cell bodies. The

showed results are the average of the thickness of each layer or the joint measure of layers in interlobule. Cerebellar volume was calculated according to the following formula: 8d(a1+a2+a3+…+a8) where d represents the distance between each section (240µm) and a1-8 represents the cerebellar area in each image. The quantification was performed in Zen 2 (blue edition) software.

1.2.8 Quantitative analysis of haemagglutinin-tagged (HA) aggregates:

Quantitative analysis of HA inclusions was performed in 8 specific sections per animal in blind fashion (selected sagittal slices corresponding to 0.12mm, 0.36mm, 0.60mm, 0.84mm, -0.12mm, -0.36mm, -0.60mm, -0.84mm lateral plans to the midline. These plans coincide with following diagrams: Figure 102, 104, 106, 108, respectively for both hemispheres in (Paxinos and Franklin, 2001)). The sections were scanned using 20x objective on Cell Observer Spinning Disk (Carl Zeiss). Number of HA inclusions were manually counted per lobule in Purkinje cells bodies region across of the 8 sections in maximum intensity orthogonal projection images and the total number of aggregates were calculated according to the following formula: 8(n1+n2+n3+…+n8) where n1-8 represents the number of aggregates in each section and 8 is the number of intermediate sections between each analysed section. Only aggregates with area between 1.51 μm^2 and 37.9 μm^2, a diameter between 1.4µm and 6.4 µm and a mean intensity value between 6258 and 33947 arbitrary units (a.u.) were considerate for the quantification.

1.2.9 Quantitative analysis of GFAP, IBA1 and calbindin Immunoreactivity:

In order to quantify GFAP, IBA1 and calbindin immunoreactivity, 8 stained sections per animal (selected sagittal slices corresponding to 0.12mm, 0.36mm, 0.60mm, 0.84mm, -0.12mm, -0.36mm, -0.60mm, -0.84mm lateral plans to the midline. These plans coincide with following diagrams: Figure 102, 104, 106, 108, respectively for both hemispheres in (Paxinos and Franklin, 2001) were scanned using 20x objective in Axio Imager Z2 (Carl Zeiss) acquiring images of maximum intensity focal plan. Quantification of the mean immunoreactivity intensity was performed blindly in Zen 2 (blue edition) system drawing the perimeter of each lobules or whole cerebellum. Final results correspond to the average intensity of the 8 analysed sections per animal.

1.2.10 Protein extraction procedure

Eight sagittal slices per animal were used to extract protein from control and treated mice. Slices were washed in PBS for 15min and then the cerebellum was dissected from each section. Cerebellum tissue lysates were obtained by incubation in a solution containing Tris-base 20mM, pH 9 (Trizma, Sigma-Aldrich) supplemented with 2% Sodium Dodecyl Sulfate (SDS, Fisher Bioreagents) for 5min on ice followed by an incubation for 20min at 100°C plus 2h at 80°C. The samples were then centrifuged for 20min at 13 200 rpm and 4°C. The samples were homogenized using the sonicator by two series of 5 sec pulse (1 pulse/sec). The protein concentration was quantified according to the BioRad Protein Assay (BioRad) and stored at -20°C.

1.2.11 Western Blot procedure

The samples were first denatured in loading buffer (Tris-HCL 0.5M/0.4%, Glycerol 30%, SDS 10%/pH 6.8, DTT 0.6M, bromophenol blue 0.01%) for 5min at 95°C and 30µg or 40µg of protein were resolved in Mini-Protean TGX Precast gels (BioRad), a 4%-15% gradient acrilamide gel and transferred to a polyvinylidene fluoride (PVDF) membranes (Merck Millipore). Membranes were blocked for 1h in 5% non-fat milk diluted in Tris-buffered saline (TBS) containing 0.1% Tween 20 (Sigma Aldrich) and incubated 1 or 2 overnights at 4°C in primary antibody followed by 2h incubation at room temperature (Table 3). Images were acquired using enhanced chemifluorescence substrate (ECF, GE Healthcare Life Sciences) in chemifluorescence imaging system (VersaDoc Imaging System model 3000, BioRad). The band quantification was performed using FIJI software and normalized to the amount of β-actin.

1.2.12 Statistical analysis

Statistical analysis was performed using GraphPad Prism6 software. Two-way analyses of variance (ANOVA) tests followed by the Bonferroni post hoc test were performed to assess statistical significance in Beam walking test. In the other graphs, unpaired t-test followed by Welch's correction was used when both groups assume Gaussian distribution while unpaired Mann-Whitney test was used when at least one comparison group do not assume Gaussian distribution. $P<0.05$ was considered statistically significant. Data are presented as the mean±standard error of the mean (SEM).

Chapter III - Results

In this work, a cohort of twelve Tg MJD mice were divided into two different groups. The control group was composed by 7 animals that were injected into the cerebellum with a control sequence, mir-scr combined with fluorescent protein mCherry as a reporter (Figure 11A, C). The treated group was composed by 5 animals that were injected with let-7 combined with fluorescent protein mCherry as a reporter (Figure 11 B,D). Both groups were subject to a set of behavioural tests, including accelerated rotarod, beam walking and swimming, performed before and every 3 weeks post-injection, for 12 weeks (Figure 11 E). After that, animals were sacrificed, and the neuropathology was evaluated as shown in the results bellow. The differences in fluorescence between non-injected and injected mice is possible to see in Figure 11 F-H.

1.1 Let-7 treatment improves motor coordination and balance

Motor incoordination and imbalance affect most of the MJD patients, thus constituting the principal hallmark of MJD disease. In this study, a Tg mouse model of MJD was used, which was firstly described by Torashima et al. as exhibiting a remarkable cerebellar atrophy and a severe impairment of motor coordination and balance early from the 3rd week of age. Two groups of animals, one treated with let-7 and the other treated with miR-scr were subjected to a set of behavioural tests, including beam walking, accelerating rotarod and swimming before and every 3 weeks post-injection, for 12 weeks (Figure 12 A-F).

In beam walking test, animals had to cross two square beams with 18mm and 9mm of square wide, until they reached the escape platform. Balance and motor coordination were evaluated in this test. At 9 weeks post injection, let-7-treated mice showed a significantly better performance to cross the 9mm square beam, thus taking less time to cross this beam, when compared to control group (Tg-mir-scr: 16.424 ± 0.980s vs Tg-let-7: 12.918 ± 0.563s, p=0.0069). In addition, a tendency for a better performance in the 18mm square beam was also observed upon let-7 treatment at this time point (Tg-mir-scr: 13.01 ± 0.618s vs Tg-let-7: 10.954 ± 0.363s, p=0.1326) (Figure 12 A). At 12 weeks post-injection, let-7 treated mice also showed a tendency to be faster crossing both beams than control mice , although not reaching statistical significance (18mm: Tg-mir-scr: 13.272 ± 0.808s vs Tg-let-7: 10.693 ± 0.730s, p=0.3229; 9mm: Tg-mir-scr: 15.474 ± 1.642s vs Tg-let-7: 12.990 ± 1.269s, p=0.3533) (Figure 12 B).

To further evaluate motor coordination and balance we have also performed accelerating rotarod test. In this test, mice were placed in rotarod apparatus and subjected to an accelerated speed from 4 r.p.m.

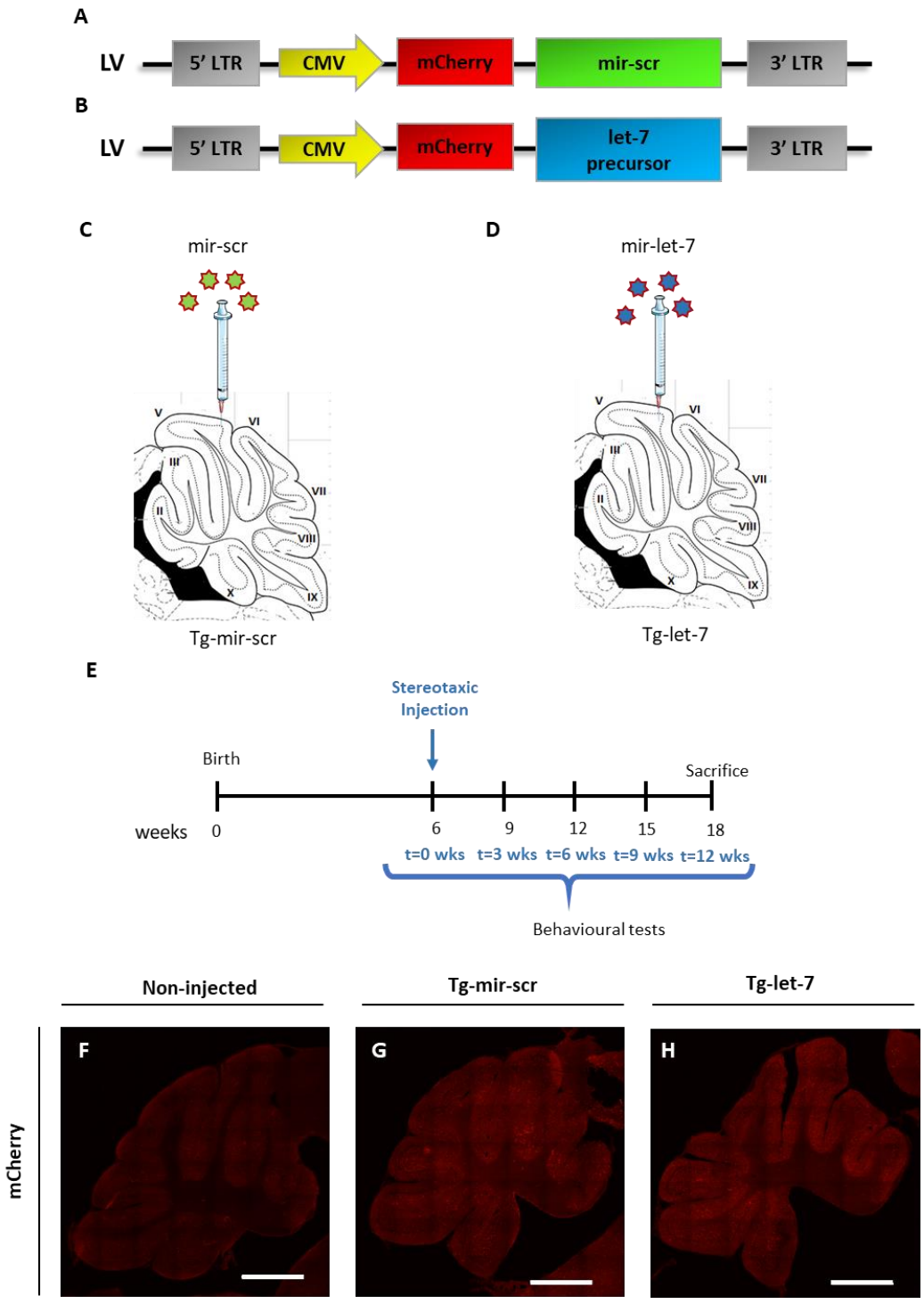

Figure 11 Scheme of cerebellar injection and study timeline. (A,B) Schematic representation of lentiviral (LV) constructs used to evaluate the effect of let-7 in MJD. (A) Control construct was composed by mir-scr clone downstream of mCherry, the gene reporter under control of CMV in a lentiviral backbone. (B) Let-7 construct includes mir-let-7 precursor clone downstream of mCherry, the gene reporter under control of CMV in a lentiviral backbone. (C-D) Representative image of cerebellum mice sagittal slice demonstrating the cerebellar injection at lobule V. The control group was injected with LV coding for mir-scr (C) and the treated group was injected with LV coding for let-7 (D). (E) Scheme of the study timeline. Mice were stereotaxically injected into the cerebellum at 6 wks post-birth and the behavioural tests were performed before and every 3 wks post-injection, for 12 wks. After that, mice were sacrificed, and neuropathology was evaluated (F-H). Transgene expression in non-injected age-matching mice (F), mice treated with mir-scr (G) and mice treated with let-7 at 12 weeks post-injection. Scale bar, 500µm. LTR-Long terminal repetition; CMV – cytomegalovirus; mir-scr – scramble microRNA; wks – weeks.

to 40 r.p.m. for a maximum of 5min. At 9 weeks post-injection, we observed that Tg-let-7 mice had a significantly higher ability to stay in the apparatus than control mice (Tg-mir-scr: 14.86 ± 3.309s vs Tg-let-7: 23.80 ± 4.325s, p=0.0440) (Figure 12 C). At the last behaviour test time-point, Tg-let-7 mice also showed to be more robust to perform this test than the control group, however a statistically significant difference was not observed (Tg-mir-scr: 16.90 ± 5.163s vs Tg-let-7: 24.27 ± 3.849s, p=0.2798) (Figure 12 D).

In the swimming test, which aims to assess coordination of limbs used during voluntary locomotion, we observed that at 9 weeks post injection let-7 treated mice had more ability to cross the pool and climb to the platform, being faster than the control mice to complete the mission (Tg-mir-scr: 9.090 ± 1.198s vs Tg-let-7: 6.151 ± 0.4611s, p=0.0527) (Figure 12 E). In the last time point, at 12 weeks post-injection, Tg-let-7 mice showed a tendency to be more agile to swim and jump to the platform than the Tg-mir-scr mice (Tg-mir-scr: 7.374 ± 0.7482s vs Tg-let-7: 6.416 ± 0.3826s, p=0.2847) (Figure 12E).

Altogether, these results show that let-7 is able to improve motor coordination and balance in a Tg MJD mouse model presenting exacerbated motor deficits at 6 weeks of age, thus ameliorating MJD phenotype.

1.2 Mice treated with let-7 present an increase of cerebellar layers

As mentioned above the Tg MJD mouse model used in this work exhibits a severe cerebellar atrophy which mimics what is observed at late stages of the disorder in humans (Torashima et al., 2008). In order to understand whether overexpression of let-7 would mitigate the neuropathology associated with MJD motor function impairments, we started by analysing both the molecular and granular layers thickness. This analysis was performed using Zen 2 (blue edition) software (Figure 13) and the results showed that let-7 could significantly increase granular layer thickness in the interlobule VII/VIII (Tg-mir-scr: 37.88 ± 1.221µm vs Tg-let-7: 41.54 ± 1.093µm, p=0.0498) (Figure 13B) when compared to the control mice (Figure 13A) as shown in Figure 13E. Regarding the measures of thickness of molecular layer (Figure 13F) (Tg-mir-scr: 86.89 ± 6.367µm vs Tg-let-7: 89.85 ± 5.095µm, p=0.7246) and granular and molecular layer together with Purkinje cells in the interlobule VII/VIII (Tg-mir-scr: 136.6 ± 7.271µm vs Tg-let-7: 144.6 ± 5.739µm, p=0.4100), a tendency to be increased in let-7 treated animals has been reported when compared to control group, though not reaching statistical significance (Figure 13G). Furthermore, in interlobule VIII/IX, a significant increase in the thickness of granular and molecular layers together with the Purkinje cells was observed in mice treated with let-7 when compared to the control ones (Tg-mir-scr: 215.2 ± 8.234µm vs Tg-let-7: 245.9 ± 9.651µm, p=0.0303) (Figure 13J). In this interlobule, there was also a tendency for an increased thickness in the granular layer (Tg-mir-scr: 69.62 ± 3.503µm vs Tg-let-7: 78.26 ± 3.703µm, p=0.1232) and molecular layer (Tg-mir-scr: 131.9 ±

5.741µm vs Tg-let-7: 155.6 ± 10.51µm, p=0.0925), when measured separately, in let-7 treated mice when compared with control mice group (Figure 13H, 13I). Overall, our results showed that let-7 treatment partially rescued the cerebellar atrophy observed in this MJD mouse model, by preserving molecular and granular layers thickness at the interlobular zones VII/VIII and VIII/IX.

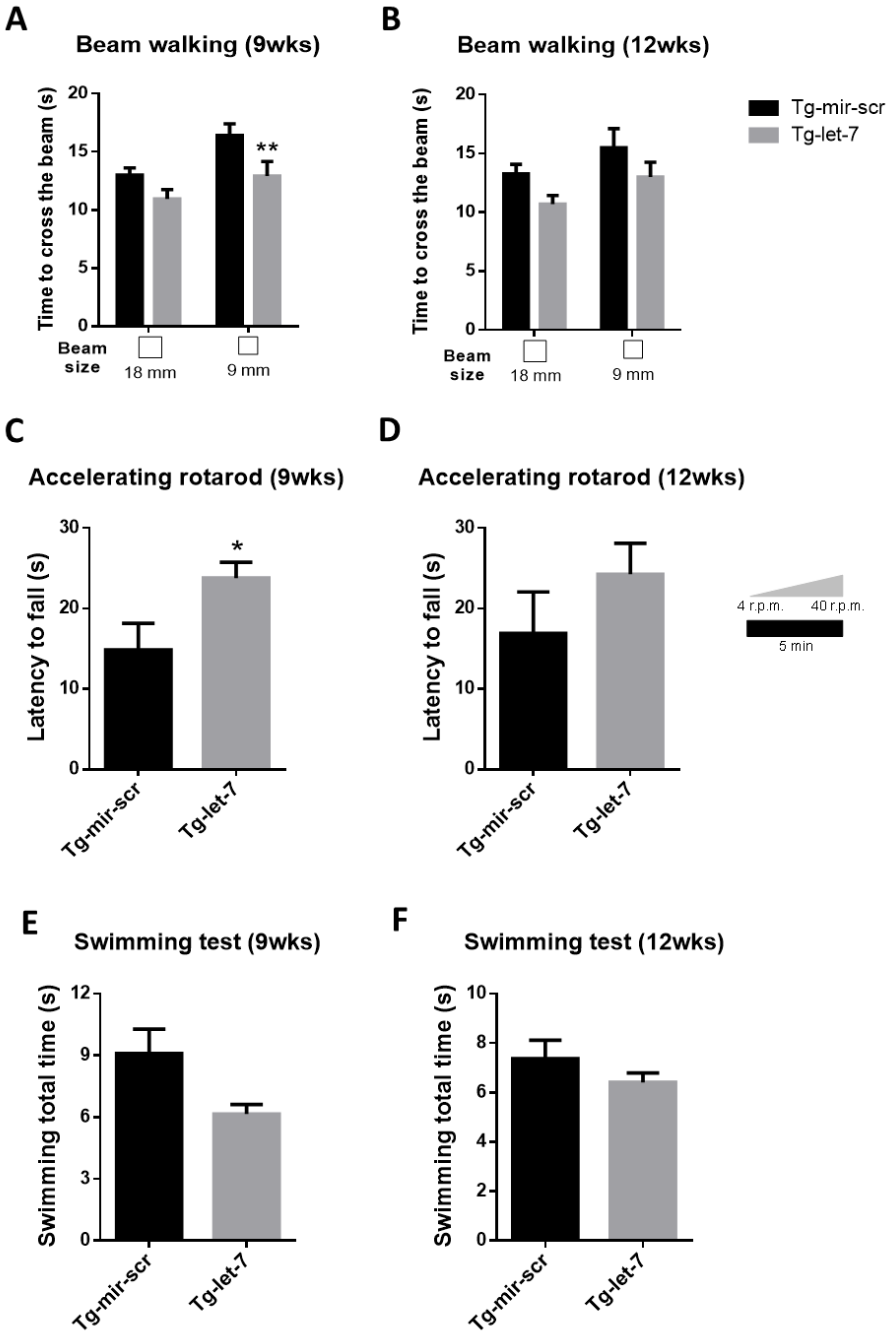

Figure 12 Let-7 treatment ameliorates motor incoordination and imbalance in a Tg MJD mouse model. (A, B) Beam walking test evaluation demonstrated that treated mice had a better performance to cross the beam at 9 (A) and 12 weeks post-injection (B), being statistically significant at 9 weeks in 9 mm square beam. (C, D) Accelerating rotarod test showed that tg-let-7 mice had a significantly higher ability to remain in apparatus than the control mice at 9 weeks post-injection (C) and also showed a tendency for a better performance at 12 weeks post-injection (D). (E, F) Swimming test demonstrated that at 9 weeks (E), as wells as 12 weeks post-injection (F) Tg-let-7 mice are able to cross the pool and climb the platform faster than control group, although not reaching statistical significance. Data represented mean ± SEM, *p<0.05 when compared with mir-scr injected mice (control group). (A, B) Two-way ANOVA with Bonferroni's post-hoc test, n=7/5. (C-F) Unpaired t-test with Welch's correction, n=7/5.

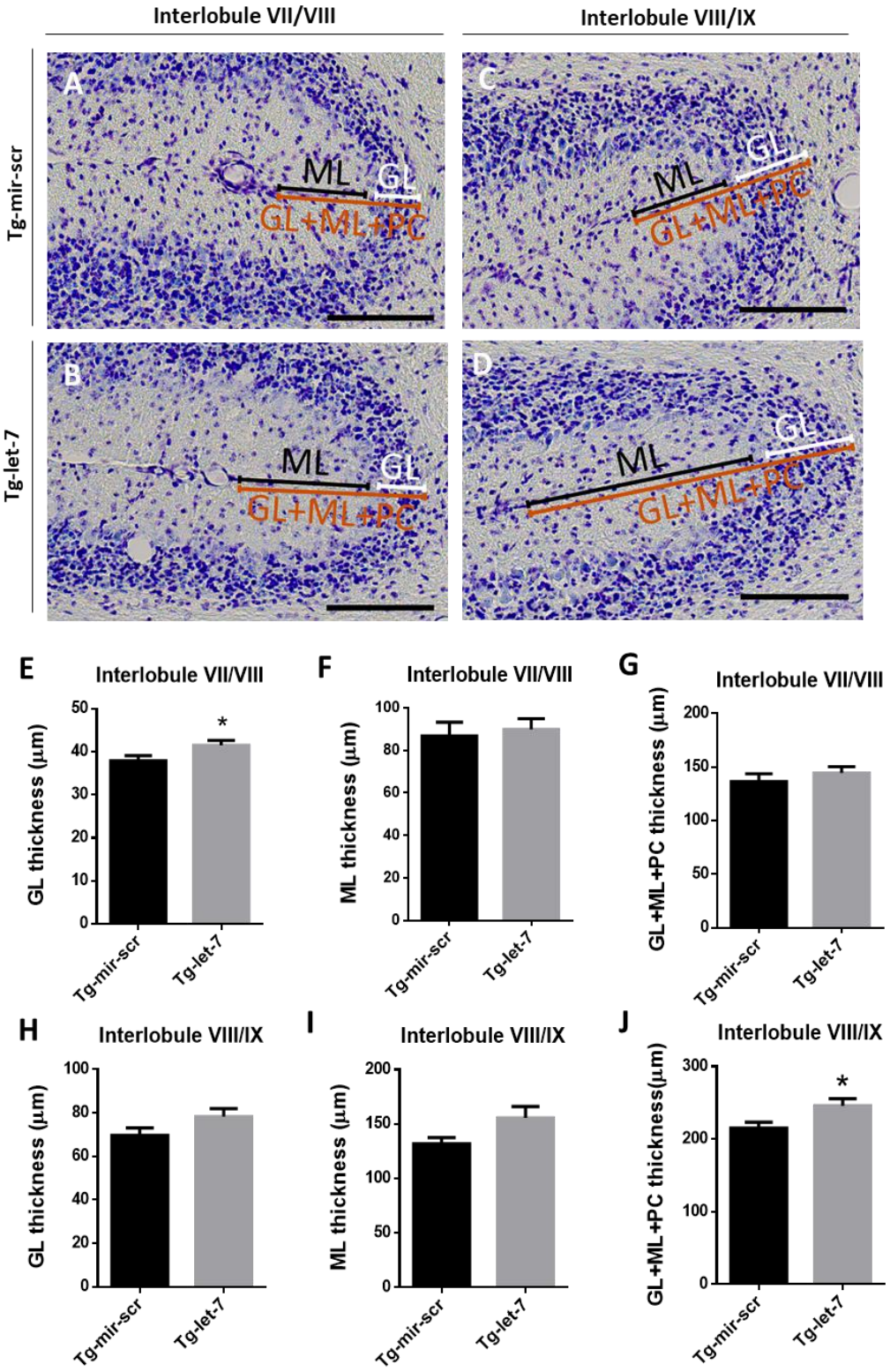

Figure 13 Let-7 treatment increases molecular and granular layers thickness. (A, B) Representative images of thickness of interlobule VII/VIII layers in control mice (A) and in treated mice with let-7 (B). (C, D) Images showing the layers thickness of interlobule VIII/IX in control mice (C) and mice treated with let-7 (D). White, black and orange lines are representative of granular layer (GL), molecular layer (ML) and granular and molecular layers together with Purkinje cells (GL+ML+PC), respectively. Scale bar, 100µm. (E-G) Quantification of layers thickness in interlobule VII/VIII in granular layer (E), molecular layer (F) and granular and molecular layers together with Purkinje cells (G). (H-J) Quantification of layers thickness in interlobule VIII/IX in granular layer (H), molecular layer (I) and granular and molecular layers together with Purkinje cells (J). Data represented mean ± SEM, *p<0.05 when compared with mir-scr mice group (control). (E-I) Unpaired t-test with Welch's correction, n=7/5; (J) Mann-Whitney test, n=7/5.

1.3 Cerebellar volume does not change upon let-7 overexpression in Tg MJD mouse model

Cerebellar atrophy present in the Tg MJD mouse model used in this work was shown to be associated not only with cerebellar layers atrophy, but also with a pronounced cerebellar volume reduction reported in comparison with WT animals (Torashima et al., 2008). Thus, we went to assess whether let-7 treatment could improve the cerebellar volume atrophy in Tg MJD mice (Figure 14). Our results showed that cerebellar volume is very similar in let-7 treated group and control group, as observed in Figure 14A and B. A quantitative analysis revealed no significant alterations in cerebellar volume between Tg-mir-scr and Tg-let-7 mice (Tg-mir-scr: $3.763x10^{10} \pm 1.690x10^{9}$ μm^3 vs Tg-let-7: $3.752x10^{10} \pm 1.238x10^{9}$ μm^3, p=0.9599), as shown in Figure 14C. This data suggests that let-7 treatment does not result in alterations of cerebellar volume.

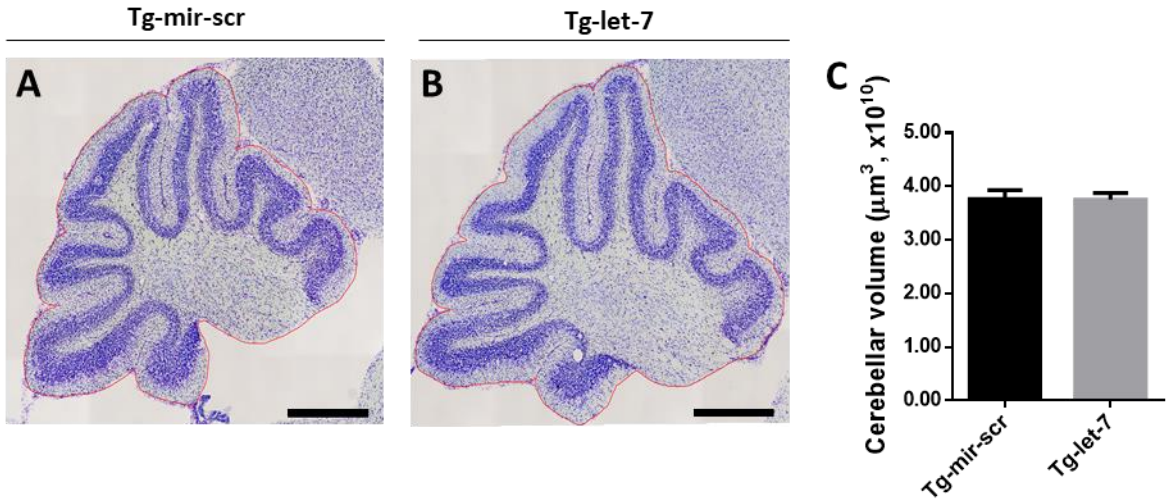

Figure 14 Cerebellar volume does not change with let-7 treatment. (A, B) Representative images of cerebellar volume at 12 weeks post-injection in control mice injected with mir-scr, (A) or in mice treated with let-7 (B) Quantification of cerebellar volume (C). Scale bar, 500µm. Red line demonstrates cerebellum contour. Data represented mean ± SEM. Unpaired t-test with Welch's correction, n=5/5.

1.4 Aggregates number is not reduced upon let-7 treatment in lobules VIII/IX

One of the most common hallmarks of the disease is the presence of misfolded proteins aggregates that induce neurodegeneration in cerebellum (Paulson et al., 1997). Taking this into consideration, we evaluated whether let-7 could diminish aggregates number in lobules VIII and IX of mice cerebellum. Thus, aggregates were manually counted using Zen 2 (blue edition) software. After the analysis of the total number of aggregates, no significant differences in the number of aggregates were observed between control mice (Figure 15C) and treated mice (Figure 15D) in lobule VIII and lobule IX together (Tg-mir-scr: 3942 ± 128.5 vs Tg-let-7: 4344 ± 443.8, p=0.4263) (Figure 15E). These results demonstrated that overexpression of let-7 did not result in misfolded protein aggregates decrease in lobules VIII and IX.

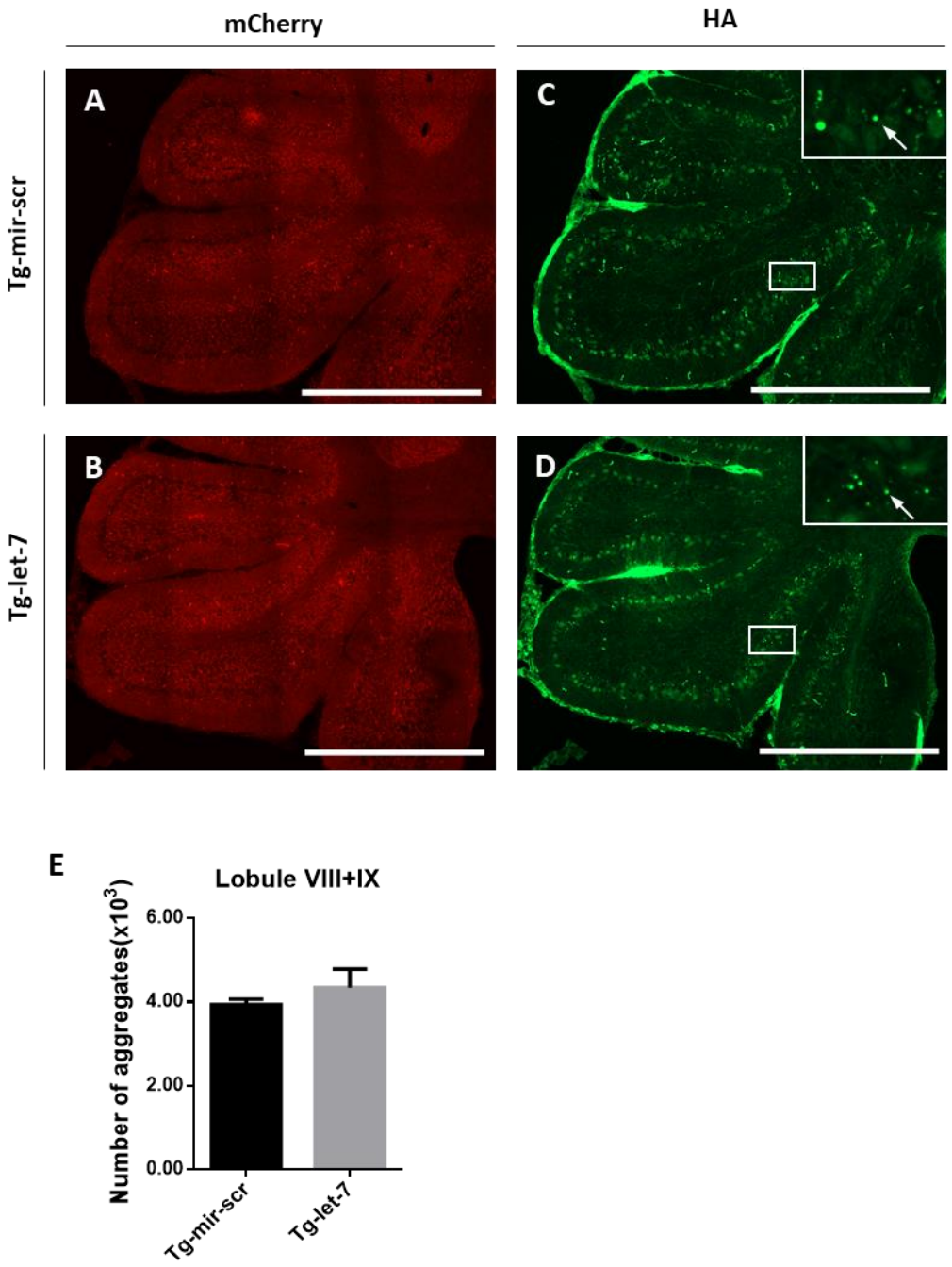

Figure 15 Let-7 treatment is not able to reduce aggregates number in lobules VIII/IX. (A, B) Images representing mCherry labelling obtained upon mir-scr plasmid overexpression (A) or let-7 plasmid overexpression (B). (C, D) Representative images of aggregates in lobules VIII and IX together quantified in E. White arrows indicate the aggregates. Scale bar, 500µm. Data represented mean ± SEM. Unpaired t-test with Welch's correction, n=7/5.

1.5 Let-7 treatment in lobules VIII and IX had no effect at preserving immunoreactivity of Purkinje cells

In our Tg MJD mouse model the disease-gene target Purkinje cells due to its cell-specific promoter L7 (Torashima et al., 2008). Since Tg MJD mice exhibit marked defects in the Purkinje cells, we went to

evaluated whether let-7 would improve immunoreactivity for calbindin. For that, we measured the immunoreactivity of Purkinje cells (Figure 16A-F) in lobules VIII and IX (represented as mean of the two lobules) in control mice (Figure 16G, H) and mice treated with let-7 (Figure 16 I, J). This analysis revealed a tendency for the decrease of calbindin intensity in Tg-let-7 (Tg-mir-scr: 3315 ± 78.91 a.u. vs Tg-let-7: 3079 ± 104.9 a.u., p=0.1090), as shown in Figure 16K. This result suggests that let-7 treatment was not able to recover immunoreactivity of Purkinje cells, at least in lobules VIII and IX.

1.6 Treatment with let-7 does not induce gliosis

The role of let-7 in neuroinflammation has been studied along the last years. In asthma, Polikepahad et al. found that let-7 displays a proinflammatory role inducing lung inflammation in allergic disorders (Polikepahad et al., 2010). More recently, deregulation of Let-7 was associated to neuroinflammation observed in depression (Wei et al., 2016). The impairment of let-7 biogenesis led to a upregulation of IL6, a proinflammatory cytokine (Wei et al., 2016). Moreover, along of the years has been observed neuroinflammation in the context of MJD reported in cell lines (Evert et al., 2001, 2003) as well as in late-stages of the disease in Tg mouse model (Silva-Fernandes et al., 2010). Regarding these, we assessed whether let-7 could be acting as an inflammatory factor (Figure 17A-H). Thus, we measured the immunoreactivity of astrocytes through GFAP labelling (Figure 17A,D) and the immunoreactivity of microglia through IBA1 labelling (Figure 17B,E). We observed no difference in astrocytes reactivity between control mice (Figure 17A) and treated mice (Figure 17D) (Tg-mir-scr: 1140 ± 83.23 a.u. vs Tg-let-7: 1064 ± 72.86 a.u., p=0.5123). At microglia level, no differences in IBA1 labelling were observed when comparing control mice (Figure 17B) and treated mice with let-7 (Figure 17E) (Tg-mir-scr: 1119 ± 97.08 a.u. vs Tg-let-7: 1129 ± 61.84 a.u., p=0.5253). Let-7 treatment does not have an effect on neuroinflammation mediated by astrocytes or microglia in Tg MJD mouse model.

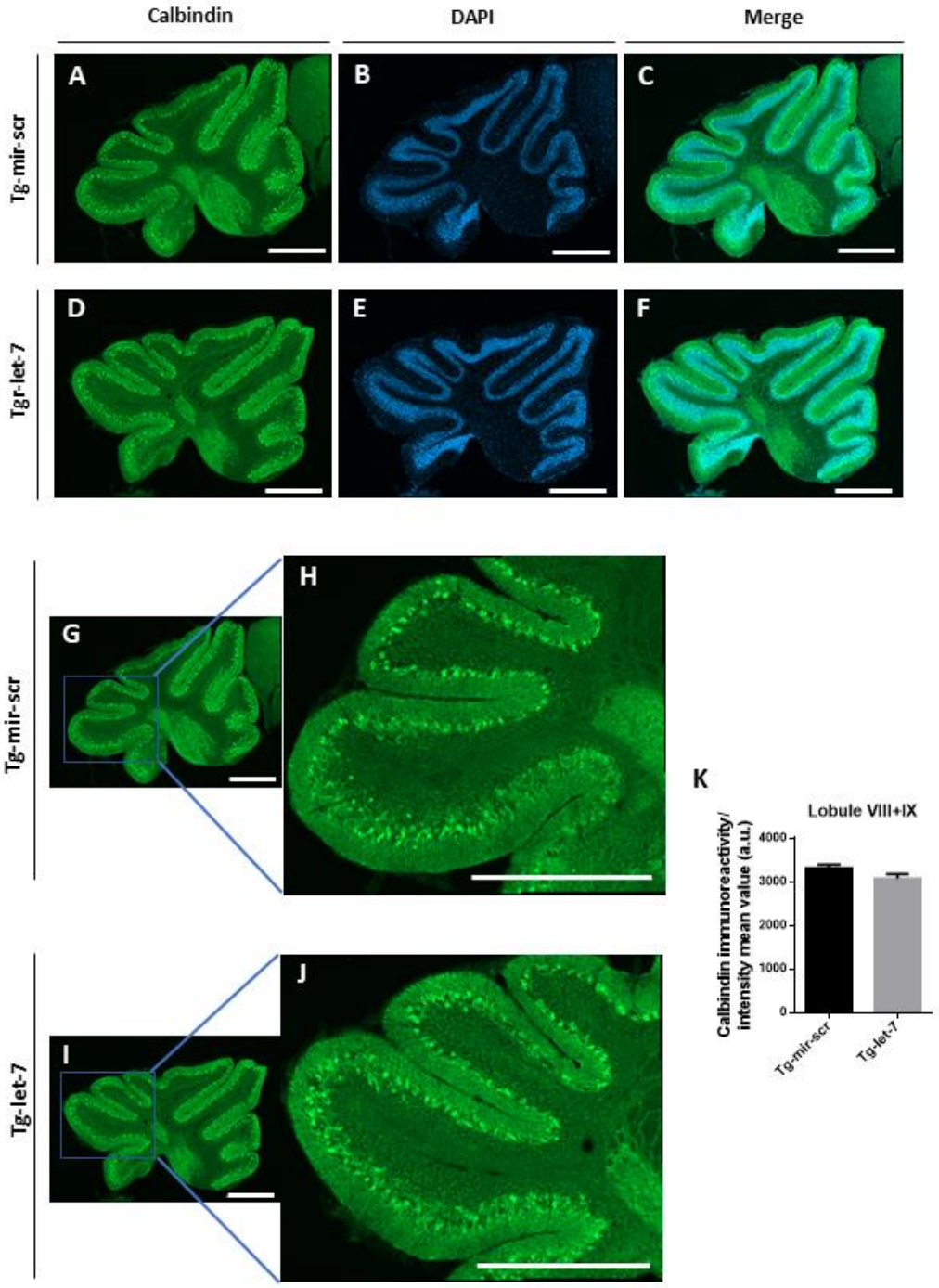

Figure 16 Calbindin immunoreactivity does not change upon treatment with let-7. (A-F) Representative images of calbindin staining in control mice (A-C) and mice treated with let-7 (D-F) after 12 weeks injection. Calbindin immunoreactivity was quantified in lobule VIII and IX (represented as mean of the two lobules), as shown in G and H for control mice and I and J for treated mice with let-7. The quantification does not demonstrate differences in immunoreactivity of calbindin as shown in K. (B, E) DAPI, nuclei, blue. Scale bar 500µm. Data represented mean ± SEM. Unpaired t-test with Welch's correction, n=7/5.

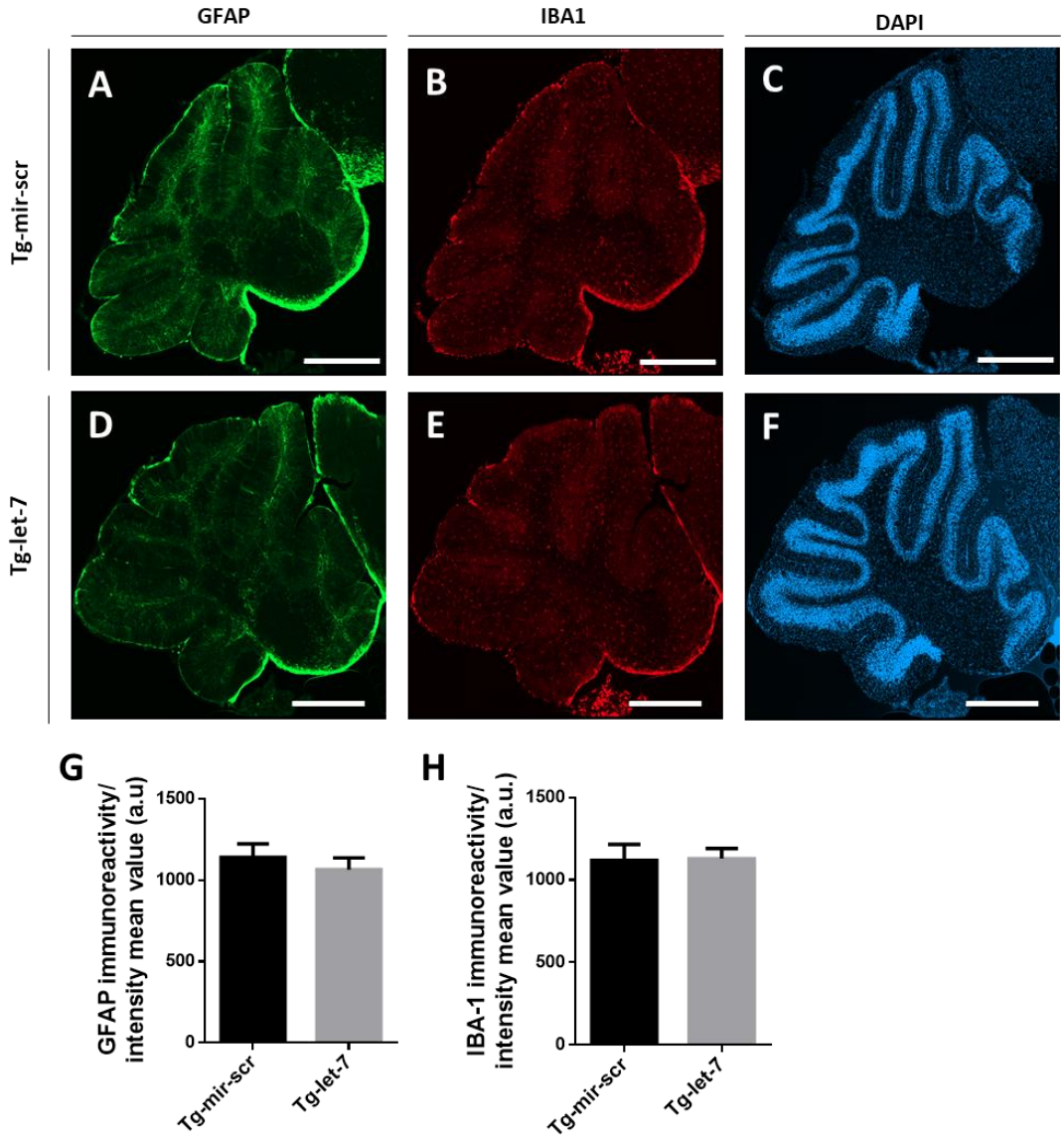

Figure 17 Treatment with let-7 does not induce gliosis(A-F) representative images of GFAP and IBA1 staining in Tg-mir-scr mice (A-C) and in treated mice with let-7 (D-F) after 12 weeks of treatment. (A,D) GFAP and (B, E) IBA1 staining were quantified in whole cerebellum. Quantification of GFAP and IBA1 does not show any differences in immunoreactivity comparing Tg-mir-scr and treated mice respectively in (G) and (H). (C,F) DAPI, nuclei, blue. Scale bar, 500µm. Data represented mean±SEM. (G) Unpaired t-test with Welch's correction, n=7/5. (H) Mann-Whitney test, n=7/5.

1.7 Autophagy is impaired in an MJD transgenic mouse model

Autophagy impairment has been shown to contribute for MJD pathogenesis. Our group had already reported autophagy deregulation in several MJD models, such as Goti et al. transgenic mouse model, human tissue and hiPSCs (Nascimento-Ferreira et al., 2011; Onofre et al., 2016). However, in our model of study, the Torashima et al. transgenic mouse model, this is not well documented. Thus, to better understand the effect of let-7 treatment in autophagy mechanism we first went to characterize autophagy impairment in this model. For that, we performed western blot analysis and found that Tg mice presented a significant decrease of LC3 I, an autophagy marker, when compared to WT mice (WT:

1.0 ± 0.2084 vs Tg: 0.4051 ± 0.05823, p=0.0317) (Figure 18A). Moreover, a tendency for an accumulation of P62 was observed in Tg mice, when compared to the WT group (WT: 1.0 ± 0.1078 vs Tg: 1.217 ± 0.06263, p=0.1111) (Figure 18B). This data correlate with a tendency for an accumulation of HA aggregates (WT: 1.0 ± 0.3274 vs Tg: 1.755 ± 0.3674, p=0.1905) (Figure 18C), as well as with a significant increase of soluble HA levels (WT: 1.0 ± 0.1997 vs Tg: 4.914 ± 0.9250, p=0.0159) observed in Tg mice in comparison to WT group (Figure 18D).

Altogether, these results demonstrated an autophagy impairment in Torashima et al. transgenic mouse model in the context of an accumulation of aggregates and soluble HA.

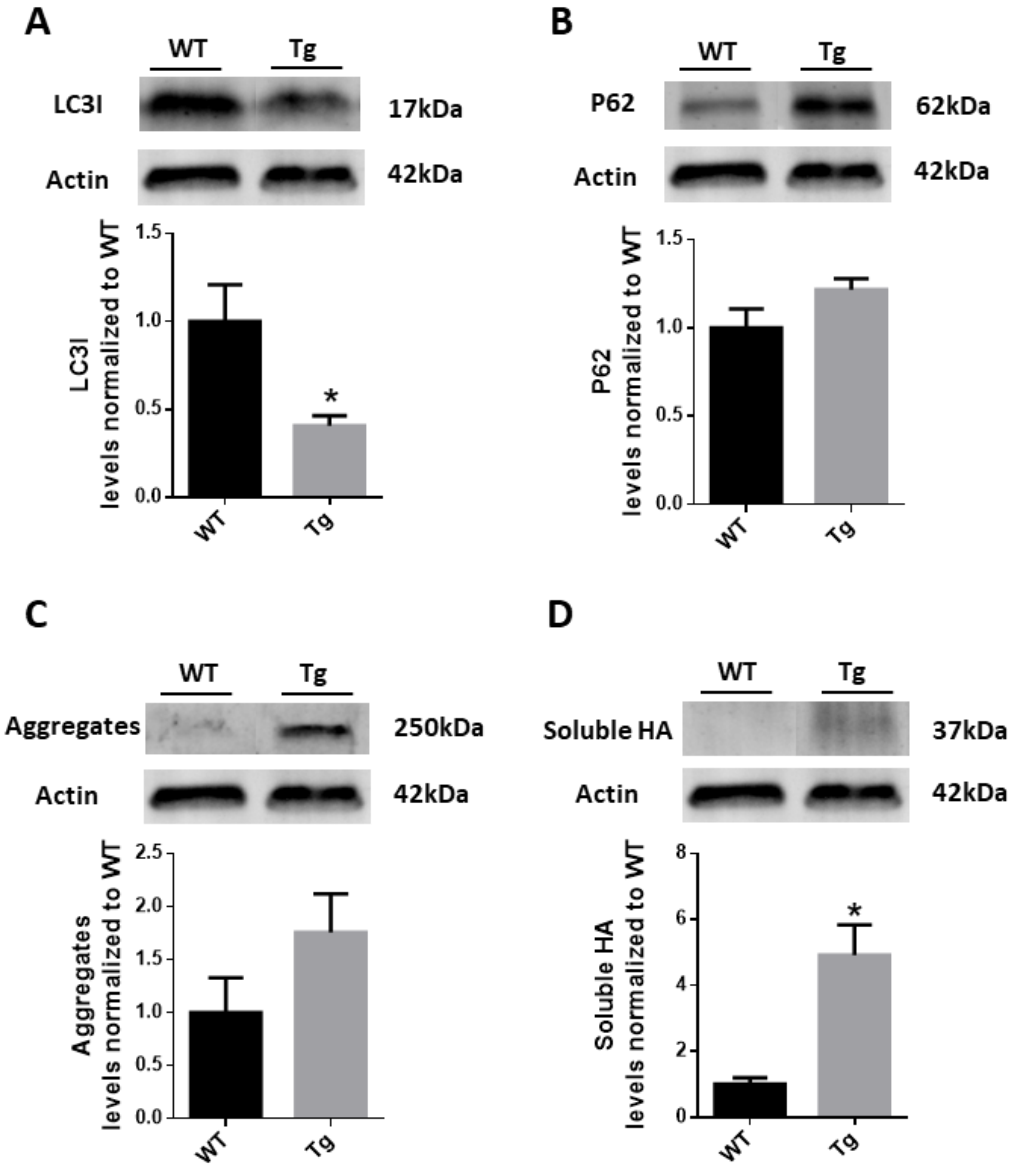

Figure 18 Autophagy is deregulated in MJD transgenic mouse model inducing aggregates and soluble HA accumulation(A,B) Autophagy is impaired in MJD tg mouse model. Tg mouse model presents a significant decrease of LC3I (A) and a tendency for P62 accumulation (B) when compared to WT mice. In Tg mouse model there is also a tendency to the accumulation of HA aggregates (C) and a significant increase of soluble HA protein (D). Data represented mean±SEM. *p<0.05 (A-D) Mann-Whitney test, n=4/5.

1.8 Autophagy is partially activated upon let-7 treatment

In order to understand whether let-7 is able to activate autophagy in Tg MJD mouse model, we have performed western blot analysis to assess the expression of autophagy markers in control and let-7 treated mice (Figure 19). We observed a slight tendency for an increase in LC3I in Tg-let-7 mice when compared to the control group (Tg-mir-scr: 1.0 ± 0.05409 vs Tg-let-7: 1.594 ± 0.5371, p=0.3316) (Figure 19A). By the opposite, P62 showed to be slightly decreased in Tg-let-7 mice (Tg-mir-scr: 1.0 ± 0.05598 vs Tg-let-7: 0.9142 ± 0.08203, p=0.4162) (Figure 19B).

The presence of aggregates was also evaluated in control and let-7 treated mice by western blot analysis. Contrarily to what we have observed by immunohistochemistry, a decrease of aggregates in let-7 treated group was reported, although not reaching statistically significance (Tg-mir-scr: 1.0 ± 0.08934 vs Tg-let-7: 0.7293 ± 0.1159, p=0.1039) (Figure 19C).

In sum, these data seem to indicate there is a partial recover of autophagy mechanism in mice treated with let-7, which seems to be correlated with the reduction of aggregates in these mice

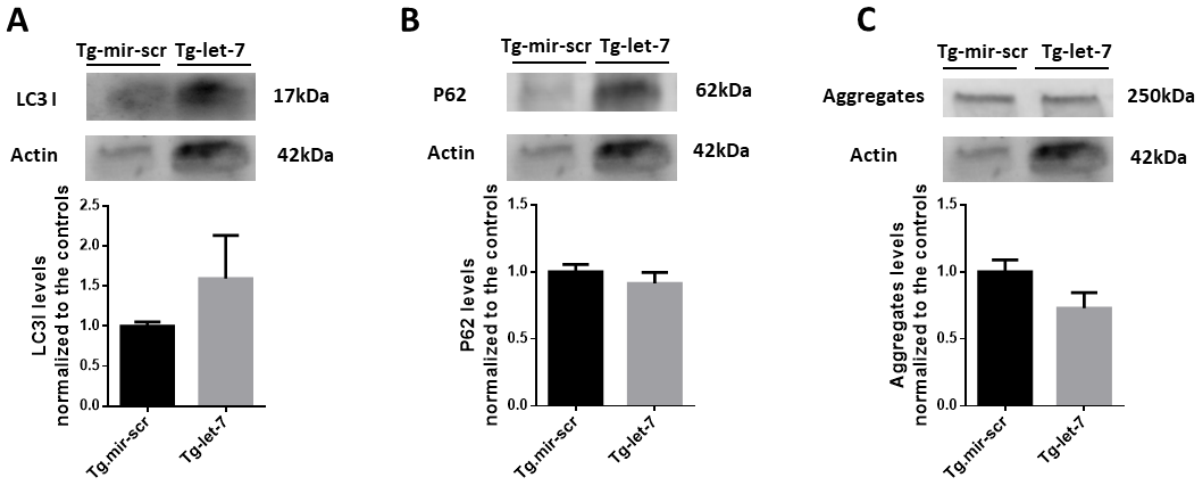

Figure 19 Let-7 treatment partially activates autophagy. (A,B) Quantification of autophagy markers revealed that let-7 may partially activate this clearance cell mechanism, demonstrated by an increase of LC3I (A) and a slight decrease of P62 (B). (C) A decrease of aggregates levels was reported in Tg-let-7, in the context of autophagy activation. Data represented mean±SEM.(A-C) Unpaired t-test with Welch's correction, n=5/5

1.9 Let-7 target is increased in a Tg mouse model and decreased under let-7 overexpression

In a previous study, several putative targets of let-7 were predicted using different bioinformatic tools, and further validated by qRT-PCR (Dubinsky et al., 2014). This study showed that many of let-7 targets belong to the amino acid sensing pathway. Basal levels of RagC, one of the validated let-7 targets, were assessed in Tg and WT mice by western blot analysis. Our results showed that RagC tended to be increased in Tg mice group when compared to the WT group (WT: 1.080 ± 0.01286 vs Tg: 1.650 ±

0.2045, p=0.250) (Figure 20A). Moreover, RagC levels were also evaluated under overexpression of let-7 in Tg mice, and a decrease of RagC has been observed in Tg-let-7, which had almost reached statistical significance (Tg-mir-scr: 1.0 ± 0.1151 vs Tg-let-7: 0.7138 ± 0.07308, p=0.0754) (Figure 20B).

These results indicate that RagC, being a let-7 target, may be involved in the mechanism of neuroprotection in MJD mediated by let-7.

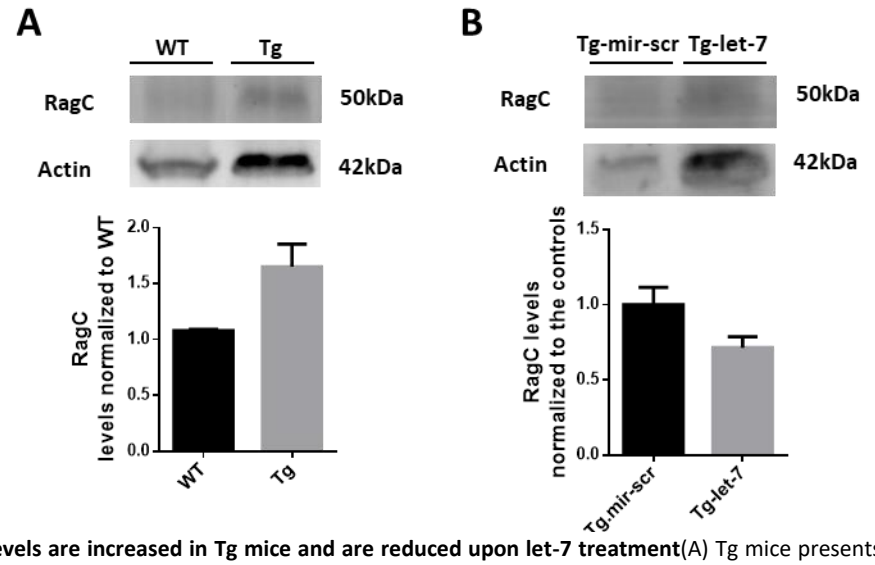

Figure 20 RagC levels are increased in Tg mice and are reduced upon let-7 treatment(A) Tg mice presents higher levels of RagC when compared to the wt group. (B) Mice treated with let-7 presents a reduction of RagC levels comparing to the control. Data represented mean±SEM. (A) Mann-Whitney test, n=3/4 (B) Unpaired t-test with Welch's correction, n=5/5.

Chapter IV - Discussion

Neurodegenerative disorders are a scourge in our society due to the lack of treatments and consequently to the loss of quality of life. Particularly, MJD having an onset during the active life period,, leads to an impairment of motor coordination and balance, among other symptoms, which will disturb the normal life of the individuals (Bettencourt and Lima, 2011; Paulson, 2012; Pedroso et al., 2013). Although MJD is a rare disease across the world, in Portugal, namely in Azores, reaches an huge incidence and consequently it is urgent to find a therapy for this disorder (Araújo et al., 2016).

The exact pathogenic mechanisms that lead to neurodegeneration in MJD are not fully understood, but it has been shown that autophagy impairment is one of the possible mechanisms contributing to the pathogenesis. Disruption of autophagy in MJD has been reported in the last years, including by our group (Nascimento-Ferreira et al., 2011; Onofre et al., 2016). Moreover, we have also shown that activation of this mechanism ameliorates MJD disease phenotype (Cunha-Santos et al., 2016; Nascimento-Ferreira et al., 2013). In the present work, we aim at understanding whether let-7, a miRNA involved in amino acids sensing pathway regulation and mTORC1 inhibition, could activate autophagy and consequently rescue neuropathology, ataxia and balance deficits observed in MJD.

We have started to evaluate motor behaviour in a Tg mouse model, before and every 3 weeks after let-7 treatment, during 12 weeks to understand whether let-7 could ameliorate motor deficits exhibited by this model. At 9 weeks post-injection, let-7 treated mice showed a better performance in all behaviour tests, including beam walking, accelerated rotarod and swimming. At 12 weeks post-injection, let-7 treated group also showed to be more agile in all testes, although not reaching statistical significance. Together these results showed that let-7 miRNA alleviates balance and motor coordination impairments in a Tg MJD mouse model.

Taking these results into account the next step was the evaluation of neuropathology in transgenic mouse model under overexpression of let-7 at 12 weeks post-injection (last behaviour time point), to understand whether behaviour data correlate with these data. First of all, we expected to observe an increase of thickness layers that would reveal the rescue of cerebellar atrophy. Here, we detected the significant increase of granular layer in interlobule VII/VIII as well as in granular and molecular layer together with the Purkinje cells in interlobule VIII/IX. We also saw a tendency to the increase of molecular layer and granular and molecular layers together with Purkinje cells in interlobule VII/VIII as well as the granular and molecular layers measured separately in interlobule VIII/IX. Our results pointed to a partial rescue of the cerebellar layers atrophy, characteristic in this MJD mouse model. These results are in agreement with what has been observed in other studies also performed by our group, in which they have reported a rescue of cerebellar atrophy in MJD upon activation of autophagy (Cunha-Santos et al., 2016). Moreover, cerebellar volume was assessed in Tg mice control and Tg mice

treated with let-7 and the results showed no difference between the two study groups. This fact may indicate that the improvement observed in cerebellar layers thickness was not sufficient to rescue the cerebellar volume atrophy.

The presence of aggregates is one of the most common hallmarks of the disease (Paulson et al., 1997). Since autophagy is a cellular clearance mechanism and previously our group had proved that its activation leads to a reduction in the number of aggregates (Cunha-Santos et al., 2016; Nascimento-Ferreira et al., 2013), we went to study the possible effect of let-7 treatment on the number of aggregates present in our Tg mouse model. Previously in our lentiviral mouse model, a reduction of ubiquitin-inclusions has been reported in striatum after 4 weeks treatment with let-7 (Dubinsky et al., 2014). Unfortunately, when we evaluated the number of aggregates in lobules VIII and IX of the cerebellum by Immunohistochemistry (IHC), we observed no differences between Tg mice treated with let-7 and control Tg mice. However, when we measured the levels of aggregates by western blot in all cerebellum, a tendency for the reduction in the number of aggregates was observed in Tg-let-7 mice. We speculate that these differences between the two analysis may be probably due to entropy of used antibody, which is anti-mouse, with the specie host, that is also mouse. This fact increased the immunoreactivity when we used IHC, and this is the reason why this may have influenced in aggregates counting. Furthermore, in IHC analysis we only evaluate aggregates number in two lobules while in western blot analysis we have measured in the whole cerebellum. There are many evidences showing that not only in MJD, but also in other neurodegenerative disorders, activation of autophagy has a crucial effect on the reduction of protein aggregates. For example, in Huntington's disease, Ravikumar and collaborators described that activation of autophagy with rapamycin caused a reduction in mutant huntingtin aggregates (Ravikumar et al., 2002). Also in a cellular model of Parkinson's Disease, rapamycin treatment resulted in the activation of autophagy and consequently in a decrease of α-synuclein (Webb et al., 2003). Thus, we believe that let-7 is able to reduce aggregates in Tg mice, through autophagy activation, similarly to what we have observed in lentiviral-striatal mouse model (Dubinsky et al., 2014).

Purkinje cells are one of the most important neurons in cerebellum. These neurons, which act as inhibitory neurons in cerebellum, receive excitatory inputs from granular cells and deliver inhibitory outputs to DCN, as well as to vestibular nuclei (reviewed by Gao et al., 2012). This circuitry allows the production of motor movements revealing the important role played by these cells in cerebellum (reviewed by Gao et al., 2012). In the case of the Tg mouse model used in this study, the truncated form of atx3 protein is driven by L7 promoter to the Purkinje cells, which determines a severe MJD phenotype (Torashima et al., 2008). Due to Purkinje cells importance in cerebellum and particularly in MJD, we assessed whether let-7 treatment would be able to rescue the immunoreactivity of Purkinje

cells Tg MJD mice. Contrarily to what we were expecting, a tendency for a decrease in Purkinje cells immunoreactivity was observed in lobules VIII and IX (mean of the two lobules) in let-7 treated mice. The antibody used in this study to evaluate calbindin immunoreactivity, calbindin D-28K, labels not only Purkinje cells, but also other type of cells. This redundancy caused us some uncertainties about this result and other analysis has to be made, namely the use of other antibodies, like PCP-4, which was used previously in our group, and that we hope will allow to reduce background produced by calbindin staining (Oliveira Miranda et al., 2018). Besides that, the number of Purkinje cells, as well as their morphology could also be evaluated upon let-7 treatment in Tg MJD mice.

In the last years, the role of let-7 in inflammation has been studied in several models, such as asthma and depression. It seems that let-7 act as proinflammatory factor in certain pathways, however acquire a preventive role in others, perhaps depending on the environment (Polikepahad et al., 2010; Wei et al., 2016). Let-7 has been shown to be involved in astrocytes differentiation (Shenoy et al., 2015) and in other studies let-7a was shown to act as an anti-inflammatory factor by regulating microglia function inducing the acquirement of M2 phenotype which is the neuroprotective form of these cells (Cho et al., 2015).

In our work, we went to understand whether overexpression of let-7 could interfere with inflammation that has been reported in MJD (Evert et al., 2001, 2003; Silva-Fernandes et al., 2010). For this purpose, we have evaluated GFAP and IBA1 levels to determine astrocytes and microglia reactivity, respectively. No differences in astrocytes, as well as microglia reactivity, were observed between control mice and let-7 treated mice evaluated by IHC. Our results seem to indicate that let-7 miRNA does not have an effect on neuroinflammation mediated by astrocytes or microglia.

Based on our previous work we knew that let-7 regulates many genes in the amino-acid sensing pathway, which mediate mTOR inhibition and ultimately induce autophagy (Dubinsky et al., 2014). Thus, we have focused our research on understanding whether the improvements observed in behaviour and neuropathology were due to the activation of autophagy mediated by let-7. In a first step we went to characterize autophagy impairment in Tg MJD mouse model, since it is not documented till now, to further understand the effect of let-7 in this model. Levels of autophagic markers, such as LC3I and P62 were determined in WT and Tg mice by western blot. Here, we detected a significant decrease of LC3I and a tendency for the accumulation of P62 in Tg mice when compared to WT. These data suggest that autophagy in this Tg mouse model is impaired in elongation step, before LC3I formation. Furthermore, the tendency for the accumulation of P62 observed in this model also suggests an autophagy impairment, since this protein is an autophagy substrate and it is supposed to be degraded across the process. This fact is also in accordance with previous studies in other MJD

models and also in other neurodegenerative disorders, where P62 was shown to accumulate under disease condition (Alves et al., 2014; Onofre et al., 2016; Simonovitch et al., 2016). Moreover, assuming that LC3I is not formed, we could guess that autophagosomes are not able to elongate (Hemelaar et al., 2003) and consequently will not fuse with lysosome, thus impairing autophagy.

Our results have shown a dysfunctional autophagy in Tg MJD mouse model. After these conclusions, we went to evaluate whether let-7 treatment would activate autophagy, and this would be responsible for the differences that we observed at behaviour and neuropathological level. We have used the same approach described before in order to evaluate levels of autophagy markers. A tendency for an increase of LC3I has been reported in let-7 treated mice comparing to the control group, while P62 showed a tendency to be decreased upon let-7 treatment. Taking all these results into consideration, we believe that treatment with let-7 partially rescue dysfunctional autophagy, here documented in Tg mice. Our group, in other study using the same Tg MJD mouse model, have also showed that the induction of autophagy resulted in a decrease of P62 (Cunha-Santos et al., 2016).

To further complete our study about autophagy activation upon let-7 treatment, we went to investigate RagC, a let-7 target. We have previously observed a RagC upregulation at the protein level under inhibition of let-7 (Dubinsky et al., 2014), thus we decided to assess RagC levels firstly in Tg mice model (basal levels) and then upon let-7 treatment. The basal levels of this protein were assessed, and the results showed a tendency for the overexpression of RagC in Tg MJD mouse model comparing to WT mice. RagC was shown to be involved in the amino acid sensing pathway leading to mTORC1 activation and consequently inhibition of autophagy (Dubinsky et al., 2014; Sancak et al., 2008). The fact that RagC had a tendency to be upregulated in Tg MJD mouse model corroborates our previous findings showing an autophagy impairment in this model.

RagC levels were then evaluated upon let-7 overexpression, and the results showed that RagC protein tended to be decreased in Tg-let-7 mice when compared to control Tg-mir-scr mice. These observations met our expectations, since we have previously reported an increase of RagC levels upon inhibition of let-7 in neuro2A cells (Dubinsky et al., 2014). These data demonstrate that RagC is one of let-7 targets involved in the mechanism of autophagy activation mediated by let-7, not only in *in vitro* cell models, but also in Tg MJD mouse model.

Altogether, our results provide evidences of an autophagy impairment in Tg MJD mouse model, which has been partially rescued by let-7 overexpression. Let-7 regulates the amino acid sensing pathway, being RagC one of the mediators, leading to autophagy activation and thus alleviating behaviour deficits and neuropathology in Tg MJD mice. With this work we are providing new insights to a new possible approach based on miRNAs for MJD therapy.

Chapter V – Conclusion and Future Perspectives

Conclusions

After this work, we are better elucidated about the role of let-7 in MJD *in vivo* models and the possible mechanism underlying autophagy activation mediated by let-7 in MJD. Therefore, we may conclude that:

- Let-7 treatment ameliorates motor deficits observed in an MJD transgenic mouse model;
- A rescue of layers thickness atrophy in lobules VIII and IX and a tendency for a reduction in levels of aggregates in whole cerebellum were observed upon Let-7 treatment;
- Let-7 treatment does not have an effect on neuroinflammation mediated by astrocytes or microglia in Tg MJD mouse model. Thus, let-7 is not acting either as a proinflammatory factor by inducing inflammation or as anti-inflammatory molecule by rescuing neuroinflammation documented in MJD;
- Let-7 partially rescue autophagy impairment in Tg MJD mice by decreasing P62 levels and increasing LC3I levels;
- RagC is one of let-7 targets involved in the mechanism of autophagy activation mediated by let-7, not only in *in vitro* cell models, but also in Tg MJD mouse model.

Future perspectives

To deeper understand the effect of let-7 in MJD, we intend to perform several other analyses to complement our results and conclusions, such as:

- Understand whether let-7 affect Purkinje cells number and morphology;
- Assess neuropathology parameters in lobule II and III, which showed to present a high expression of mCherry reporter gene;
- Evaluate the expression levels of other let-7 targets involved in the amino acid sensing pathway in Tg MJD mice, before and after treatment with let-7;
- Elucidate the mechanism of autophagy activation mediated by let-7, by defining which of the let-7 targets are more relevant in an MJD context.

Chapter VI - References

Agarraberes, F.A., and Dice, J.F. (2001). A molecular chaperone complex at the lysosomal membrane is required for protein translocation. J. Cell Sci. *114*, 2491–2499.

Albrecht, M., Golatta, M., Wüllner, U., and Lengauer, T. (2004). Structural and functional analysis of ataxin-2 and ataxin-3. Eur. J. Biochem. *271*, 3155–3170.

de Almeida, L.P., Ross, C.A., Zala, D., Aebischer, P., and Deglon, N. (2002). Lentiviral-mediated delivery of mutant huntingtin in the striatum of rats induces a selective neuropathology modulated by polyglutamine repeat size, huntingtin expression levels, and protein length. J. Neurosci. *22*, 3473–3483.

De Almeida, L.P., Zala, D., Aebischer, P., and Déglon, N. (2001). Neuroprotective effect of a CNTF-expressing lentiviral vector in the quinolinic acid rat model of Huntington's disease. Neurobiol. Dis. *8*, 433–446.

Alves, S., Régulier, E., Nascimento-Ferreira, I., Hassig, R., Dufour, N., Koeppen, A., Carvalho, A.L., Simões, S., Pedroso de Lima, M.C., Brouillet, E., et al. (2008). Striatal and nigral pathology in a lentiviral rat model of Machado-Joseph disease. Hum. Mol. Genet. *17*, 2071–2083.

Alves, S., Nascimento-Ferreira, I., Dufour, N., Hassig, R., Auregan, G., Nóbrega, C., Brouillet, E., Hantraye, P., Pedroso de Lima, M.C., Déglon, N., et al. (2010). Silencing ataxin-3 mitigates degeneration in a rat model of Machado – Joseph disease : no role for wild-type ataxin-3? Hum. Embryol. Dev. Biol. *19*, 2380–2394.

Alves, S., Cormier-Dequaire, F., Marinello, M., Marais, T., Muriel, M.P., Beaumatin, F., Charbonnier-Beaupel, F., Tahiri, K., Seilhean, D., El Hachimi, K., et al. (2014). The autophagy/lysosome pathway is impaired in SCA7 patients and SCA7 knock-in mice. Acta Neuropathol. *128*, 705–722.

Antony, P.M.A., Mäntele, S., Mollenkopf, P., Boy, J., Kehlenbach, R.H., Riess, O., and Schmidt, T. (2009). Identification and functional dissection of localization signals within ataxin-3. Neurobiol. Dis. *36*, 280–292.

Araújo, M.A. De, Raposo, M., Kazachkova, N., Vasconcelos, J., Kay, T., and Lima, M. (2016). Trends in the Epidemiology of Spinocerebellar Ataxia Type 3 / Machado-Joseph Disease in the Azores Islands , Portugal. JSM Brain Sci. *1*, 1–5.

Atlashkin, V., Kreykenbohm, V., Eskelinen, E., Wenzel, D., Fayyazi, A., and Mollard, G.F. Von (2003). Deletion of the SNARE vti1b in Mice Results in the Loss of a Single SNARE Partner , Syntaxin 8. Mol. Cell. Biol. *23*, 5198–5207.

Balzeau, J., Menezes, M.R., Cao, S., Hagan, J.P., and Hagan, J.P. (2017). The LIN28 / let-7 Pathway in Cancer. Front. Genet. *8*, 1–16.

Bar-Peled, L., Schweitzer, L.D., Zoncu, R., and Sabatini, D.M. (2012). Ragulator is a GEF for the rag GTPases that signal amino acid levels to mTORC1. Cell *150*, 1196–1208.

Berezikov, E., Chung, W.-J., Willis, J., Cuppen, E., and Lai, E.C. (2007). Mammalian Mirtron Genes. Mol. Cell *28*, 328–336.

Berg, T.O., Fengsrud, M., Strømhaug, P.E., Berg, T., and Seglen, P.O. (1998). Isolation and Characterization of Rat Liver Amphisomes. J. Biol. Chemestry *273*, 21883–21892.

Berger, Z., Ravikumar, B., Menzies, F.M., Oroz, L.G., Underwood, B.R., Pangalos, M.N., Schmitt, I., Wullner, U., Evert, B.O., Kane, C.J.O., et al. (2006). Rapamycin alleviates toxicity of different aggregate-prone proteins. Hum. Embryol. Dev. Biol. *15*, 433–442.

Bettencourt, C., and Lima, M. (2011). Machado-Joseph disease: From first descriptions to new perspectives. Orphanet J. Rare Dis. *6*, 1–12.

Bettencourt, C., Santos, C., Kay, T., Vasconcelos, J., and Lima, M. (2008). Analysis of segregation patterns in Machado-Joseph disease pedigrees. J. Hum. Genet. *53*, 920–923.

Bilen, J., and Bonini, N.M. (2007). Genome-Wide Screen for Modifiers of Ataxin-3 Neurodegeneration in Drosophila. PLoS Genet. *3*, e177.

Bjørkøy, G., Lamark, T., Brech, A., Outzen, H., Perander, M., Øvervatn, A., and Stenmark, H. (2005). p62/SQSTM1 forms protein aggregates degraded by autophagy and has a protective effect on huntingtin-induced cell death. J. Cell Biol. *171*, 603–614.

Burnett, B.G., and Pittman, R.N. (2005). The polyglutamine neurodegenerative protein ataxin 3 regulates aggresome formation. PNAS *102*, 4330–4335.

Burnett, B., Li, F., and Pittman, R.N. (2003). The polyglutamine neurodegenerative protein ataxin-3 binds polyubiquitylated proteins and has ubiquitin protease activity. Hum. Mol. Genet. *12*, 3195–3205.

Carmona, V., Cunha-santos, J., Onofre, I., Simões, A.T., Vijayakumar, U., Davidson, B.L., and de Almeida, L.P. (2017). Unravelling Endogenous MicroRNA System Dysfunction as a New Pathophysiological Mechanism in Machado-Joseph Disease. Mol. Ther. *25*, 1–18.

Cemal, C.K., Carroll, C.J., Lawrence, L., Lowrie, M.B., Ruddle, P., Al-mahdawi, S., King, R.H.M., Pook, M.A., Huxley, C., Chamberlain, S., et al. (2002). YAC transgenic mice carrying pathological alleles of the MJD1 locus exhibit a mild and slowly progressive cerebellar deficit. Hum. Mol. Genet. *11*, 1075–1094.

Chai, Y., Koppenhafer, S.L., Bonini, N.M., and Paulson, H.L. (1999). Analysis of the Role of Heat Shock Protein (Hsp) Molecular Chaperones in Polyglutamine Disease. J. Neurosci. *19*, 10338–10347.

Chai, Y., Wu, L., Griffin, J.D., and Paulson, H.L. (2001). The Role of Protein Composition in Specifying Nuclear Inclusion Formation in Polyglutamine Disease *. J. Biol. Chemestry *276*, 44889–44897.

Chang, H., Triboulet, R., Thornton, J.E., and Gregory, R.I. (2013). A role for the Perlman syndrome exonuclease Dis3l2 in the Lin28-let-7 pathway. Nat. Lett. 1–5.

Chang, Y., Yan, W., He, X., Zhang, L., Li, C., Huang, H., Nace, G., Geller, D.A., Lin, J., and Tsung, A. (2012). miR-375 inhibits autophagy and reduces viability of hepatocellular carcinoma cells under hypoxic conditions. Gastroenterolgy *143*, 177–187.

Charroux, B., and Fanto, M. (2010). The fine line between waste disposal and recycling: DRPLA fly models illustrate the importance of completing the autophagy cycle for rescuing neurodegeneration. Autophagy *6*, 667–669.

Chatterjee, A., Chattopadhyay, D., and Chakrabarti, G. (2014). miR-17-5p Downregulation Contributes to Paclitaxel Resistance of Lung Cancer Cells through Altering Beclin1 Expression. PLoS One *9*, 1–14.

Chatterjee, A., Chattopadhyay, D., and Chakrabarti, G. (2015). miR-16 targets Bcl-2 in paclitaxel-resistant lung cancer cells and overexpression of miR-16 along with miR-17 causes unprecedented sensitivity by simultaneously modulating autophagy and apoptosis. Cell. Signal. *27*, 189–203.

Cho, K.J., Song, J., Oh, Y., and Lee, J.E. (2015). MicroRNA-Let-7a regulates the function of microglia in inflammation. Mol. Cell. Neurosci. *68*, 167–176.

Chou, A., Yeh, T., Ouyang, P., Chen, Y., Chen, S., and Wang, H. (2008). Polyglutamine-expanded ataxin-3 causes cerebellar dysfunction of SCA3 transgenic mice by inducing transcriptional dysregulation. Neurobiol. Dis. *31*, 89–101.

Coutinho, P. (1992). Doença de machado-joseph: tentativa de definição.

Coutinho, P., and Andrade, C. (1978). Autosomal dominant system degeneration in Portuguese families of the Azores Islands. Neurology *28*, 703–709.

Cuervo, A.M., and Dice, J.F. (1996). A Receptor for the Selective Uptake and Degradation of Proteins by Lysosomes. Science (80-.). *273*, 501–503.

Cunha-Santos, J., Duarte-Neves, J., Carmona, V., Guarente, L., de Almeida, L.P., and Cavadas, C. (2016). Caloric restriction blocks neuropathology and motor deficits in Machado–Joseph disease mouse models through SIRT1 pathway. Nat. Commun. *7*, 1–14.

Diener, K., Wang, X.S., Chen, C., Meyer, C.F., Keesler, G., Zukowski, M., Tan, T.H., and Yao, Z. (1997). Activation of the c-Jun N-terminal kinase pathway by a novel protein kinase related to human germinal center kinase. Proc. Natl. Acad. Sci. U. S. A. *94*, 9687–9692.

Donaldson, K.M., Li, W., Ching, K.A., Batalov, S., Tsai, C., Joazeiro, C.A.P., Donaldson, K.M., Li, W., Ching, K.A., Batalov, S., et al. (2003). Ubiquitin-mediated sequestration of normal cellular proteins into polyglutamine aggregates. PNAS *100*.

Doss-pepe, E.W., Stenroos, E.S., Johnson, W.G., and Madura, K. (2003). Ataxin-3 Interactions with Rad23 and Valosin-Containing Protein and Its Associations with Ubiquitin Chains and the Proteasome Are Consistent with a Role in Ubiquitin-Mediated Proteolysis. Mol. Cell. Biol. *23*, 6469–6483.

Dubinsky, A.N., Dastidar, S.G., Hsu, C.L., Zahra, R., Djakovic, S.N., Duarte, S., Esau, C.C., Spencer, B., Ashe, T.D., Fischer, K.M., et al. (2014). Let-7 Coordinately Suppresses Components of the Amino Acid Sensing Pathway to Repress mTORC1 and Induce Autophagy. Cell Metab. *20*, 626–638.

Dunn, W.A. (1990). Studies on the Mechanisms of Autophagy: Formation of the Autophagic Vacuole. J. Cell Biol. *110*, 1923–1933.

Durr, A., Stevanin, G., Cancel, G., Duyckaerts, C., Abbas, N., Didierjean, O., Benomar, A., Lyon-caen, O., Julien, J., Serdaru, M., et al. (1996). Spinocerebellar Ataxia 3 and Machado-Joseph Disease : Clinical , Molecular , and Neuropathological Features. Ann Neurol *39*, 490–499.

de Duve, C., and Wattiaux, R. (1966). Functions of Lysosomes. Annu. Rev. Physiol. *28*, 435–492.

Ellisdon, A.M., Thomas, B., and Bottomley, S.P. (2006). The Two-stage Pathway of Ataxin-3 Fibrillogenesis Involves a Polyglutamine-independent Step *. J. Biol. Chemestry *281*, 16888–16896.

Ellisdon, A.M., Pearce, M.C., and Bottomley, S.P. (2007). Mechanisms of Ataxin-3 Misfolding and Fibril Formation : Kinetic Analysis of a Disease-associated Polyglutamine Protein. J. Mol. Biol. *368*, 595–605.

Eulalio, A., Huntzinger, E., and Izaurralde, E. (2008). GW182 interaction with Argonaute is essential for miRNA-mediated translational repression and mRNA decay. Nat. Struct. Mol. Biol. *15*, 346–353.

Evert, B.O., Vogt, I.R., Kindermann, C., Ozimek, L., Vos, R.A.I. De, Brunt, E.R.P., Schmitt, I., Klockgether, T., and Wu, U. (2001). Inflammatory Genes Are Upregulated in Expanded Ataxin-3- Expressing Cell Lines and Spinocerebellar Ataxia Type 3 Brains. J. Neurosci. *21*, 5389–5396.

Evert, B.O., Vogt, I.R., Vieira-Saecker, A., Ozimek, L., Vos, R.A.I. De, Brunt, E.R.P., Klockgether, T., and Wüllner, U. (2003). Gene Expression Profiling in Ataxin-3 Expressing Cell Lines Reveals Distinct Effects of Normal and Mutant Ataxin-3. J. Neuropathol. Exp. Neurol. *62*, 1006–1018.

Faehnle, C.R., Walleshauser, J., and Joshua-Tor, L. (2017). Multi-domain utilization by TUT4 and TUT7 in control of let-7 biogenesis. Nat. Struct. Mol. Biol. 1–8.

Fan, W., Nassiri, A., and Zhong, Q. (2011). Autophagosome targeting and membrane curvature sensing by Barkor / Atg14 (L). PNAS *108*, 7769–7774.

Findlay, G.M., Yan, L., Procter, J., Mieulet, V., and Lamb, R.F. (2007). A MAP4 kinase related to *Ste20* is a nutrient-sensitive regulator of mTOR signalling. Biochem. J. *403*, 13–20.

Frankel, L.B., Wen, J., Lees, M., Høyer-hansen, M., Farkas, T., and Krogh, A. (2011). microRNA-101 is a

potent inhibitor of autophagy. EMBO J. *30*, 4628–4641.

Furuta, N., Fujita, N., Noda, T., Yoshimori, T., and Amano, A. (2010). Combinational Soluble N - Ethylmaleimide-sensitive Factor Attachment Protein Receptor Proteins VAMP8 and Vti1b Mediate Fusion of Antimicrobial and Canonical Autophagosomes with Lysosomes. Mol. Biol. Cell *21*, 1001–1010.

Gao, Z., Van Beugen, B.J., and De Zeeuw, C.I. (2012). Distributed synergistic plasticity and cerebellar learning. Nat. Rev. Neurosci. *13*, 619–635.

Gatchel, J.R., and Zoghbi, H.Y. (2005). Diseases of Unstable Repeat Expansion: Mechanisms and Common Principles. Nat. Rev. Genet. *6*, 743–755.

Goti, D., Katzen, S.M., Mez, J., Kurtis, N., Kiluk, J., Ben-haı, L., Jenkins, N.A., Copeland, N.G., Kakizuka, A., Sharp, A.H., et al. (2004). A Mutant Ataxin-3 Putative – Cleavage Fragment in Brains of Machado – Joseph Disease Patients and Transgenic Mice Is Cytotoxic above a Critical Concentration. J. Neurosci. *24*, 10266–10279.

Gregory, R.I., Yan, K., Amuthan, G., Chendrimada, T., Doratotaj, B., Cooch, N., and Shiekhattar, R. (2004). The Microprocessor complex mediates the genesis of microRNAs. Nat. Lett. *432*, 235–240.

Gregory, R.I., Chendrimada, T.P., Cooch, N., and Shiekhattar, R. (2005). Human RISC Couples MicroRNA Biogenesis and Posttranscriptional Gene Silencing. Cell *123*, 631–640.

Gutierrez, M.G., Munafó, D.B., Berón, W., and Colombo, M.I. (2004). Rab7 is required for the normal progression of the autophagic pathway in mammalian cells. J. Cell Sci. *117*, 2687–2697.

Haacke, A., Hartl, F.U., and Breuer, P. (2007). Calpain inhibition is sufficient to suppress aggregation of polyglutamine-expanded ataxin-3. J. Biol. Chem. *282*, 18851–18856.

Hagan, J.P., Piskounova, E., and Gregory, R.I. (2009). Lin28 recruits the TUTase Zcchc11 to inhibit let-7 maturation in mouse embryonic stem cells. Nat. Struct. Mol. Biol. *16*, 1021–1025.

Hailey, D.W., Rambold, A.S., Satpute-krishnan, P., Mitra, K., Sougrat, R., and Kim, P.K. (2010). Mitochondria Supply Membranes for Autophagosome Biogenesis during Starvation. Cell *141*, 656–667.

Hara, T., Nakamura, K., Matsui, M., Yamamoto, A., Nakahara, Y., Suzuki-migishima, R., Yokoyama, M., Mishima, K., Saito, I., Okano, H., et al. (2006). Suppression of basal autophagy in neural cells causes neurodegenerative disease in mice. Nat. Lett. *441*, 885–889.

Harding, T.M., Hefner-gravink, A., Thumm, M., and Klionsky, D.J. (1996). Genetic and Phenotypic Overlap between Autophagy and the Cytoplasm to Vacuole Protein Targeting Pathway. The *271*, 17621–17625.

Harris, G.M., Dodelzon, K., Gong, L., Gonzalez-alegre, P., and Paulson, H.L. (2010). Splice Isoforms of the Polyglutamine Disease Protein Ataxin-3 Exhibit Similar Enzymatic yet Different Aggregation Properties. PLoS One *5*.

Hemelaar, J., Lelyveld, V.S., Kessler, B.M., and Ploegh, H.L. (2003). A Single Protease, Apg4B, is Specific for the Autophagy-related Ubiquitin-like Proteins GATE-16 , MAP1-LC3, GABARAP, and Apg8L. J. Biol. Chemestry *278*, 51841–51850.

Heo, I., Ha, M., Lim, J., Yoon, M., Park, J., Kwon, S.C., Chang, H., and Kim, V.N. (2012). Mono-Uridylation of Pre-MicroRNA as a Key Step in the Biogenesis of Group II let-7 MicroRNAs. Cell *151*, 521–532.

Hsu, C.L., Lee, E.X., Gordon, K.L., Paz, E.A., Shen, W.C., Ohnishi, K., Meisenhelder, J., Hunter, T., and La Spada, A.R. (2018). MAP4K3 mediates amino acid-dependent regulation of autophagy via phosphorylation of TFEB. Nat. Commun. *9*.

Hu, J., Matsui, M., Gagnon, K.T., Schwartz, J.C., Gabillet, S., Arar, K., Wu, J., Bezprozvanny, I., Corey,

D.R., and America, N. (2009). Allele-specific silencing of mutant huntingtin and ataxin-3 genes by targeting expanded CAG repeats in mRNAs. Nat. Biotechnol. *27*, 478–484.

Huang, Y., Chuang, A.Y., and Ratovitski, E.A. (2011). Phospho- Δ Np63 α/miR - 885-3p axis in tumor cell life and cell death upon cisplatin exposure. Cell Cycle *10*, 3938–3947.

Ichikawa, Y., Goto, J., Hattori, M., Toyoda, A., Ishii, K., Jeong, S.Y., Hashida, H., Masuda, N., Ogata, K., Kasai, F., et al. (2001). The genomic structure and expression of MJD, the Machado-Joseph disease gene. J. Hum. Genet. *46*, 413–422.

Ichimura, Y., Kumanomidou, T., Sou, Y., Mizushima, T., Ezaki, J., Ueno, T., Kominami, E., Yamane, T., Tanaka, K., and Komatsu, M. (2008). Structural Basis for Sorting Mechanism of p62 in Selective Autophagy. J. Biol. Chemestry *283*, 22847–22857.

Ikeda, H., Yamaguchi, M., Sugai, S., Aze, Y., Narumiya, S., and Kakizuka, A. (1996). Expanded polyglutamine in Machado-Joseph disease protein induces cell death in vitro and in vivo. Nat. Genet. *13*, 196–202.

Iwata, A., Christianson, J.C., Bucci, M., Ellerby, L.M., Nukina, N., Forno, L.S., and Kopito, R.R. (2005). Increased susceptibility of cytoplasmic over nuclear polyglutamine aggregates to autophagic degradation. PNAS *102*, 13135–12140.

Jaber, N., Dou, Z., Chen, J., Catanzaro, J., Jiang, Y., Ballou, L.M., and Selinger, E. (2011). Class III PI3K Vps34 plays an essential role in autophagy and in heart and liver function. PNAS *109*, 2003–2008.

Jäger, S., Bucci, C., Tanida, I., Ueno, T., Kominami, E., and Saftig, P. (2004). Role for Rab7 in maturation of late autophagic vacuoles. J. Cell Sci. *117*, 4837–4848.

Jegga, A.G., Schneider, L., Ouyang, X., and Zhang, J. (2011). Systems biology of the autophagy-lysosomal pathway. Autophagy *7*, 477–489.

Kabeya, Y., Mizushima, N., Ueno, T., Yamamoto, A., Kirisako, T., Noda, T., Kominami, E., Ohsumi, Y., and Yoshimori, T. (2000). LC3, a mammalian homologue of yeast Apg8p, is localized in autophagosome membranes after processing. EMBO J. *19*, 5520–5528.

Kamada, Y., Funakoshi, T., Shintani, T., Nagano, K., Ohsumi, M., and Ohsumi, Y. (2000). Tor-mediated Induction of Autophagy Via an Apg1 Protein Kinase Complex. J. Cell Biol. *150*, 1507–1513.

Kaur, J., and Debnath, J. (2015). Autophagy at the crossroads of catabolism and anabolism. Nat. Rev. Mol. Cell Biol. 1–12.

Kawaguchi, Y., Okamoto, T., Taniwaki, M., and Aizawa, M. (1994). CAG expansions in a novel gene for Machado-Joseph disease at chromosome 14q32.1. Nat. Genet. *8*, 221–228.

Khan, L.A., Bauer, P.O., Miyazaki, H., Lindenberg, K.S., Landwehrmeyer, B.G., and Nukina, N. (2006). Expanded polyglutamines impair synaptic transmission and ubiquitin – proteasome system in Caenorhabditis elegans. J. Neurochem. *98*, 576–587.

Kim, E., Goraksha-Hicks, P., Li, L., Neufeld, T.P., and Guan, K.L. (2008). Regulation of TORC1 by Rag GTPases in nutrient response. Nat. Cell Biol. *10*, 935–945.

Kimura, S., Noda, T., and Yoshimori, T. (2008). Dynein-dependent Movement of Autophagosomes Mediates Efficient Encounters with Lysosomes. Cell Struct. Funct. *33*, 109–122.

Klockgether, T., Skalej, M., Wedekind, D., Luft, A.R., Welte, D., Schulz, J.B., Abele, M., Laccone, F., Brice, A., and Dichgans, J. (1998). Autosomal dominant cerebellar ataxia type I MRI-based volumetry of posterior fossa structures and basal ganglia in spinocerebellar ataxia types 1 , 2 and 3. Brain *121*, 1687–1693.

Komatsu, M., Waguri, S., Chiba, T., Murata, S., Iwata, J., Tanida, I., Ueno, T., Koike, M., Uchiyama, Y., Kominami, E., et al. (2006). Loss of autophagy in the central nervous system causes neurodegeneration in mice. Nat. Lett. *441*, 880–884.

Korkmaz, G., le Sage, C., Tekirdag, K.A., Agami, R., and Gozuacik, D. (2012). miR-376b controls starvation and mTOR inhibition- related autophagy by targeting ATG4C and BECN1. Autophagy *8*, 165–176.

Korkmaz, G., Tekirdag, K.A., Ozturk, D.G., Kosar, A., and Sezerman, O.U. (2013). MIR376A Is a Regulator of Starvation-Induced Autophagy. PLoS One *8*, e82556.

Kovaleva, V., Mora, R., Park, Y.J., Plass, C., Chiramel, A.I., Stilgenbauer, S., Pscherer, A., Bartenschlager, R., and Hartmut, D. (2012). miRNA-130a Targets ATG2B and DICER1 to Inhibit Autophagy and Trigger Killing of Chronic Lymphocytic Leukemia Cells. Cancer Res. *72*, 1763–1773.

Laço, M.N., Oliveira, C.R., Paulson, H.L., and Rego, A.C. (2011). Compromised mitochondrial complex II in models of Machado – Joseph disease. BBA - Mol. Basis Dis. *1822*, 139–149.

Lagos-Quintana, M., Rauhut, R., Lendeckel, W., and Tuschl, T. (2001). Identification of Novel Genes Coding for Small Expressed RNAs. Science (80-.). *294*, 853–858.

Lamb, C.A., Yoshimori, T., and Tooze, S.A. (2013). The autophagosome: origins unknown , biogenesis complex. Nat. Rev. Mol. Cell Biol. 1–16.

Landthaler, M., Yalcin, A., and Tuschl, T. (2004). The Human DiGeorge Syndrome Critical Region Gene 8 and its D. melanogaster homolog are required for miRNA biogenesis. Curr. Biol. *14*, 2162–2167.

Lee, J., Beigneux, A., Ahmad, S.T., Young, S.G., and Gao, F. (2007). ESCRT-III Dysfunction Causes Autophagosome Accumulation and Neurodegeneration. Curr. Biol. *17*, 1561–1567.

Lee, R.C., Feinbaum, R.L., and Ambros, V. (1993). The C . elegans Heterochronic Gene lin-4 Encodes Small RNAs with Antisense Complementarity to lin-14. Cell *75*, 843–854.

Lee, Y., Ahn, C., Han, J., Choi, H., Kim, J., Yim, J., Lee, J., Provost, P., Kim, S., and Kim, V.N. (2003). The nuclear RNase III Drosha initiates microRNA processing. Nat. Lett. *425*, 415–419.

Lee, Y., Kim, M., Han, J., Yeom, K., Lee, S., Baek, S.H., and Kim, V.N. (2004a). MicroRNA genes are transcribed by RNA polymerase II. EMBO J. *23*, 4051–4060.

Lee, Y.S., Nakahara, K., Pham, J.W., Kim, K., He, Z., Sontheimer, E.J., and Carthew, R.W. (2004b). Distinct Roles for Drosophila Dicer-1 and Dicer-2 in the siRNA / miRNA Silencing Pathways. Cell *117*, 69–81.

Li, F., Macfarlan, T., Pittman, R.N., and Chakravarti, D. (2002). Ataxin-3 Is a Histone-binding Protein with Two Independent Transcriptional Corepressor Activities. J. Biol. Chemestry *277*, 45004–45012.

Li, W., Li, J., and Bao, J. (2012). Microautophagy: lesser-known self-eating. Cell. Mol. Life Sci. *69*, 1125–1136.

Macedo-Ribeiro, S., Cortes, L., Maciel, P., and Carvalho, A.L. (2009). Nucleocytoplasmic Shuttling Activity of Ataxin-3. PLoS One *4*.

Maciel, P., Gaspar, C., DeStefano, A.L., Silveira, I., Coutinho, P., Radvany, J., Dawson, D.M., Sudarsky, L., Guimarães, J., and Loureiro, J.E. (1995). Correlation between CAG repeat length and clinical features in Machado-Joseph disease. Am. J. Hum. Genet. *57*, 54–61.

Maciel, P., Costa, M.C., Ferro, A., Rousseau, M., Santos, C.S., Gaspar, C., Barros, J., Rouleau, G. a, Coutinho, P., and Sequeiros, J. (2001). Improvement in the molecular diagnosis of Machado-Joseph disease. Arch. Neurol. *58*, 1821–1827.

Masino, L., Musi, V., Menon, R.P., Fusi, P., Kelly, G., Frenkiel, T.A., Trottier, Y., and Pastore, A. (2003). Domain architecture of the polyglutamine protein ataxin-3: A globular domain followed by a flexible tail. FEBS Lett. *549*, 21–25.

Matos, C.A., de Macedo-Ribeiro, S., and Carvalho, A.L. (2011). Polyglutamine diseases: The special case of ataxin-3 and Machado-Joseph disease. Prog. Neurobiol. *95*, 26–48.

Mazzucchelli, S., Palma, A. De, Riva, M., Urzo, A.D., Pozzi, C., Pastori, V., Comelli, F., Fusi, P., Vanoni, M., Tortora, P., et al. (2009). Proteomic and biochemical analyses unveil tight interaction of ataxin-3 with tubulin. Int. J. Biochem. Cell Biol. *41*, 2485–2492.

McLoughlin, H.S., Moore, L.R., Chopra, R., Komlo, R., McKenzie, M., Blumenstein, K.G., Zhao, H., Kordasiewicz, H.B., Shakkottai, V.G., and Paulson, H.L. (2018). Oligonucleotide therapy mitigates disease in Spinocerebellar Ataxia Type 3 mice. Ann. Neurol. 1–24.

Menghini, R., Casagrande, V., Marino, A., Marchetti, V., Cardellini, M., Stoehr, R., Rizza, S., Martelli, E., Greco, S., and Mauriello, A. (2014). MiR-216a : a link between endothelial dysfunction and autophagy. Cell Death Dis. *5*, e1029.

Menzies, F.M., Huebener, J., Renna, M., Bonin, M., Riess, O., and Rubinsztein, D.C. (2010). Autophagy induction reduces mutant ataxin-3 spinocerebellar ataxia type 3. Brain *133*, 93–104.

Milkereit, R., Persaud, A., Vanoaica, L., Guetg, A., Verrey, F., and Rotin, D. (2015). LAPTM4b recruits the LAT1-4F2hc Leu transporter to lysosomes and promotes mTORC1 activation. Nat. Commun. *6*, 1–9.

Mizushima, N., Noda, T., Yoshimori, T., Tanaka, Y., Ishii, T., George, M.D., Klionsky, D.J., Ohsumi, M., and Ohsumi, Y. (1998). A protein conjugation system essential for autophagy. Nature *395*, 395–398.

Mizushima, N., Yoshimori, T., and Ohsumi, Y. (2002). Mouse Apg10 as an Apg12-conjugating enzyme : analysis by the conjugation-mediated yeast two-hybrid method. FEBS Lett. *532*, 450–454.

Mizushima, N., Kuma, A., Kobayashi, Y., Yamamoto, A., and Matsubae, M. (2003). Mouse Apg16L, a novel WD-repeat protein , targets to the autophagic isolation membrane with the Apg12- Apg5 conjugate. J. Cell Sci. *116*, 1679–1688.

Mizushima, N., Yamamoto, A., Matsui, M., Yoshimori, T., and Ohsumi, Y. (2004). In Vivo Analysis of Autophagy in Response to Nutrient Starvation Using Transgenic Mice Expressing a Fluorescent Autophagosome Marker. Mol. Biol. Cell *15*, 1101–1111.

Mookerjee, S., Papanikolaou, T., Guyenet, S.J., Sampath, V., Lin, A., Vitelli, C., Degiacomo, F., Sopher, B.L., Chen, S.F., Spada, A.R. La, et al. (2009). Posttranslational Modification of Ataxin-7 at Lysine 257 Prevents Autophagy-Mediated Turnover of an N-Terminal Caspase-7 Cleavage Fragment. Neurobiol. Dis. *29*, 15134–15144.

Moore, L.R., Rajpal, G., Dillingham, I.T., Qutob, M., Blumenstein, K.G., Gattis, D., Hung, G., Kordasiewicz, H.B., Paulson, H.L., and Mcloughlin, H.S. (2017). Evaluation of Antisense Oligonucleotides Targeting ATXN3 in SCA3 Mouse Models. Mol. Ther. Nucleic Acid *7*, 200–210.

Mortimore, G.E., Lardeuxt, B.R., and Adams, C.E. (1988). Regulation of Microautophagy and Basal Protein Turnover in Rat Liver. Effects of short-term stravation. J. Biol. Chemestry *263*, 2506–2512.

Muñoz, E., Rey, M.J., Milá, M., Cardozo, A., Ribalta, T., Tolosa, E., and Ferrer, I. (2002). Intranuclear inclusions , neuronal loss and CAG mosaicism in two patients with Machado – Joseph disease. J. Neurol. Sci. *200*, 19–25.

Nagai, Y., Inui, T., Popiel, H.A., Fujikake, N., Hasegawa, K., Urade, Y., Goto, Y., Naiki, H., and Toda, T. (2007). A toxic monomeric conformer of the polyglutamine protein. Nat. Strucutural Mol. Biol. *14*, 332–

340.

Nakano, K., Spence, A., and Dawson, D. (1972). Machado disease. Neurology *22*, 49–55.

Nascimento-Ferreira, I., Santos-Ferreira, T., Sousa-Ferreira, L., Auregan, G., Onofre, I., Alves, S., Dufour, N., Gould, V.F.C., Koeppen, A., Déglon, N., et al. (2011). Overexpression of the autophagic beclin-1 protein clears mutant ataxin-3 and alleviates Machado–Joseph disease. Brain *134*, 1400–1415.

Nascimento-Ferreira, I., Nóbrega, C., Vasconcelos-Ferreira, A., Onofre, I., Albuquerque, D., Aveleira, C., Hirai, H., Déglon, N., and de Almeida, L.P. (2013). Beclin 1 mitigates motor and neuropathological deficits in genetic mouse models of Machado-Joseph disease. Brain *136*, 2173–2188.

Neff, N.T., Bourret, L., Miao, P., and Dice, J.F. (1981). Degradation of Proteins Microinjected into IMR-90 Human Diploid Fibroblasts. J. Cell Biol. *91*, 184–194.

Nicklin, P., Bergman, P., Zhang, B., Triantafellow, E., Wang, H., Nyfeler, B., Yang, H., Hild, M., Kung, C., Wilson, C., et al. (2009). Bidirectional Transport of Amino Acids Regulates mTOR and Autophagy. Cell *136*, 521–534.

Nisoli, I., Chauvin, J.P., Napoletano, F., Calamita, P., Zanin, V., Fanto, M., and Charroux, B. (2010). Neurodegeneration by polyglutamine Atrophin is not rescued by induction of autophagy. Cell Death Differ. *17*, 1577–1587.

Nóbrega, C., and de Almeida, L.P. (2012). Machado-Joseph Disease/Spinocerebellar Ataxia type3. In Spinocerebellar Ataxia, (INTECH), p. 109.

Nóbrega, C., Nascimento-Ferreira, I., Onofre, I., Albuquerque, D., Conceição, M., Déglon, N., and de Almeida, L.P. (2012). Overexpression of Mutant Ataxin-3 in Mouse Cerebellum Induces Ataxia and Cerebellar Neuropathology. Cerebellum *12*, 441–455.

Nóbrega, C., Nascimento-Ferreira, I., Onofre, I., Albuquerque, D., Hirai, H., Déglon, N., and de Almeida, L.P. (2013). Silencing Mutant Ataxin-3 Rescues Motor Deficits and Neuropathology in Machado-Joseph Disease Transgenic Mice. PLoS One *8*.

Okamura, K., Hagen, J.W., Duan, H., Tyler, D.M., and Lai, E.C. (2007). The Mirtron Pathway Generates microRNA-Class Regulatory RNAs in Drosophila. Cell *130*, 89–100.

Oliveira Miranda, C., Marcelo, A., Silva, T.P., Barata, J., Vasconcelos-Ferreira, A., Pereira, D., Nóbrega, C., Duarte, S., Barros, I., Alves, J., et al. (2018). Repeated Mesenchymal Stromal Cell Treatment Sustainably Alleviates Machado-Joseph Disease. Mol. Ther. *26*, 1–21.

Onofre, I., Mendonça, N., Lopes, S., Nobre, R., Melo, J.B. de, Carreira, I.M., Januário, C., Gonçalves, A.F., and de Almeida, L.P. (2016). Fibroblasts of Machado Joseph Disease patients reveal autophagy impairment. Sci. Rep. *6*, 1–10.

Orr, H.T., and Zoghbi, H.Y. (2007). Trinucleotide repeat disorders. Annu. Rev. Neurosci. *30*, 575–621.

Ou, Z., Luo, M., Niu, X., Chen, Y., Xie, Y., He, W., Song, B., Xian, Y., Fan, D., Ouyang, S., et al. (2016). Autophagy Promoted the Degradation of Mutant ATXN3 in Neurally Differentiated Spinocerebellar Ataxia-3 Human Induced Pluripotent Stem Cells. Biomed Res. Int. 1–11.

Pattingre, S., Tassa, A., Qu, X., Garuti, R., Liang, X.H., Mizushima, N., Packer, M., Schneider, M.D., and Levine, B. (2005). Bcl-2 Antiapoptotic Proteins Inhibit Beclin 1-Dependent Autophagy. Cell *122*, 927–939.

Paulson, H. (2012). Machado – Joseph disease / spinocerebellar ataxia type 3 (Elsevier B.V.).

Paulson, H.L., Perez, M.K., Trottier, Y., Trojanowski, J.Q., Subramony, S.H., Das, S.S., Vig, P., Mandel, J., Fischbeck, K.H., and Pittman, R.N. (1997). Intranuclear Inclusions of Expanded Polyglutamine Protein

in Spinocerebellar Ataxia Type 3. Neuron *19*, 333–344.

Paxinos, G., and Franklin, K.B.J. (2001). The mouse Brain in stereotaxic coordinates.

Pedroso, L., Franc, M.C., Braga-neto, P., Caramelli, P., Saraiva-pereira, M.L., Saute, J.A., Jardim, L.B., Lopes-cendes, I., Barsottini, O.G.P., and Society, D. (2013). Nonmotor and Extracerebellar Features in Machado-Joseph Disease : A Review. Mov. Disord. *28*, 1200–1208.

Perez, M.K., Paulson, H.L., Pendse, S.J., Saionz, S.J., Bonini, N.M., and Pittman, R.N. (1998). Recruitment and the Role of Nuclear Localization in Polyglutamine-mediated Aggregation. J. Cell Biol. *143*, 1457–1470.

Polikepahad, S., Knight, J.M., Naghavi, A.O., Oplt, T., Creighton, C.J., Shaw, C., Benham, A.L., Kim, J., Soibam, B., Harris, R.A., et al. (2010). Proinflammatory role for let-7 microRNAS in experimental asthma. J. Biol. Chem. *285*, 30139–30149.

Ravikumar, B., Duden, R., and Rubinsztein, D.C. (2002). Aggregate-prone proteins with polyglutamine and polyalanine expansions are degraded by autophagy. Hum. Mol. Genet. *11*, 1107–1117.

Ravikumar, B., Acevedo-arozena, A., Imarisio, S., Berger, Z., Vacher, C., Kane, C.J.O., Brown, S.D.M., and Rubinsztein, D.C. (2005). Dynein mutations impair autophagic clearance of aggregate-prone proteins. Nat. Genet. *37*, 771–776.

Rego, A.C., and de Almeida, L.P. (2005). Molecular targets and therapeutic strategies in Huntington's disease. Curr. Drug Targets. CNS Neurol. Disord. *4*, 361–381.

Reinhart, B.J., Slack, F.J., and Basson, M. (2000). The 21-nucleotide let-7 RNA regulates developmental timing in Caenorhabditis elegans. Nat. Lett. *403*, 901–906.

Rodríguez-Lebrón, E., Costa, M.D., Luna-Cancalon, K., Peron, T.M., Fischer, S., Boudreau, R.L., Davidson, B.L., and Paulson, H.L. (2013). Silencing mutant ATXN3 expression resolves molecular phenotypes in SCA3 transgenic mice. Mol. Ther. *21*, 1909–1918.

Rodriguez, A., Griffiths-Jones, S., Ashurst, J.L., and Bradley, A. (2004). Identification of Mammalian microRNA Host Genes and Transcription Units. Genome Res. *14*, 1902–1910.

Rosenberg, R.N. (1992). Machado-Joseph Disease : An Autosomal Dominant Motor System Degeneration. Mov. Disord. *7*, 193–203.

Ruano, L., Melo, C., Silva, M.C., and Coutinho, P. (2014). The global epidemiology of hereditary ataxia and spastic paraplegia: A systematic review of prevalence studies. Neuroepidemiology *42*, 174–183.

Rüb, U., Vos, R.A.I. de, Schultz, C., Brunt, E.R., Paulson, H., and Braak, H. (2002). Spinocerebellar ataxia type 3 (Machado - Joseph disease): severe destruction of the lateral reticular nucleus. Brain *125*, 2115–2124.

Rüb, U., Vos, R.A.I. De, Brunt, E.R., Sebestény, T., Schöls, L., Auburger, G., Bohl, J., Ghebremedhin, E., and Gierga, K. (2006). Spinocerebellar Ataxia Type 3 (SCA3): Thalamic Neurodegeneration Occurs Independently from Thalamic Ataxin-3 Immunopositive Neuronal Intranuclear Inclusions. Brain Pathol. *16*, 218–227.

Rüb, U., Brunt, E.R., and Deller, T. (2008). New insights into the pathoanatomy of spinocerebellar ataxia type 3 (Machado – Joseph disease). Curr Opin Neurol *21*, 11–116.

Ruby, J.G., Jan, C.H., and Bartel, D.P. (2007). Intronic microRNA precursors that bypass Drosha processing. Nat. Lett. *448*, 83–86.

Rusten, T.E., Vaccari, T., Lindmo, K., Rodahl, L.M.W., Nezis, I.P., Sem-jacobsen, C., Wendler, F., Vincent, J., Brech, A., Bilder, D., et al. (2007). ESCRTs and Fab1 Regulate Distinct Steps of Autophagy. Curr. Biol.

17, 1817–1825.

Sancak, Y., Peterson, T.R., Shaul, Y.D., Lindquist, R.A., Thoreen, C.C., Bar-Peled, L., and Sabatini, D.M. (2008). The Rag GTPases bind raptor and mediate amino acid signaling to mTORC1. Science (80-.). *320*, 1496–1501.

Sancak, Y., Bar-Peled, L., Zoncu, R., Markhard, A.L., Nada, S., and Sabatini, D.M. (2010). Ragulator-Rag complex targets mTORC1 to the lysosomal surface and is necessary for its activation by amino acids. Cell *141*, 290–303.

Schmitt, I., Brattig, T., Gossen, M., and Riess, O. (1997). Characterization of the rat spinocerebellar ataxia type 3 gene. Neurogenetics *1*, 103–112.

Schulz, J.B., Borkert, J., Wolf, S., Schmitz-hübsch, T., Rakowicz, M., Mariotti, C., Schoels, L., Timmann, D., Warrenburg, B. Van De, Dürr, A., et al. (2010). Visualization , quantification and correlation of brain atrophy with clinical symptoms in spinocerebellar ataxia types 1 , 3 and 6. Neuroimage *49*, 158–168.

Schwarz, D.S., Hutvágner, G., Du, T., Xu, Z., Aronin, N., and Zamore, P.D. (2003). Asymmetry in the assembly of the RNAi enzyme complex. Cell *115*, 199–208.

Shenoy, A., Danial, M., and Blelloch, R.H. (2015). Let-7 and miR-125 cooperate to prime progenitors for astrogliogenesis. EMBO J. *34*, 1180–1194.

Shi, Y., Huang, F., Tang, B., Li, J., Wang, J., Shen, L., Xia, K., and Jiang, H. (2014). MicroRNA profiling in the serums of SCA3/MJD patients. Int. J. Neurosci. *124*, 97–101.

Shibata, M., Lu, T., Furuya, T., Degterev, A., Mizushima, N., Yoshimori, T., Macdonald, M., Yankner, B., and Yuan, J. (2006). Regulation of Intracellular Accumulation of Mutant Huntingtin by Beclin 1 *. J. Biol. Chemestry *281*, 14474–14485.

Silva-Fernandes, A., Costa, C., Duarte-Silva, S., Oliveira, P., Botelho, C.M., Martins, L., Mariz, J.A., Ferreira, T., Ribeiro, F., Correia-Neves, M., et al. (2010). Motor uncoordination and neuropathology in a transgenic mouse model of Machado – Joseph disease lacking intranuclear inclusions and ataxin-3 cleavage products. Neurobiol. Dis. *40*, 163–176.

Silva-Fernandes, A., Duarte-Silva, S., Neves-Carvalho, A., Amorim, M., Soares-Cunha, C., Oliveira, P., Thirstrup, K., Teixeira-Castro, A., and Maciel, P. (2014). Chronic Treatment with 17-DMAG Improves Balance and Coordination in A New Mouse Model of Machado-Joseph Disease. Neurotherapeutics *11*, 433–449.

Simões, A.T., Gonçalves, N., Koeppen, A., Déglon, N., Kügler, S., Duarte, C.B., and de Almeida, L.P. (2012). Calpastatin-mediated inhibition of calpains in the mouse brain prevents mutant ataxin 3 proteolysis, nuclear localization and aggregation, relieving Machado-Joseph disease. Brain *135*, 2428–2439.

Simões, A.T., Gonçalves, N., Nobre, R.J., Duarte, C.B., and Pereira de Almeida, L. (2014). Calpain inhibition reduces ataxin-3 cleavage alleviating neuropathology and motor impairments in mouse models of Machado-Joseph Disease. Hum. Mol. Genet. *23*, 4932–4944.

Simonovitch, S., Schmukler, E., Bespalko, A., Iram, T., Frenkel, D., Holtzman, D.M., Masliah, E., Michaelson, D.M., and Pinkas-Kramarski, R. (2016). Impaired Autophagy in APOE4 Astrocytes. J. Alzheimer's Dis. *51*, 915–927.

Singh, R., and Saini, N. (2012). Downregulation of BCL2 by miRNAs augments drug- induced apoptosis – a combined computational and experimental approach. J. Cell Sci. *125*, 1568–1578.

Sokol, N.S., Xu, P., Jan, Y., and Ambros, V. (2008). Drosophila let-7 microRNA is required for remodeling of the neuromusculature during metamorphosis. Genes Dev. *22*, 1591–1596.

La Spada, A.R., Wilson, E.M., Lubanh, D.B., Harding, A.E., and Fischbeck, K.H. (1991). Androgen receptor gene mutations in X-linked spinal and bulbar muscular atophy. Nature *352*, 77–79.

Suite, N.D.A., Sequeiros, J., and Mckhann, G.M. (1986). Machado-Joseph Disease in a Sicilian-American Family. J. Neurogenet. *3*, 177–182.

Suzuki, K., Kubota, Y., Sekito, T., and Ohsumi, Y. (2007). Hierarchy of Atg proteins in pre-autophagosomal structure organization. Genes to Cells *12*, 209–218.

Takahashi, K., and Yamanaka, S. (2006). Induction of Pluripotent Stem Cells from Mouse Embryonic and Adult Fibroblast Cultures by Defined Factors. Cell *126*, 663–676.

Takahashi, K., Tanabe, K., Ohnuki, M., Narita, M., Ichisaka, T., Tomoda, K., and Yamanaka, S. (2007). Induction of Pluripotent Stem Cells from Adult Human Fibroblasts by Defined Factors. Cell *131*, 861–872.

Takiyama, Y., Nishizawa, M., Tanaka, H., and Kawashima, S. (1993). The gene for Machado-Joseph Diasease maps to human chromosome 14q. Nat. Genet. *4*, 300–304.

Taroni, F., and Didonato, S. (2004). Pathways to motor incoordination: the inherited ataxias. Nat. Rev. Neurosci. *5*, 641–655.

Todi, S. V, Scaglione, K.M., Blount, J.R., Basrur, V., Conlon, K.P., Pastore, A., Elenitoba-johnson, K., and Paulson, H.L. (2010). Activity and Cellular Functions of the Deubiquitinating Enzyme and Polyglutamine Disease Protein Ataxin-3 Are Regulated by Ubiquitination at Lysine 117. J. Biol. Chemestry *285*, 39303–39313.

Toonen, L.J.A., Rigo, F., van Attikum, H., and van Roon-Mom, W.M.C. (2017). Antisense Oligonucleotide-Mediated Removal of the Polyglutamine Repeat in Spinocerebellar Ataxia Type 3 Mice. Mol. Ther. - Nucleic Acids *8*, 232–242.

Torashima, T., Koyama, C., Iizuka, A., Mitsumura, K., Takayama, K., Yanagi, S., Oue, M., Yamaguchi, H., and Hirai, H. (2008). Lentivector-mediated rescue from cerebellar ataxia in a mouse model of spinocerebellar ataxia. EMBO Rep. *9*, 393–399.

Trottier, Y., Cancel, G., An-Gourfinkel, I., Lutz, Y., Weber, C., Brice, A., Hirsch, E., and Mandel, J.L. (1998). Heterogeneous intracellular localization and expression of ataxin-3. Neurobiol. Dis. *5*, 335–347.

Wang, C.-W., and Klionsky, D.J. (2003). The Molecular Mechanism of Autophagy. Mol. Med. *9*, 65–76.

Wang, Y., Hsi, E., Cheng, H., Hsu, S., Liao, Y., and Juo, S.H. (2017). Let-7g suppresses both canonical and non-canonical NF-κB pathways in macrophages leading to anti-atherosclerosis. Oncotarget 1–16.

Warrick, J.M., Paulson, H.L., Gray-board, G.L., Bui, Q.T., Fischbeck, K.H., Pittman, R.N., and Bonini, N.M. (1998). Expanded Polyglutamine Protein Forms Nuclear Inclusions and Causes Neural Degeneration in Drosophila. Cell *93*, 939–949.

Warrick, J.M., Morabito, L.M., Bilen, J., Gordesky-gold, B., Faust, L.Z., Paulson, H.L., and Bonini, N.M. (2005). Ataxin-3 Suppresses Polyglutamine Neurodegeneration in Drosophila by a Ubiquitin-Associated Mechanism. Mol. Cell *18*, 37–48.

Watchon, M., Yuan, K.C., Mackovski, N., Svahn, A.J., Cole, N.J., Goldsbury, C., Rinkwitz, S., Becker, T.S., Nicholson, G.A., and Laird, A.S. (2017). Calpain inhibition is protective in Machado–Joseph Disease Zebrafish due to induction of autophagy. J. Neurosci. *37*, 7782–7794.

Webb, J.L., Ravikumar, B., Atkins, J., Skepper, J.N., and Rubinsztein, D.C. (2003). α-synuclein is degraded by both autophagy and the proteasome. J. Biol. Chem. *278*, 25009–25013.

Wei, Y., Sinha, S.C., and Levine, B. (2008). Dual Role of JNK1-mediated phosphorylation of Bcl-2 in

autophagy and apoptosis regulation. Autophagy *4*, 949–951.

Wei, Y.B., Liu, J.J., Villaescusa, J.C., Åberg, E., Brené, S., Wegener, G., Mathé, A.A., and Lavebratt, C. (2016). Elevation of Il6 is associated with disturbed let-7 biogenesis in a genetic model of depression. Transl. Psychiatry *6*, e869.

Wightman, B., Ha, I., and Ruvkun, G. (1993). Posttranscriptional Regulation of the Heterochronic Gene lin-14 by W -4 Mediates Temporal Pattern Formation in C . elegans. Cell *75*, 855–862.

Winter, J., Jung, S., Keller, S., Gregory, R.I., and Diederichs, S. (2009). Many roads to maturity: microRNA biogenesis pathways and their regulation. Nat. Cell Biol. *11*, 228–234.

Woods, B.T., and Schaumburg, H.H. (1972). Nigro-spino-dentatal Degeneration with Nuclear Ophthalmoplegia. J. Neurol. Sci. *17*, 149–166.

Xiao, J., Zhu, X., He, B., Zhang, Y., Kang, B., Wang, Z., and Ni, X. (2011). MiR-204 regulates cardiomyocyte autophagy induced by ischemia-reperfusion through LC3-II. J. Biomed. Sci. *18*, 1–6.

Yamamoto, A., Tagawa, Y., Yoshimori, T., and Moriyama, Y. (1998). Bafilomycin A1 Prevents Maturation of Autophagic Vacuoles by Inhibiting Fusion between Autophagosomes and Lysosomes in Rat Hepatoma Cell Line, H-4-II-E cells. Cell Struct. Funct. *42*, 33–42.

Yang, X., Zhong, X., Tanyi, J.L., Shen, J., Xu, C., Gao, P., Zheng, T.M., Demichele, A., and Zhang, L. (2013). mir-30d Regulates multiple genes in the autophagy pathway and impairs autophagy process in human cancer cells. Biochem. Biophys. Res. Commun. *431*, 617–622.

Yao, Y., Jones, E., and Inoki, K. (2017). Lysosomal Regulation of mTORC1 by Amino Acids in Mammalian Cells. Biomolecules *1*, 1–18.

Yi, R., Qin, Y., Macara, I.G., and Cullen, B.R. (2003). Exportin-5 mediates the nuclear export of pre-microRNAs and short hairpin RNAs. Genes Dev. *17*, 3011–3016.

Zander, C., Takahashi, J., Hachimi, K.H. El, Fujigasaki, H., Albanese, V., Lebre, A.S., Stevanin, G., Duyckaerts, C., and Brice, A. (2001). Similarities between spinocerebellar ataxia type 7 (SCA7) cell models and human brain : proteins recruited in inclusions and activation of caspase-3. Hum. Mol. Genet. *10*, 2569–2580.

Zheng, S., Clabough, E.B.D., Sarkar, S., Futter, M., Rubinsztein, D.C., and Scott, O. (2010). Deletion of the Huntingtin Polyglutamine Stretch Enhances Neuronal Autophagy and Longevity in Mice. PLoS Genet. *6*.

Zhu, H., Wu, H., Liu, X., Li, B., Chen, Y., Ren, X., Liu, C.-G., and Yang, J.-M. (2009). Regulation of autophagy by a beclin 1 -targeted microRNA , miR-30a, in cancer cells. Autophagy *5*, 816–823.